

Electrolytes and Interphases in Sodium-Based Rechargeable Batteries: Recent Advances and Perspectives

*Original*

Electrolytes and Interphases in Sodium-Based Rechargeable Batteries: Recent Advances and Perspectives / Eshetu, G.G., Elia, G.A., Armand, M., Forsyth, M., Komaba, S., Rojo, T., Passerini, S.. - In: ADVANCED ENERGY MATERIALS. - ISSN 1614-6832. - ELETTRONICO. - 10:20(2020), p. 2000093. [10.1002/aenm.202000093]

*Availability:*

This version is available at: 11583/2959174 since: 2022-03-23T10:49:41Z

*Publisher:*

Wiley-VCH Verlag

*Published*

DOI:10.1002/aenm.202000093

*Terms of use:*

This article is made available under terms and conditions as specified in the corresponding bibliographic description in the repository

*Publisher copyright*

(Article begins on next page)

# Electrolytes and Interphases in Sodium-Based Rechargeable Batteries: Recent Advances and Perspectives

*Gebrekidan Gebresilassie Eshetu, Giuseppe Antonio Elia, Michel Armand, Maria Forsyth, Shinichi Komaba, Teofilo Rojo, and Stefano Passerini\**

For sodium (Na)-rechargeable batteries to compete, and go beyond the currently prevailing Li-ion technologies, mastering the chemistry and accompanying phenomena is of supreme importance. Among the crucial components of the battery system, the electrolyte, which bridges the highly polarized positive and negative electrode materials, is arguably the most critical and indispensable of all. The electrolyte dictates the interfacial chemistry of the battery and the overall performance, having an influence over the practical capacity, rate capability (power), chemical/thermal stress (safety), and lifetime. In-depth knowledge of electrolyte properties provides invaluable information to improve the design, assembly, and operation of the battery. Thus, the full-scale appraisal of both tailored electrolytes and the concomitant interphases generated at the electrodes need to be prioritized. The deployment of large-format Na-based rechargeable batteries also necessitates systematic evaluation and detailed appraisal of the safety-related hazards of Na-based batteries. Hence, this review presents a comprehensive account of the progress, status, and prospect of various Na<sup>+</sup>-ion electrolytes, including solvents, salts and additives, their interphases and potential hazards.

technologies. Unlike lithium, whose market is already very tight, sodium mineral deposits are almost infinite, evenly distributed worldwide, much easier to extract and thereby attainable at low cost.<sup>[1–4]</sup> If the realization of Na-rechargeable batteries could be practically possible, there will be nearly three orders of magnitude relaxation in the constraints on lithium-based resources, accompanied by sustainability, improved environmental benevolence, and cost reduction (Table 1). Even more appealing is the possible use of the widely available and lighter aluminum, rather than copper, as negative current collector and hard carbon from renewable sources instead of graphite for the negative electrode. Finally, the stability of sodium-ion batteries (SIBs) in the fully discharged state would significantly enhance the safety associated with the shipment of large-format SIBs worldwide.

These beneficial features of sodium-

based cells revived the research work on Na-based rechargeable batteries and accordingly captured the attention of both the academic research and industry sectors. However, similar to LIB, most of the research work in Na-based batteries have focused on the development and elaboration of negative and positive

## 1. Introduction

Among the post-lithium (Li) electrochemical energy storage devices, room temperature (RT) sodium (Na)-based rechargeable batteries appear to be one most appealing and viable

Dr. G. G. Eshetu, Prof. M. Armand, Prof. T. Rojo  
CIC Energigune  
Parque Tecnológico de Álava  
Albert Einstein 48, Miñano, Álava, Vitoria-Gasteiz 01510, Spain

Dr. G. G. Eshetu, Dr. G. A. Elia, Prof. S. Passerini  
Helmholtz Institute Ulm (HIU)  
Helmholtzstrasse 11, Ulm 89081, Germany

Dr. G. G. Eshetu, Dr. G. A. Elia, Prof. S. Passerini  
Karlsruhe Institute of Technology (KIT)  
P.O. Box 3640, Karlsruhe 76021, Germany  
E-mail: stefano.passerini@kit.edu

 The ORCID identification number(s) for the author(s) of this article can be found under <https://doi.org/10.1002/aenm.202000093>.

© 2020 Karlsruher Institut für Technologie. Published by WILEY-VCH Verlag GmbH & Co. KGaA, Weinheim. This is an open access article under the terms of the Creative Commons Attribution-NonCommercial-NoDerivs License, which permits use and distribution in any medium, provided the original work is properly cited, the use is non-commercial and no modifications or adaptations are made.

DOI: 10.1002/aenm.202000093

Dr. G. G. Eshetu  
Institute for Power Electronics and Electrical Drives (ISEA)  
RWTH Aachen University  
Jägerstraße 17/19, Aachen 52066, Germany

Dr. G. G. Eshetu  
Department of Chemistry  
College of Natural and Computational Sciences  
Mekelle University  
P.O. Box-231, Mekelle 07000, Ethiopia

Prof. M. Forsyth  
Institute for Frontier Materials  
Deakin University  
Burwood, Victoria 03217, Australia

Prof. S. Komaba  
Department of Applied Chemistry  
Tokyo University of Science  
1-3 Kagurazaka, Shinjuku, Tokyo 162-8061, Japan

Prof. T. Rojo  
Department of Inorganic Chemistry  
Faculty of Science and Technology  
University of the Basque Country (UPV/EHU)  
P.O. Box. 644, Bilbao 48080, Spain

**Table 1.** Comparison of the physical properties of lithium and sodium relevant to their use in rechargeable batteries.<sup>1,3]</sup>

Characteristics	Chemistry	
	<sup>11</sup> Na	<sup>3</sup> Li
Atomic weight [g mol <sup>-1</sup> ]	23	6.94
Mass to electron ratio	23	6.94
Ionic volume [Å <sup>3</sup> ]	4.44	1.84
Shannon's ionic radius [Å]	0.76	1.02
Melting point [°C]	98	182
Voltage [V] vs SHE <sup>a)</sup>	-2.714	-3.045
Ratio of reserves (ppm in the earth crust)	2830	6.5
Distribution	Everywhere	70% in S. America <sup>o)</sup>
Material abundance in earth's crust [ppm]	23 000	20
Material abundance in water [mg L <sup>-1</sup> ]	11 000	0.18
Price of carbonates [\$ per ton]	150	5000
Price of anode current collector [\$ per metric ton.]	1885 (Al)	5719 (Cu)
Metal electrode theoretical capacity [mAh g <sup>-1</sup> ] <sup>b)</sup>	1165	3829
Metal electrode theoretical capacity [mAh cm <sup>-3</sup> ]	1131	2062
Desolvation energy [kJ mol <sup>-1</sup> ] in	≈40–70 kJ mol <sup>-1</sup> higher than Li	
DEC	148	208
EC	152	211
PC	158	218
Coordination preference	Octahedral and prismatic	Octahedral and tetrahedral
Reactivity/flammability of the metal	Highly flammable	Less reactive

<sup>a)</sup>Standard hydrogen electrode; <sup>b)</sup>Metal; <sup>o)</sup>South America.

electrode materials, with only a relatively small activity dedicated to electrolytes and their interphases with the electrodes. In fact, being sandwiched between the highly reducing negative and highly oxidizing positive electrodes, the electrolyte is in close interaction with both electrodes and the corresponding electrified interfaces. Indeed, stable electrolytes and interphases are the most indispensable elements for the proper functioning of the emerging Na-based batteries. Hence, the viable future deployment of SIB technology will profoundly depend on the further discovery and development of tailored electrolytes and full-scale mastering of their interphases with both active electrodes.

A bibliometric analysis of the research progress on SIBs, SIBs electrolytes, and SIBs interphases was carried out using the Scopus database utilizing titles, abstracts or keywords as searching inputs for the period from 2010–2019 (2nd September 2019). The results reported in **Figure 1** shows an exponential growth of research papers. The experiences and knowhow stockpiled from LIBs provide insights into the development of electrolytes and understanding of their interphases. On the other hand, there is no guarantee that the direct transition of behaviors from Li- to Na-based battery chemistries is appropriate. Peculiar characteristics of sodium versus lithium, like the less negative redox potential (≈0.33 V), the milder Lewis acidity resulting in higher solubility of Na-based SEI/CEI compounds (e.g., Na<sub>2</sub>CO<sub>3</sub>



**Gebrekidan Gebresilassie**

**Eshetu** obtained his PhD in Materials Science in 2013 from the LRCS (CNRS) laboratory in France under the supervision of Prof. Michel Armand, Prof. Stephane Laruele, and Dr. Sylvie Grugeon. He then carried out his first postdoctoral research at the Karlsruhe Institute of Technology (KIT), Helmholtz Institute Ulm

(HIU) in the group of Prof. Stefano Passerini. In 2017, he joined CIC Energigune (Spain) as senior postdoctoral fellow in the Prof. Armand group. Currently, he is a senior researcher at RWTH Aachen University (Germany) in the group of Egbert Figgemeier. His research interest focuses on next generation electrochemical energy storage devices.



**Giuseppe Antonio Elia**

received his Ph.D. in Chemistry in 2013 from La Sapienza University of Rome. During his Ph.D. studies, he spent a few visiting scientist stages in highly qualified research centers, namely, Hanyang University, Munster Electrochemical Energy Technology (MEET), Argonne National Laboratory

(ANL), and Helmholtz-Institut Ulm (HIU). Afterward, he spent three and a half years at TU Berlin (2014–2019) as a scientist, focusing its activity on Al-battery systems. Currently, he is a senior researcher at Helmholtz-Institut Ulm (Germany) in the group of Professor Stefano Passerini. His research interest focuses on next-generation electrochemical energy storage devices.



**Stefano Passerini** is Professor at the Karlsruhe Institute of Technology, Helmholtz Institute Ulm (Germany) since January 1, 2014. Formerly Professor at the University of Muenster (Germany), he cofounded the MEET battery research center at the University of Muenster (Germany). His research activities are focused on electrochemical energy storage in batteries and supercapacitors.

vs Li<sub>2</sub>CO<sub>3</sub>), the lower desolvation energy of Na<sup>+</sup> (by ≈25–30%), the larger ionic radii (>30%), the larger coordination shell, the higher reactivity of Na metal, and the lower equivalent volume of most Na-based SEI species, certainly affect the evolving interphases differently, requiring the screening of varying electrolyte

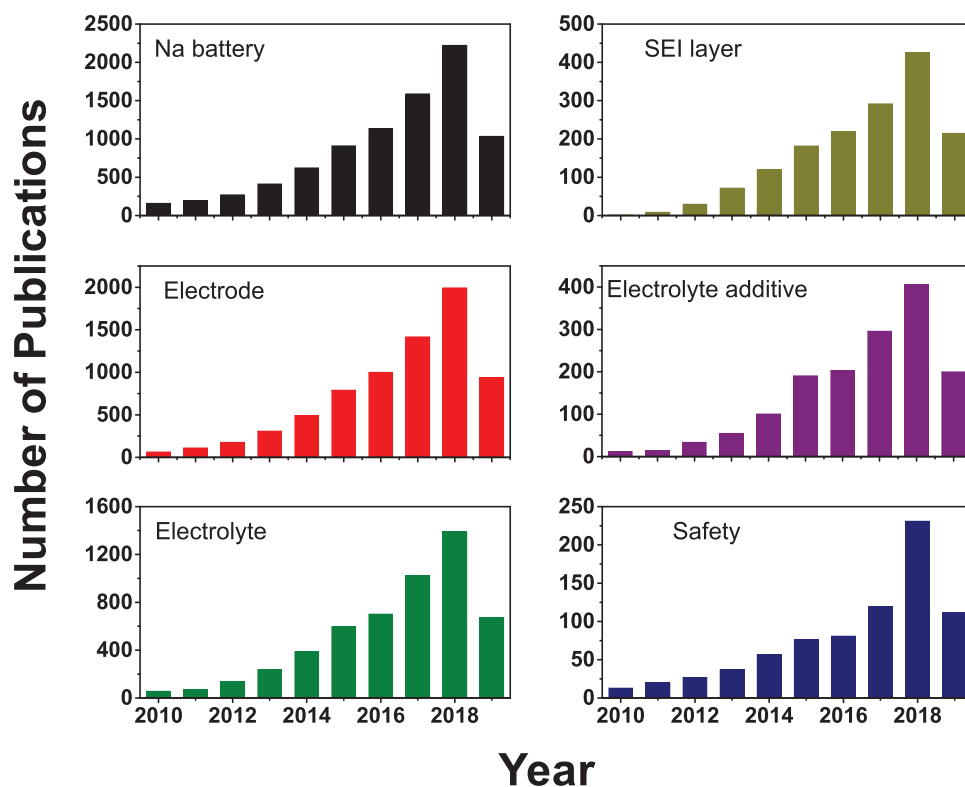


**Figure 1.** Number of publications dealing with Na-based rechargeable batteries, their electrolytes and interphases (last updated on 2nd September 2019). The key words used for the search in scopus were “sodium battery,” “sodium battery + electrode,” “sodium battery + electrolyte,” “sodium battery + solid electrolyte interphase,” “sodium battery + electrolyte additive,” and “sodium battery + safety.”

chemistries. So, to assess the viability and potential deployment of SIBs, a new paradigm of thinking, including the screening of electrolytes and optimization of each electrolyte’s constituent and their interphases, is necessary.

The purpose of this review is to consolidate and provide a comprehensive account of the progress, status, and prospects of various Na<sup>+</sup> ion conductive electrolytes (including solvents, salts, and additives), the interphases they form with SIB electrodes and potential hazards. We anticipate that this comprehensive review will spur new concepts, ideas and research directions, eventually enabling the deployment of rechargeable SIBs operating at RT.

For the sake of clarity, the review is divided into three broad sections dealing with electrolytes, interphases, and the safety of Na-based rechargeable batteries. These sections are further organized into different sub-headings. Also, the definition “half-cell” refers to cells employing Na metal as the anode while “sodium-ion” or “Na-ion” or “full-cell” refers to cells using two non-Na metal electrodes.

## 2. Electrolytes for Na-Based Rechargeable Batteries

The electrolyte electronically insulates the negative (anode) and positive (cathode) electrodes, acting, under ideal condition, as a medium for solely the ion charge transfer while the electrons pass through the external circuit. As it is placed between the highly reducing and oxidizing active materials (electrodes),

its stability or metastability is of supreme significance. That is to say that a given electrolyte must satisfy the needs of both electrodes. Upon interaction with the electrodes, it supplies the chemistry for the formation of interphases at both the electrodes, which govern the overall performance of the battery system.

Adopting from the properties of the optimized electrolytes for LIBs, the generic list of required characteristics for a SIB electrolyte includes:

- i) Chemical inertness: the electrolyte should stay inert toward all inactive and active battery components (e.g., separator, binder, current collectors, packaging materials, etc.) during operation;
- ii) Wider liquidus range and thermal stability: low melting and high boiling temperatures extend the operative range of the SIB cell;
- iii) Wide electrochemical stability window: the large separation of high and low onset potentials for decomposition by oxidation and reduction, respectively, enables a high cell voltage;
- iv) High ionic and no electronic conductivity: to enable facile Na<sup>+</sup> transport and minimize the cell self-discharge, respectively;
- v) Environmentally benign and nontoxic: to enable limited environmental hazards and thereby safer batteries;
- vi) Sustainable chemistry: based on abundant chemicals, and low impact and simple synthesis, preparation and scaling processes (e.g., energy, pollution, etc.);

- vii) Cost reduction: to enable low total cost, including materials, production, and others;
- viii) Tunable interphase property: formation of stable, electronically insulating but ionically highly conductive interphases layers on both electrodes.

In principle, the electrolyte component should be inert in the battery and act only as a medium for the ion transfer, but in practice, the inertness is only kinetically granted by the formation of the passive layer at the electrode/electrolyte interphases (EEI). The chemistry and morphology of these interfacial layers are fundamental parameters influencing the battery performance. In fact, besides the optimization of the electrolyte composition to improve the bulk properties (e.g., ionic mobility, stability, etc.), the composition of the electrolyte dictates the composition and quality of the interphase layer(s), and thereby severely impacts the cell performance. Although the research on electrolyte development for SIBs is still in its infancy,

various electrolyte systems, mostly derived from those of LIBs, have been investigated, and the relevant research results and progress are discussed below.

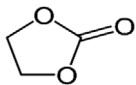
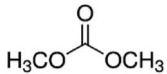
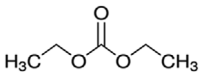
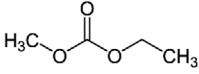
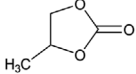
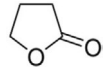
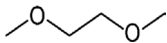
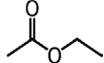
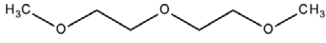
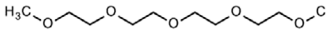
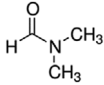
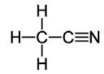
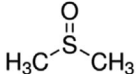
## 2.1. Nonaqueous Liquid Electrolytes

Following the historical development of electrolytes for LIBs, most of the nonaqueous electrolytes fall into the following families: organic esters and ethers (Table 2), ionic liquids, and concentrated electrolytes.

### 2.1.1. Carbonate Ester-Based Electrolytes

Analogous to LIBs, carbonate esters have been the primarily adopted solvents for SIBs, thanks to their higher electrochemical stability and ability to dissolve alkali metal ( $\text{Li}^+$ ,  $\text{Na}^+$ , etc.)

**Table 2.** Physicochemical and electrochemical properties of frequently utilized organic solvents/co-solvents in SIBs.

Solvent-co-solvent	Chemical structure	$T_m$ [°C]	$T_b$ [°C]	$T_f$ [°C]	$\eta$ (25 °C) [cP]	$\epsilon/25$ °C	D.M debye	AN/DN	$E_{\text{Lumo}}$ [eV]
EC		36.4	248	160	1.9 (40 °C)	89.78	4.61	-/16.4	1.175
DMC		4.6	91	18	0.59 (20 °C)	3.1	0.76	-/17.2	1.054
DEC		-74.3	126	31	0.75	2.8	0.96	-/16	1.288
EMC		-53	110		0.65	2.96	0.89	-	1.248
PC		48.8	242	132	2.53	64.92	4.81	18.3/15.1	1.235
BC		-53	240	97	3.2	53	4.23	-	1.049
GBL		-43.5	204		1.73	39			
DME		-58	84	0	0.46	7.2	1.15	10.2/18.6	-
EA		-84	102	-3	0.45	6	-	-	-
DEGDME		-64	162	57	1.06	7.18	-	9.9/19.2	-
TEGDME		-46	216	111	3.39	7.53	-	10.5/16.6	-
DMF		-60.4	153	67	0.8	37	-	-/26.6	-
ACN		-44	81.6	2	0.35	38	-	-/14.1	-
DMSO		18.4	189	95	1.99	46.7	-	19.3/29.8	-

**Table 3.** Physicochemical and electrochemical properties of salts for SIBs.

Salt	Anion-chemical-structure	$T_m$ [°C] Na(Li)	Al-corrosion	$\sigma$ in 1 M solution [mS cm <sup>-1</sup> ] (solvent)	Anodic stability/V vs. Na/Na <sup>+</sup>	Refs.
NaClO <sub>4</sub>		468 (236)	No	6.4 (PC) 8 (EC:PC) 5 (EC:DMC)	4.7	[3,369]
NaPF <sub>6</sub>		dec 300 (dec)	No	7.98 (PC) 6.8 (EC:DMC)	5	[3,339]
NaBF <sub>4</sub>		384 (293)	No	–	5	[3,369]
NaTFSI		257 (234)	High	6.2 (PC)	Limited to 3.4 V by Al dissolution, but up to 5 V with 5% NaPF <sub>6</sub>	[3]
NaFSI		118 (130)	High	–	Limited to 3.4 V by Al dissolution, but up to 5 V with 5% NaPF <sub>6</sub>	[3]
NaFTFSI		160 (94.5)	High	–	Limited to 3.4 V by Al dissolution	[3]
NaOTf		248 (≥300)	High	3.7 (EC:DMC)	–	[3]
NaBOB		345(302)	No	0.07–0.26 (PC)	–	[370]
NaDFOB		–	No	4.27/PC 5.32/EC:DEC 7.74/EC:DMC 5.36 (EC:PC)	5.51 5.76 – 5.79	[371]

salts. The most widely used are the cyclic propylene carbonate (PC) and ethylene carbonate (EC), and the linear ethyl methyl carbonate (EMC), dimethyl carbonate (DMC), and diethyl carbonate (DEC). Most sodium ion electrolytes employ one or more Na-salts dissolved (Table 3) in mixtures of two or more solvents, while single solvent formulations are very rare, except a few using PC.<sup>[5]</sup> The impetus behind the use of multiple solvents (and sometimes salts) originates from the various and often contradicting requirements of battery electrolytes, which can hardly be met by a single compound/molecule. The recent review of Bommier and Ji,<sup>[6]</sup> reporting a statistical analysis of electrolyte compositions, revealed that the EC:DEC is the most used followed by the EC:PC and PC based systems and afterward by the EC:DMC mixture. Regarding the salt, NaClO<sub>4</sub> is the most used, followed by NaPF<sub>6</sub>; NaCF<sub>3</sub>SO<sub>3</sub>; NaTFSI and the other salts are less reported.

*Interaction of the Na<sup>+</sup> Ions with Carbonate Ester Solvents:* The interaction of the Na<sup>+</sup> ions with carbonate ester solvents has been extensively investigated. Jónsson and Johansson<sup>[7]</sup>

evaluated the cation–anion interaction using DFT methods to evaluate the ion-pair dissociation reaction for sodium and lithium salts, evidencing that the sodium salts are characterized by a lower ion-pair dissociation energy (≈15–20% lower than lithium salts). The results were later confirmed by Okoshi et al.<sup>[8]</sup> also proving, using DFT calculations, that the desolvation energy of Na ions is commonly smaller than that of Li ions in similar electrolytes, due to the weaker Lewis acidity of Na<sup>+</sup>. Cresce et al.<sup>[9]</sup> measured the weaker Na<sup>+</sup> interaction with solvents using electrospray mass spectrometry, infrared and Raman spectroscopy, <sup>17</sup>O, <sup>23</sup>Na pulse field gradient double-stimulated-echo pulse sequence nuclear magnetic resonance (NMR), and conductivity measurements. These results have been confirmed by Pham et al.<sup>[10]</sup> using first-principles molecular dynamics simulations. Kamath et al.<sup>[11]</sup> employed an in silico strategy based on both thermodynamic and kinetic descriptors derived from molecular dynamics simulations to rationally derive optimal electrolytes for Na-ion batteries. Thermodynamic considerations based on free energy evaluation

**Table 4.** Summary of the Na-batteries employing carbonate-based electrolyte.

Electrolyte formulation	Ionic conductivity @ RT [mS cm <sup>-1</sup> ]	Electrodes	Electrode capacity [mAh g <sup>-1</sup> ]	Life cycles	Capacity retention [%]	Notes	Refs.
1 M NaPF <sub>6</sub> in EC:PC	6.2	Na/hard carbon	200	180	≥99%	Major influence of solvent than the salt on the electrochemical performance	[14]
1 M NaPF <sub>6</sub> in EC <sub>0.45</sub> :PC <sub>0.45</sub> :DMC <sub>0.1</sub>	10.0	Na/hard carbon	320	100	≥99%	DMC as co-solvent to decrease viscosity and improve ionic conductivity	[15]
		Na/ Na <sub>3</sub> V <sub>2</sub> (PO <sub>4</sub> ) <sub>2</sub> F <sub>3</sub>	120	80	≥99%		
		Hard carbon/Na <sub>3</sub> V <sub>2</sub> (PO <sub>4</sub> ) <sub>2</sub> F <sub>3</sub>	97 (with respect to the cathode mass)	120	90%		
1 M NaClO <sub>4</sub> EC:PC (1/1, vol)	6.0	Na/Na <sub>4</sub> Fe <sub>3</sub> (PO <sub>4</sub> ) <sub>2</sub> (P <sub>2</sub> O <sub>7</sub> )	110	100	90%	Superior performance of EC:PC with respect to EC:DEC	[17]
0.6 M NaPF <sub>6</sub> in EC:DMC (3:7 wt)	6.8	Na/Na <sub>0.7</sub> CoO <sub>2</sub>	80	Only 1 cycle reported		The electrolyte favors electrode kinetics due to the formation of an electrochemically stable SEI layer	[19]
1 M NaClO <sub>4</sub> /EC:PC (1:1 vol) and 1 M NaClO <sub>4</sub> /PC	–	Na/NaTi <sub>2</sub> (PO <sub>4</sub> ) <sub>3</sub>	–	–	–	Nonreliability of the Na electrode, resulting in the continuous increase of the SEI layer	[20]
NaPF <sub>6</sub> and NaTFSI in PC and EC:DEC (1:2 vol) electrolytes	–	Na/NaCrO <sub>2</sub> and symmetrical NaCrO <sub>2</sub> cell	90	50	90%	Sodium metal counter electrode instability. Use of symmetrical cell to improve reliability of tests.	[22]
1 M LiPF <sub>6</sub> in EC: PC: FEC (49:49:2)	–	Na/Na <sub>0.75</sub> Fe <sub>2.08</sub> (CN) <sub>6</sub> ·3.4H <sub>2</sub> O	130	40	87%	Influence of the binder has been investigated. PVDF has been selected as the best choice for the Na/Na <sub>0.75</sub> Fe <sub>2.08</sub> (CN) <sub>6</sub> ·3.4H <sub>2</sub> O cell	[40]
0.5 M NaPF <sub>6</sub> EC:EMC	–	Na/graphite (anion intercalation)	86.2	140	≥99%		[369]
1.5 M NaPF <sub>6</sub> in EC	–	HC/Na <sub>3</sub> V <sub>2</sub> (PO <sub>4</sub> ) <sub>2</sub> F <sub>3</sub>	100	500	≥80%		[24]
1 M NaClO <sub>4</sub> in EMS + 2 vol% FEC	6.2	Na/Fe <sub>3</sub> O <sub>4</sub>	200	50	≥99%		[41]
		Na/Na[Ni <sub>0.25</sub> Fe <sub>0.5</sub> Mn <sub>0.25</sub> ]O <sub>2</sub>	125	50	90%		
		Fe <sub>3</sub> O <sub>4</sub> /Na[Ni <sub>0.25</sub> Fe <sub>0.5</sub> Mn <sub>0.25</sub> ]O <sub>2</sub>	130 (referred to the mass of the cathode)	150	80%		
0.8 M NaPF <sub>6</sub> in TMP + 10 vol% FEC	5.5	Na/Sb	500	80	95%		[42]
		Na/NaNi <sub>0.35</sub> Mn <sub>0.35</sub> Fe <sub>0.3</sub> O <sub>2</sub>	120	50	95%		
		Sb/NaNi <sub>0.35</sub> Mn <sub>0.35</sub> Fe <sub>0.3</sub> O <sub>2</sub>	450 (referred to the mass of the anode)	50	75%		

indicated EC:PC as the preferred electrolyte formulation under equilibrium conditions, while kinetic descriptors indicated EC:DMC and EC:EMC to be the best formulations. Experimental tests in sodium cells employing TiO<sub>2</sub> nanotubes as the working electrode demonstrated the best rate capability with the EC:EMC solvent mixture, while the EC:DMC formulation resulted in higher delivered capacity at low current rate. The same research group<sup>[12]</sup> further investigated the trends in solvation behavior of various carbonate solvents and mixtures showing that the formation of Na carbonate complexes is exothermic and proceeds favorably. The values for the interaction of Na<sup>+</sup> ion with carbonate solvents indicate that pure EC and binary mixture of (EC:PC) are the best electrolytes for sodium based batteries. The use of the EC has been criticized by Kumar et al.<sup>[13]</sup> indicating, by quantum chemistry simulations,

that the high reduction potential and low barrier for the ring-opening of EC are the main causes for the continuous growth of SEI observed in SIBs.

*Electrolyte Composition Dependence of Electrochemical Stability against Different Electrode Chemistries:* Besides to the investigations on the interaction of Na<sup>+</sup> ions with organic solvents, it is of fundamental importance to evaluate the electrolyte stability against electrodes active material (Table 4). Ponrouch et al.<sup>[14]</sup> reported a detailed investigation of electrolyte formulations with different sodium salts (NaClO<sub>4</sub>, NaPF<sub>6</sub>, and NaTFSI) and solvents (PC, EC, DMC, DME, DEC, THF, and triglyme) or solvent mixtures (EC:DMC, EC:DME, EC:PC and EC:triglyme), including viscosity, ionic conductivity, and electrochemical and thermal stabilities. The reported results evidence relatively similar conductivities for NaPF<sub>6</sub> (798 × 10<sup>-3</sup> S cm<sup>-1</sup>),

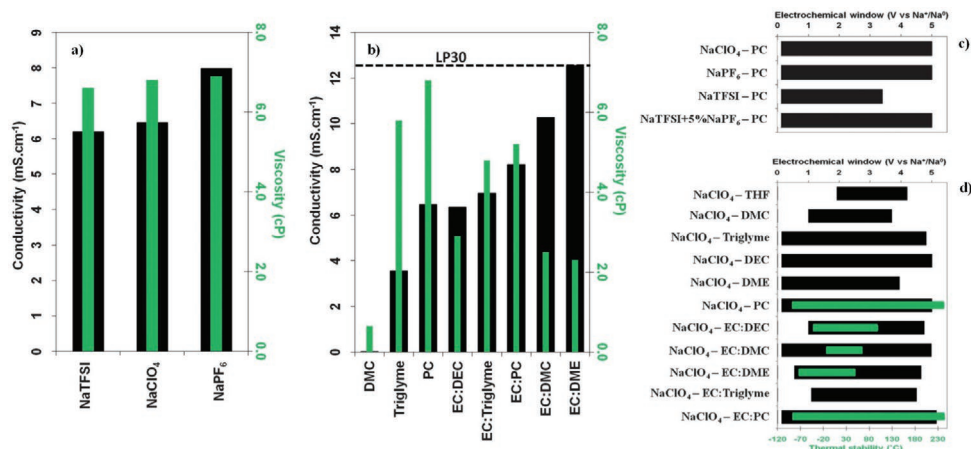


**Figure 2.** Conductivity (black bars and left hand side Y axis) and viscosity (green bars and right hand side Y axis) of a) PC-based electrolytes with 1 M of various Na salts, b) electrolytes based on 1 M NaClO<sub>4</sub> dissolved in various solvents and solvent mixtures. c,d) Electrochemical potential window stability (black bars and upper y axis) and thermal range (green bars and lower y axis) values of c) PC based electrolytes with 1 M of various Na salts and d) electrolytes based on 1 M NaClO<sub>4</sub> dissolved in various solvents and solvent mixtures. Reproduced with permission.<sup>[2]</sup> Copyright 2015, RSC Publishing group.

NaClO<sub>4</sub> ( $6.35 \times 10^{-3} \text{ S cm}^{-1}$ ) and NaTFSI ( $6.2 \times 10^{-3} \text{ S cm}^{-1}$ ), indicating that the anion does not remarkably influence the conductivity value (Figure 2a). In contrast, larger variations are found changing the solvent/s. Considering, e.g., 1 M solutions of NaClO<sub>4</sub>, the conductivity follows the trend EC:DME > EC:DMC > EC:PC > EC:triglyme > EC:DEC > PC > triglyme, DME, DMC, DEC (Figure 2b), indicating that the proper selection of the solvent/s can enhance the electrolyte conductivity by increasing the dissociation of the salt (high dielectric constant) and/or lowering the viscosity of the solution, thus improving the ionic mobility. The investigation of the electrochemical stability window indicates that the anion choice does not influence the stability except for the TFSI anion, which does not protect the anodic aluminum dissolution (Figure 2c). On the contrary, the selection of the solvent/s have a major influence for the electrochemical stability window, as revealed by the highest stabilities being obtained with PC, DEC, and their mixture and the EC:DME mixture (Figure 2d). However, the thermodynamic stability is not the final indication as the electrode materials may induce catalytic electrolyte decomposition reactions. Rather than by thermodynamics, the electrolyte inertness with the electrodes, especially the negative one, is usually ruled by kinetic limitations and the formation of passivation layers (SEI). To evaluate the suitability of the investigated electrolytes for SIB application, their behavior was investigated in sodium cells using hard carbon electrodes. The investigation identified the NaPF<sub>6</sub> in EC:PC composition as the best choice. The same research group<sup>[15]</sup> explored the effect of DME, DMC, and DEC as additional cosolvents to NaPF<sub>6</sub> in EC:PC, confirming that the addition of a third co-solvent decreases the viscosity thus enhancing the ionic conductivity following the trend: DME > DMC > DEC. These electrolytes were tested in sodium cells employing hard carbon electrode, showing large polarization and insufficient capacity retention when DME was used, while EC:PC:DMC (4.5:4.5:1, mol) was found to be the optimum composition resulting in good rate capability and high capacity upon cycling. This latter electrolyte was found to be compatible with Na<sub>3</sub>V<sub>2</sub>(PO<sub>4</sub>)<sub>2</sub>F<sub>3</sub> (NVPF) cathode material, allowing the assembly

of a full Na-ion cells displaying the operative voltage of 3.65 V, very low polarization, excellent capacity retention upon cycling, i.e., 97 mAh g<sup>-1</sup> (of NVPF) after more than 120 cycles, satisfactory coulombic efficiency (>98.5%) and very good power performance. In a following work,<sup>[16]</sup> the 1 M NaPF<sub>6</sub> in EC:PC:DMC (4.5:4.5:1, mol) electrolyte was investigated in a wide temperature range, i.e., from -15 °C up to 75 °C, employing carbon-coated hard carbon characterized by a reduced surface area with respect to conventional hard carbon. The use of the carbon-coated electrode material led to significant improvements, especially in terms of the first cycle coulombic efficiency, but also showing good electrochemical stability in the investigated temperature range.

Jang et al.<sup>[17]</sup> evaluated the electrochemical performance of 1 M NaClO<sub>4</sub> in EC:DEC (1:1, vol) and EC:PC (1:1, vol) in sodium cells employing a Na<sub>4</sub>Fe<sub>3</sub>(PO<sub>4</sub>)<sub>2</sub>(P<sub>2</sub>O<sub>7</sub>) cathode as working electrode. Using <sup>13</sup>CNMR spectroscopy, the authors evidenced that the electrolytes containing DEC were unstable in contact with Na metal. Lee et al.<sup>[18]</sup> tested Na<sub>2</sub>Zn<sub>3</sub>[Fe(CN)<sub>6</sub>]<sub>2</sub>·xH<sub>2</sub>O as cathode material in sodium cells, evincing an improved capacity retention for 1 M NaPF<sub>6</sub>/EC:DMC (1:1, vol) with respect to 1 M NaClO<sub>4</sub>/PC and 1M NaClO<sub>4</sub>/EC:DMC (1:1). Bhide et al.<sup>[19]</sup> investigated the effect of salt concentration in nonaqueous electrolytes based on NaPF<sub>6</sub>, NaClO<sub>4</sub>, and NaCF<sub>3</sub>SO<sub>3</sub> salts in EC:DMC (30/70 w/w), the best conductivities were achieved by 0.6 M NaPF<sub>6</sub>, 1 M NaClO<sub>4</sub> and 0.8 M NaCF<sub>3</sub>SO<sub>3</sub>. The various electrolytes were also studied in sodium cells employing a Na<sub>0.7</sub>CoO<sub>2</sub> cathode material, proving that the NaPF<sub>6</sub>-based electrolytes improved electrode kinetics due to the formation of an electrochemically stable SEI layer.

*Effect of Electrolyte Composition on Electrode Performance—Reliability of Na Metal Counter Electrode:* Rudola and co-workers<sup>[20]</sup> evaluated the effect of the electrolyte solvent on NaTi<sub>2</sub>(PO<sub>4</sub>)<sub>3</sub> (NTP) cathode material, comparing its electrochemical behavior in 1 M NaClO<sub>4</sub>/EC:PC (1:1 vol) and 1 M NaClO<sub>4</sub>/PC. The results showed a difference in the voltage profile, which was attributed to increased polarization of the sodium metal anode for the latter electrolyte resulting from the different SEI formed

on the Na metal surface in presence of only PC or EC:PC mixtures. As suggested by the authors, special care should be taken in the evaluation of electrode materials for sodium-ion batteries in half cells because of the pronounced effects related to the sodium metal electrode; similar issue has been also recently reported by Komaba and co-workers for potassium metal.<sup>[21]</sup> Hatchard et al.<sup>[22]</sup> studied the NaCrO<sub>2</sub> cathode material using NaPF<sub>6</sub> and NaTFSI in PC and EC:DEC (1/2 vol) electrolytes in sodium half-cells and symmetric cells, confirming that half-cell tests were not useful for evaluating the cycling performance due to a high impedance increase at the Na metal electrode. Using symmetric cells, the authors achieved a columbic efficiency of 99.97% for the cell employing 1 M NaTFSI in EC:DEC electrolyte, suggesting this as a more reliable method for the characterization of a given cathode material, i.e., excluding the influence of the counter Na metal electrode. The reliability of the Na metal counter electrode has been investigated in detail by Conder and Villeveille<sup>[23]</sup> evaluating the EIS response of symmetric Na/Na cells. The report evidenced the importance of the thickness of the Na metal and its uniformity, as well as the absence of surface pollutants. The reliability of the Na metal counter electrode was improved by simply scratching the surface impurity (mainly sodium oxide) and by calendering the Na metal, thus obtaining a uniform thickness on a renewed surface.

A recent paper from Tarascon's group<sup>[24]</sup> explored the effect of various NaPF<sub>6</sub>-based electrolytes containing either single linear carbonates DMC, EMC, DEC, or single cyclic carbonates PC, EC, on the stability of the SEI formed in full Na<sub>3</sub>V<sub>2</sub>(PO<sub>4</sub>)<sub>2</sub>F<sub>3</sub> (NVPF) or Na<sub>3</sub>V<sub>2</sub>(PO<sub>4</sub>)<sub>3</sub> (NVP)/HC cells via complementary in-situ UV-Vis spectroscopy and in situ cyclic voltammetry (CV) measurements together with galvanostatic charge-discharge tests. In this case, only full cell systems were investigated to

avoid any influence of the sodium metal counter electrode. Furthermore, a high electrode loading was used being, hard carbon (HC, 6.0 mg cm<sup>-2</sup>), Na<sub>3</sub>V<sub>2</sub>(PO<sub>4</sub>)<sub>3</sub> (NVP, 13.5 and 16.0 mg cm<sup>-2</sup>), and Na<sub>3</sub>V<sub>2</sub>(PO<sub>4</sub>)<sub>2</sub>F<sub>3</sub> (NVPF, 12.0 mg cm<sup>-2</sup>). The investigation demonstrated that linear carbonates are not stable under low potential, forming highly soluble decomposition products, evidencing their inability to build an efficient SEI layer. On the contrary, cyclic carbonates can achieve an outstanding cycle capability under similar conditions (**Figure 3**).

*Effect of Additive in Carbonate-Based Electrolyte:* Another strategy to improve the bulk properties of electrolytes and the accompanying electrochemical performance lies in the incorporation of functional additives in the electrolyte. In fact, additives can serve as sacrificial components for the formation of highly regulated interphases in the initial activation cycles of the battery. However, the additives properties in SIBs are quite different in comparison to LIBs due to the difference in the two chemistries. Komaba et al.<sup>[25]</sup> screened various additives, i.e., FEC, DFEC, VC, and ES, finding that only FEC boosted the electrochemical performance of hard carbon or NaNi<sub>1/2</sub>Mn<sub>1/2</sub>O<sub>2</sub> half-cells. However, the improved cycling performance of both materials was assigned to the influence of FEC on the reversibility of the Na metal anode and not to a beneficial effect on the investigated electrodes. As it can be seen in **Figure 4**, FEC clearly enhances the electroplating rate and reversibility of the Na metal anode.

Darwiche et al.<sup>[26]</sup> investigated the effect of FEC as an electrolyte additive in half-cells employing Sb as alloying anode material. An outstanding capacity retention of 100% was reported for the cell with FEC, while only 2% of the initial capacity was retained in the FEC-free electrolyte after 100 cycles. The same behavior was reported by several other

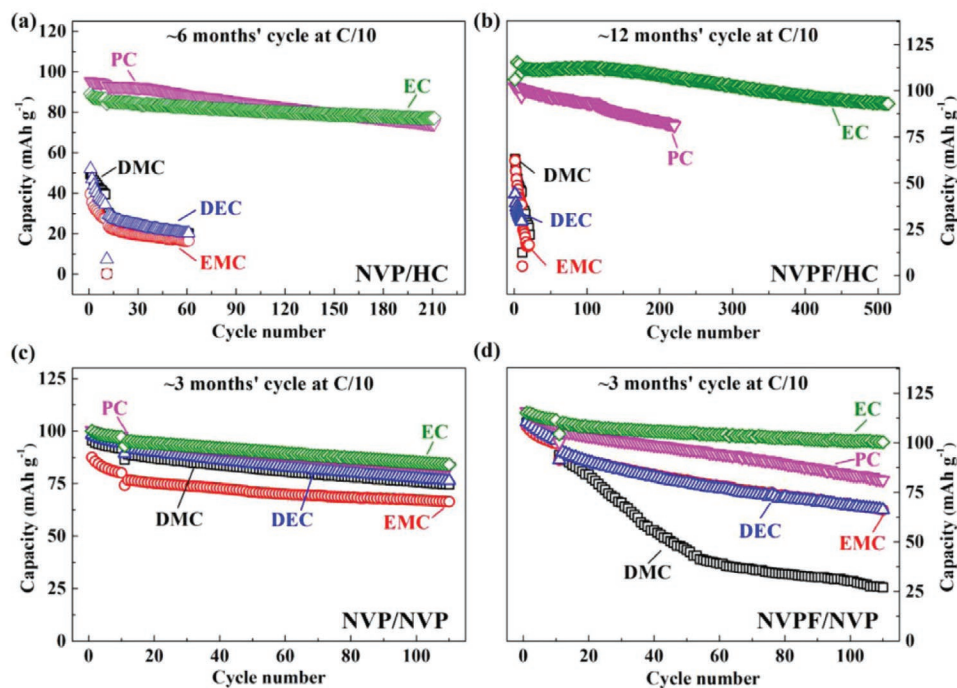


**Figure 3.** The cycling performance of a) DMC, EMC, DEC, PC, and EC electrolyte in NVP/HC, b) NVPF/HC, c) NVP/NVP and d) NVPF/NVP full cells at C/10 under room temperature. Reproduced with permission.<sup>[24]</sup> Copyright 2018, Electrochemical Society.

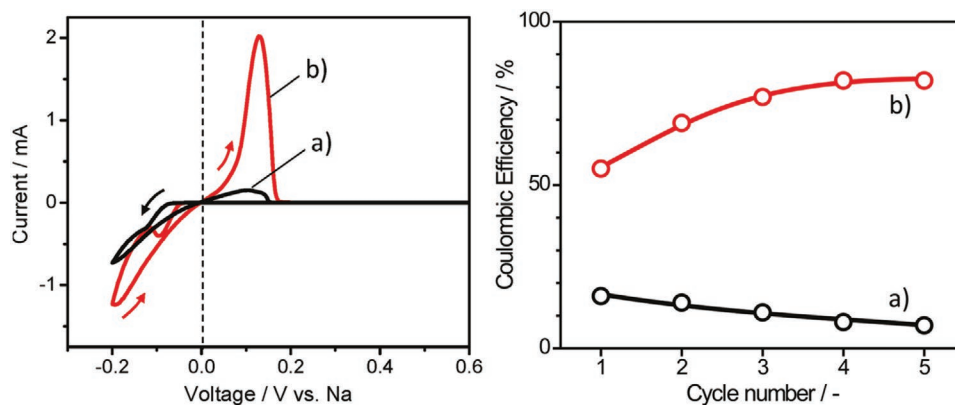


**Figure 4.** (Left) cyclic voltammograms on Al foil electrodes at a rate of  $3 \text{ mV min}^{-1}$  and (right) Coulombic efficiency during the voltammetry tested in a) FEC free and b) 2 vol% FEC added 1 M  $\text{NaClO}_4/\text{PC}$  solutions in coin-type Na cells. Reproduced with permission.<sup>[25]</sup> Copyright 2011, American Chemical Society.

research groups,<sup>[27–30]</sup> emphasizing the importance of the use of this additive to stabilize the alloy-based anode material. Such a striking improvement was associated with the formation of a very thin and stable protective film on the Sn- or Sb-based electrodes, resulting from the FEC ring opening polymerization upon reduction.<sup>[26,31,32]</sup> This protective film prevented the further decomposition of the electrolyte. The formed SEI lowered the electrode/electrolyte interphase resistance facilitating the transport of Na ions and thus improving the capacity retention and rate performance.<sup>[30]</sup> Hasa et al.<sup>[33]</sup> evidenced the beneficial effect of FEC as additive in half- and full-cells employing  $\text{P2-Na}_{0.6}\text{Ni}_{0.22}\text{Fe}_{0.11}\text{Mn}_{0.66}\text{O}_2$  layered oxide cathode and nanostructured Sb–C alloying anode. The full cell showed a working voltage of about 2.7 V and delivered a reversible capacity of about  $120 \text{ mAh g}^{-1}$  (with respect to active cathode material). Darwiche et al.<sup>[34]</sup> investigated the influence of the electrolyte formulations on the performance of the Sb alloy anode making use of  $\text{NaClO}_4$  and  $\text{NaPF}_6$  salts in PC or EC:DMC as solvents, including 5 wt% FEC as additive. The results showed a higher first cycle irreversible capacity for PC relative to EC:DMC. On the other hand,  $\text{NaClO}_4/\text{PC}$  showed excellent capacity retention, ascribed to the formation of a homogeneous, electrochemically stable and mechanically robust SEI due to the presence of FEC. Dall'Asta et al.<sup>[35]</sup> evaluated various nonaqueous electrolytes in sodium cells employing  $\text{Na}_{0.44}\text{MnO}_2$  (NMO) as cathode material showing the poor performance of PC-based electrolyte, which was later found to be greatly improved by the addition of FEC. The authors also reported a weighty influence of the salt, in contrast with previous reports,<sup>[14]</sup> on the electrochemical performance, indicating 1 M  $\text{NaPF}_6/\text{EC}:\text{DEC}$  (3:7, v:v) with 2 wt% FEC as the electrolyte of choice for the tested cell. In contrast to the above reports showing favorable effects of FEC, Ponrouch<sup>[36]</sup> inspected the electrochemical behavior of hard carbon prepared from sugar pyrolysis, proving its better performance when using the additive-free 1 M  $\text{NaClO}_4/\text{EC}:\text{PC}$  based electrolyte with respect to the one containing FEC (2%) as additive. Similarly, Wu et al.<sup>[37]</sup> showed that FEC did not improve the performance of half-cells employing the anatase  $\text{TiO}_2$  (nanoparticles) electrode. The effect of FEC as electrolyte additive in half-cells employing HC electrodes made using either PVDF or CMC binders was further evaluated by

Komaba's group.<sup>[38]</sup> The results indicated that FEC affects positively the performance of the HC electrodes using PVDF and negatively those based on CMC binder. Dugas et al.<sup>[39]</sup> evaluated the use of FEC as additive in 1 M  $\text{NaPF}_6/\text{EC}:\text{DMC}$  electrolyte, showing a reduction of the irreversible capacity of Na-half cells when NVPF is used as the positive electrode. However, a continuous release of small quantities of gases was reported, which in the long term could be detrimental to cell performance. Piernas-Muñoz et al.<sup>[40]</sup> explored several electrolytes containing  $\text{NaClO}_4$  or  $\text{NaPF}_6$  as salts and EC:PC, EC:DMC, EC:DEC solvent mixtures, with and without a small amount of FEC as additive (2%) in cells employing sodium Prussian blue,  $\text{Na}_{0.75}\text{Fe}_{2.08}(\text{CN})_6 \cdot 3.4\text{H}_2\text{O}$  as cathode material. The results showed that the use of  $\text{NaPF}_6$  salt in EC:PC solvent mixture is the best choice in terms of delivered capacity, coulombic efficiency, capacity retention, and rate capability, in agreement with previous work.<sup>[14]</sup> The addition of FEC to the electrolyte stabilizes the interfacial resistance at lower values, improving the coulombic efficiency of the cell. On the contrary, the effect on the delivered capacity and stability is limited. It appears from the literature results summarized above that there is inconsistent and contrasting behavior when FEC additive is used in SIBs. A more detailed overview of the use of additives in SIBs will be reported in Section 3.

**Alternative Solvents:** Besides the use of conventional carbonates, other organic solvents have been proposed for the further realization of SIBs. Oh et al.<sup>[41]</sup> reported the use of ethyl methanesulfonate (EMS) as electrolyte solvent. The comparison between 1M  $\text{NaClO}_4/\text{PC} + 2 \text{ vol}\% \text{ FEC}$  and 1 M  $\text{NaClO}_4/\text{EMS} + 2 \text{ vol}\% \text{ FEC}$  evidenced the slightly higher ionic conductivity and very large improvement (ca. by over 1 V) in the electrochemical window stability of the latter electrolyte (4.5 V vs  $\text{Na}/\text{Na}^+$  with PC, 5.6 V vs  $\text{Na}/\text{Na}^+$  with EMS). The electrolyte was successfully tested in SIBs using  $\text{Fe}_3\text{O}_4$  as conversion anode material and layered  $\text{Na}[\text{Ni}_{0.25}\text{Fe}_{0.5}\text{Mn}_{0.25}]\text{O}_2$  as cathode material. The full cell delivered a capacity of  $130 \text{ mAh g}^{-1}$  with respect to the cathode weight at  $13 \text{ mA g}^{-1}$  with a working voltage of 2 V. Zeng et al.<sup>[42]</sup> proposed the use of a non-flammable phosphate ester (trimethyl phosphate, TMP) as electrolyte solvent. The 0.8 M  $\text{NaPF}_6/\text{TMP}$  electrolyte, including FEC (10 vol%), showed comparable conductivity with 1 M  $\text{NaPF}_6/\text{EC}:\text{DEC}$  (1:1 vol) selected

as the benchmark, yielding good stability against sodium metal and most importantly, no flammability issues. The electrolyte was successfully employed in SIB cells using Sb alloy anode and  $\text{NaNi}_{0.35}\text{Mn}_{0.35}\text{Fe}_{0.3}\text{O}_2$  cathode, which showed good capacity retention for 50 cycles. Yu et al.<sup>[43]</sup> investigated the use of trimethyl phosphate (TMP) and 1,1,2,2-tetrafluoroethyl-2,2,3,3-tetrafluoropropyl ether (F-EPE) as nonflammable solvents and fluoroethylene carbonate (FEC) as additive with different concentration of Na salts. The electrolyte, tested in full cells employing  $\text{NaNi}_{1/3}\text{Fe}_{1/3}\text{Mn}_{1/3}\text{O}_2$  (NFM) cathode and hard carbon (HC) anode, showed superior performance (70.8% retention after 500 cycles) with respect to the standard EC-DEC-FEC electrolyte used as the benchmark.

### 2.1.2. Ether-Based Electrolytes

Glyme-based electrolytes have received attention in the field of SIBs because of their ability to enable the  $\text{Na}^+$ -solvent cointercalation in graphite electrodes and build stable SEI (Table 5).<sup>[44]</sup>

*Ether-Based Electrolyte Enabling Na-Solvent Cointercalation:* Graphite, the most widely used anode material for LIBs, cannot be used for SIBs due to the inability of  $\text{Na}^+$  ion to intercalate in graphite.<sup>[44,45]</sup> Nobuhara et al.<sup>[46]</sup> evaluated, by using first-principle calculations, the formation energies of graphite intercalation compounds (GICs) with Li, Na, and K, revealing that while the Li and K intercalated GICs are energetically stable, Na GICs are not, even for rather limited intercalation levels. However, Jache and Adelhelm<sup>[47]</sup> demonstrated the possibility to cointercalate  $[\text{Na}^+\text{-diglyme}]$  complex ions into graphite using a diglyme-based electrolyte. Figure 5a compares the voltage profiles of Li/graphite and Na/graphite cells in conventional carbonate-based electrolyte, revealing the electrochemical

inactivity of the graphite electrode towards sodium. On the contrary, Figure 5b shows that the graphite half-cell employing 1 M  $\text{NaCF}_3\text{SO}_3$ /diglyme electrolyte delivers a capacity approaching 100  $\text{mAh g}^{-1}$  with good coulombic efficiency, exceeding 99%, and an extremely good cycle life (Figure 5c).

Kang's group<sup>[48]</sup> evaluated the electrochemical behavior of graphite electrodes using various glymes, i.e., TEGDME, DEGDM, and DME, as solvents and  $\text{NaPF}_6$ ,  $\text{NaClO}_4$ , and  $\text{NaCF}_3\text{SO}_3$  salts. The results clearly highlighted that, while the salt has negligible influence, the solvent plays a key role on both intercalation potential and rate capability. An increase of the glyme molecular weight was found to increase the intercalation potential but decreasing the rate capability. The  $\text{NaPF}_6$  in DEGDM electrolyte was selected for the realization of a full cell in combination with  $\text{Na}_{1.5}\text{VPO}_{4.8}\text{F}_{0.7}$  cathode, characterized by a working voltage of 3 V, capacity of 45  $\text{mAh g}^{-1}$  (with respect to the mass of both the electrodes), good rate capability and promising capacity retention (80% after 250 cycles).<sup>[48]</sup> The correlation between the glyme molecular weight with the intercalation potential and the rate capability was later confirmed by Jache and co-workers.<sup>[49]</sup> Kang's group<sup>[50]</sup> investigated the solvated  $\text{Na}^+$  intercalation mechanism using operando X-ray diffraction analysis, electrochemical titration, real-time optical observation, and density functional theory (DFT) calculations. The reported results revealed that Na intercalation occurs through multiple staging reactions, finally forming a stage-1 graphite intercalated compound, identifying the  $[\text{Na-ether}]^+$  as intercalated species in the form of complexes double stacked in parallel with graphene layers in the graphite galleries. The same group<sup>[51]</sup> also examined the influence of  $[\text{Na-solvent}]^+$  intercalation into graphite by DFT calculations, and indicated that a solvation energy  $>1.75$  eV is required to achieve the co-intercalation process (Figure 5d). A second condition required

**Table 5.** Summary of the Na-batteries employing glyme based electrolyte.

Electrolyte formulation	Cell chemistry	Electrode capacity [ $\text{mAh g}^{-1}$ ]	Cycle life/cycles	Capacity retention [%]	Details	Refs.
1 M $\text{NaCF}_3\text{SO}_3$ in diglyme	Na/graphite $\text{Na}^+$ cointercalation with the solvent	100	1000	$\geq 99\%$	$\text{Na}^+$ ion cannot be intercalated in the graphite, the glyme solvent coordinated to the $\text{Na}^+$ ion enable the intercalation process	[47]
$\text{NaPF}_6$ in DEGDM	Na/graphite $\text{Na}^+$ cointercalation with the solvent	150	300	$\geq 99\%$	An increase of the glyme molecular weight was found to increase the intercalation potential and decrease the rate capability.	[48]
	Na/ $\text{Na}_{1.5}\text{VPO}_{4.8}\text{F}_{0.7}$	120	20	$\geq 99\%$		
1 M $\text{NaCF}_3\text{SO}_3$ /diglyme	Graphite/ $\text{Na}_{1.5}\text{VPO}_{4.8}\text{F}_{0.7}$	100 (in respect to the cathode mass)	250	80%		
	Na/graphite $\text{Na}^+$ cointercalation with the solvent	110	6000	$\geq 99\%$		[55]
1 M $\text{NaClO}_4$ in TEGDME	Graphite/ $\text{Na}_3\text{V}_2(\text{PO}_4)_3\text{@C}$	90 (in respect to the cathode weight)	400	80%		
	Na/graphite $\text{Na}^+$ cointercalation with the solvent	100	500	$\geq 99\%$		[57]
	Na/ $\text{Na}_{0.7}\text{CoO}_2$	90	100	$\geq 99\%$		
	Graphite/ $\text{Na}_{0.7}\text{CoO}_2$	80 $\text{mAh g}^{-1}$ (in respect to the cathode weight)	1250	$\geq 99\%$		

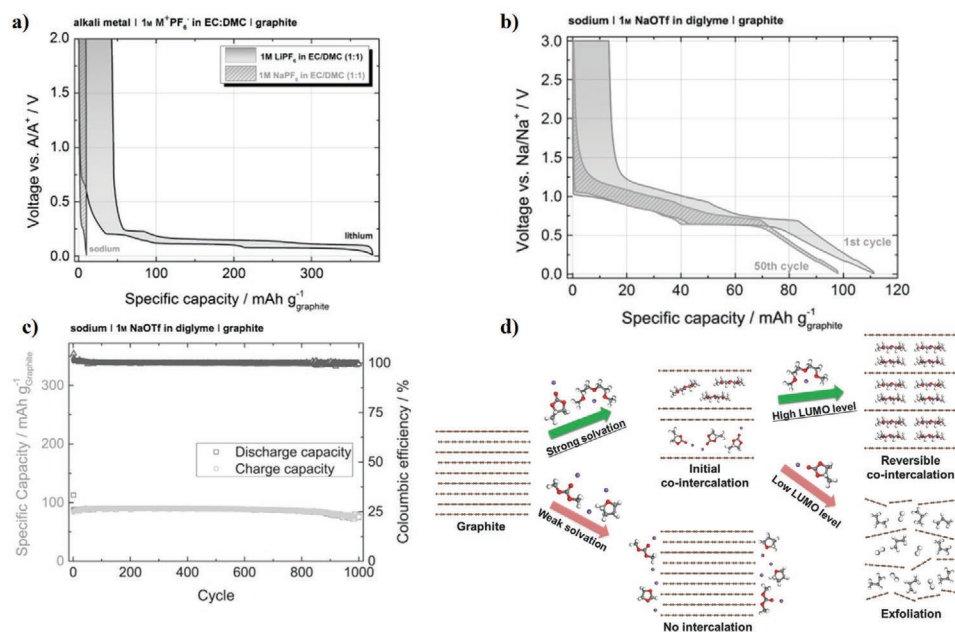


**Figure 5.** Voltage profiles of lithium/graphite and sodium/graphite half-cells cycled using a current of  $37.2 \text{ mA g}^{-1}$  in different electrolytes. a)  $1 \text{ M LiPF}_6/\text{EC}:\text{DMC}$  and  $1 \text{ M NaPF}_6/\text{EC}:\text{DMC}$ , b)  $1 \text{ M NaCF}_3\text{SO}_3/\text{diglyme}$ . Reproduced with permission.<sup>[47]</sup> Copyright 2014, Wiley. c,d) The long-term cycling performance and the mechanism of  $\text{Na}^+$ -solvent cointercalation in graphite is depicted in panel d, respectively, for the latter half-cell. Reproduced with permission.<sup>[51]</sup> Copyright 2017, Wiley.

for the cointercalation process is the stability of Na-solvent complexes in the graphite galleries for the reversible Na-solvent co-intercalation. In this regard, the lowest unoccupied molecular orbital (LUMO) levels of the  $[\text{Na-solvent}]^+$  molecules must be higher with respect to the Fermi level of the graphite. In that condition, will be difficult for electrons to be injected into these complexes (i.e. for complexes to be reduced). Gotoh et al.<sup>[52]</sup> explored the dynamics and coordination structure of  $[\text{Na-diglyme}_x]^+$  intercalated in graphite by  $^2\text{H}$  solid-state NMR, finding that two diglyme molecules coordinate each sodium ion rigidly, except for rotation of the methyl groups at low temperatures below 233 K. The active motion of sodium–diglyme complexes is favorable for Na diffusion between graphene layers in the graphite intercalated compound. Yu and co-workers<sup>[53]</sup> used ab initio calculations to study the atomistic structure and the electrochemical properties of intercalated graphite  $[\text{Na-diglyme}]^+\text{C}_n$ , revealing that the graphite intercalated compound has the lowest energy at  $n \approx 21$ , and in that case,  $[\text{Na-diglyme}]^+$  complex diffuses relatively fast in the interlayer space, and the electronic conductivity can be enhanced upon the cointercalation compared to the initial graphite. Maibach et al.<sup>[54]</sup> investigated the surface layer evolution of graphite in a sodium cell employing  $1 \text{ M NaFSI}$  in TEGDME electrolyte using soft X-ray photoelectron spectroscopy and confirmed the formation of a thin ( $\approx 3\text{--}8 \text{ nm}$ ) SEI layer. However, owing to the large volume expansion upon intercalation, the formed SEI breaks up leading to an irreversible phenomenon during the electrochemical process. Zhu et al.<sup>[55]</sup> scrutinized the electrochemical performances of various graphite anodes in different electrolyte systems for SIBs. The tests revealed that the best performance can be obtained employing natural graphite as electrode material and  $1 \text{ M NaCF}_3\text{SO}_3/\text{diglyme}$  as electrolyte, demonstrating a cycling

stability of 6000 cycles and an extraordinary rate capability up to current rates of  $10 \text{ A g}^{-1}$ . Moreover, a SIB cell using natural graphite and  $\text{Na}_3\text{V}_2(\text{PO}_4)_3$  as anode and cathode, respectively, and  $1 \text{ M NaCF}_3\text{SO}_3/\text{diglyme}$  as electrolyte, provided a capacity of about  $100 \text{ mAh g}^{-1}$  (on the basis of the cathode mass) at a working voltage of  $2 \text{ V}$ , and an extremely good rate capability until  $2 \text{ A g}^{-1}$ . Liu et al.<sup>[56]</sup> investigated in detail the irreversible capacity loss phenomena associated to the co-intercalation process, evaluating the solvation structures, desolvation process, and the corresponding electrochemical reduction stability of ether-based solvated  $\text{Na}^+$  ions. The study indicated the reductive decomposition of a small fraction of  $\text{PF}_6^-$  in the  $\text{Na}^+$  solvation sheath as partially responsible for the initial capacity loss, linked to the formation of an incomplete SEI on graphite. The PVDF binder, however, is identified as the main contributor to the initial capacity loss, because it immobilizes  $\text{Na}^+$  ions via a physical trapping mechanism. These are no longer accessible even at low discharging current density. Replacing PVDF with SA, i.e., a binder with less electronegative groups, significantly decreases the population of the “physically immobilized”  $\text{Na}^+$ , bringing the initial coulombic efficiency to an unprecedented level of 95%. Hasa et al.<sup>[57]</sup> reported a SIB cell assembled by coupling a layered  $\text{P2-Na}_{0.7}\text{CoO}_2$  cathode, a graphite anode and a  $1 \text{ M NaClO}_4$  TEGDME electrolyte, characterized by a capacity of  $80 \text{ mAh g}^{-1}$  (in respect to the cathode mass), extremely good cycle life of 1250 cycles and an excellent rate capability until  $10\text{C}$ , i.e.,  $1.75 \text{ A g}^{-1}$ . Glymes therefore enable the use of graphite as an effective anode material and are found to be extremely promising solvents for Na-based rechargeable batteries. On the other hand, the cointercalated solvent molecules depleted by the electrolyte solution requires an elevated amount of electrolyte that must be considered as an active material in the battery,

similar to dual-ion systems,<sup>[58,59]</sup> thus reducing the practical energy density attainable from such systems.

**Ether Based Electrolyte for Efficient Na Plating-Stripping Process:** Besides their use to activate the Na<sup>+</sup> intercalation in the graphite, glyme-based solvents revealed excellent reversibility for the sodium metal stripping/deposition process. Cui group<sup>[60]</sup> demonstrated that NaPF<sub>6</sub> in glymes (mono-, di-, and tetraglyme), can enable highly reversible and non-dendritic plating–stripping of sodium metal anodes at RT. High average coulombic efficiencies of 99.9% were achieved over 300 plating–stripping cycles at 0.5 mA cm<sup>-2</sup>. The long-term reversibility was found to arise from the formation of a uniform and, inorganic rich SEI layer, which is highly impermeable to electrolyte solvent and helpful to nondendritic growth. Westman et al.<sup>[61]</sup> investigated in detail the physicochemical and electrochemical properties of NaPF<sub>6</sub> in diglyme. The authors evidenced the suitability of the Na metal as counter/reference electrode in the NaPF<sub>6</sub>-diglyme electrolyte. The electrolyte showed an excellent ESW with no major reductive or oxidative decomposition within 0–4.4 V versus Na<sup>+</sup>/Na. The elevated ESW was associated to the absence of side reactions, which was supported by DFT calculations of oxidation and reduction potentials for various complexes of diglyme with Na<sup>+</sup> and PF<sub>6</sub><sup>-</sup>, as also evidenced with GC/MS analyses.

### 2.1.3. Ionic Liquids-Based Electrolytes

Ionic liquids (ILs) are RT molten salts formed by the combination of large organic cations such as imidazolium or pyrrolidinium and high-charge delocalized anions such as bis(trifluoromethanesulfonyl)imide (TFSI) (Figure 6).<sup>[62]</sup> This class of electrolyte offers unique characteristics including high conductivity, environmental compatibility and, especially, high thermal stability.<sup>[63–66]</sup> In contrast to organic carbonate-based electrolytes, which are highly volatile and flammable, IL-based solutions are generally stable up to 300–400 °C.<sup>[67]</sup> Furthermore, ILs are basically composed of organic ions allowing unlimited structural variation with the possibility to tune the properties of the IL to satisfy specific requirements.<sup>[68]</sup>

**Pure IL-Based Electrolytes:** Even if more than 10<sup>6</sup> possible ILs can be available, the research on lithium batteries as well as for sodium is mainly focused on imidazolium or pyrrolidinium based IL electrolytes. In 2010, Yamaki and co-workers<sup>[69]</sup> employed a 1-ethyl-3-methyl imidazolium tetrafluoroborate, (EMIMBF<sub>4</sub>) NaBF<sub>4</sub>, in a symmetric Na full cell using Na<sub>3</sub>V<sub>2</sub>(PO<sub>4</sub>)<sub>3</sub> both as cathode and anode material. The authors demonstrated an improved thermal stability and cyclability at elevated temperatures compared with the cell employing the

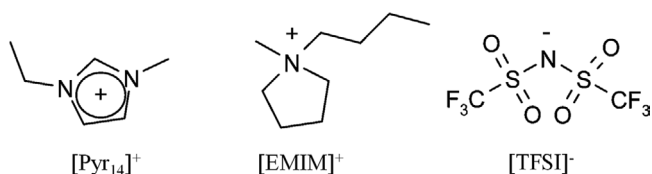


**Figure 6.** Chemical structure of the 1-butyl-1-methylpyrrolidinium [Pyr<sub>14</sub>]<sup>+</sup> and 1-ethyl-3-methylimidazolium [EMIM]<sup>+</sup> cations and of the bis(trifluoromethylsulfonyl)imide [TFSI]<sup>-</sup> anion.

conventional flammable carbonate-based electrolyte. The same IL-based electrolyte was recently characterized by Wu et al.,<sup>[70]</sup> reporting excellent ionic conductivity of  $9.8 \times 10^{-3}$  S cm<sup>-1</sup> at 20 °C, nonflammability and good thermal resistance. Monti et al.<sup>[71]</sup> reported a systematic investigation of imidazolium-based electrolyte using 1-ethyl-3-methylimidazolium (EMIM) and 1-butyl-3-methylimidazolium (BMIM) cations with TFSI anion doped with NaTFSI at different concentrations. The investigation evidences an increase of the viscosity and a decrease of the ionic conductivity with increased Na salt concentration, which was associated with the formation of ionic aggregates, thus limiting the mobility of the ionic species, due to the introduction of high charge density alkali metal ions. The use of imidazolium for LIBs or SIBs is limited by its low cathodic stability. The proton positioned at C2 can be reduced at cathodic redox potentials higher than that needed for lithiation/sodiation. This causes an irreversible decomposition of the RTIL, which results in poor reversibility at the negative electrode. However, Hosokawa and co-workers<sup>[72]</sup> recently demonstrated that the use of FSI anion, in place of TFSI, can greatly improve the stability of the imidazolium ionic liquid against sodium metal (Figure 7a). Figure 7b,c shows the comparison of the cyclic voltammetry performed using a Cu disk as working electrode and EMIMFSI (Figure 7b) or EMIMTFSI (Figure 7c) as electrolytes, demonstrating that the Na stripping/deposition can be efficiently performed in the electrolyte containing FSI anion.

Thanks to the widened electrochemical stability, pyrrolidinium-based ILs are the most widely investigated for LIBs as well as for SIBs applications.<sup>[63–65]</sup> One of the first attempts of using pyrrolidinium based ILs in SIBs was reported by Hagiwara's group,<sup>[73]</sup> describing the physicochemical properties of Pyr<sub>13</sub>FSI–NaFSI mixtures in different molar ratio. The study

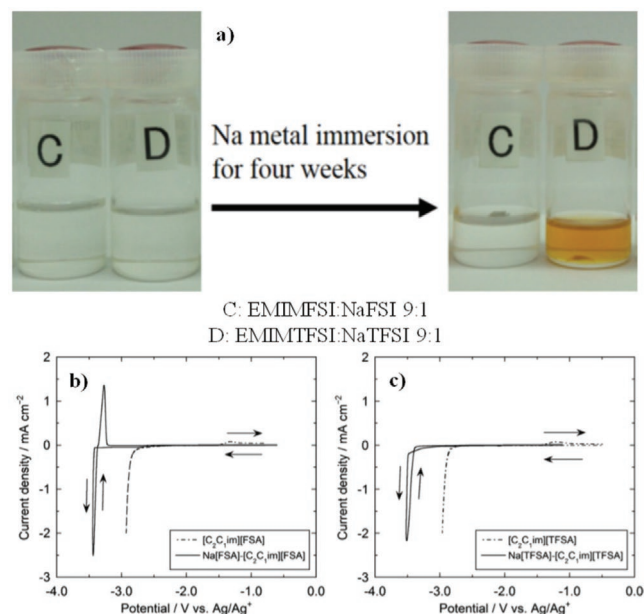


**Figure 7.** a) Photographic images of the EMIMFSI–NaFSI and of the EMIMTFSI–NaTFSI ionic liquids before Na metal immersion and after Na metal immersion for 4 weeks. Cyclic voltammograms of a Cu disk electrode in b) EMIMFSI–NaFSI c) EMIMTFSI–NaTFSI. Reproduced with permission.<sup>[72]</sup> Copyright 2016, American Chemical Society.

verified the conventional decrease of the ionic conductivity with increasing Na salt concentration, reporting a conductivity of  $3.2 \times 10^{-3} \text{ S cm}^{-1}$  at  $25 \text{ }^\circ\text{C}$  for the 8:2 IL:Na salt mole ratio, however, the electrolyte showed a good stability against sodium metal, and an electrochemical window stability extended up to  $5.2 \text{ V}$  versus  $\text{Na}/\text{Na}^+$ . Finally, the IL was successfully employed in a sodium cell using  $\text{NaCrO}_2$  cathode, which exhibited a stable charge–discharge behavior, delivering capacities of 92 and  $106 \text{ mAh g}^{-1}$  at 25 and  $80 \text{ }^\circ\text{C}$ , respectively, using a current of  $20 \text{ mA g}^{-1}$ . The coulombic efficiency was higher than 99% during the (dis-)charge tests except for the initial few cycles. The same research group tested the  $\text{Pyr}_{13}\text{FSI}-\text{NaFSI}$  electrolyte with several cathode and anode materials, such as hard carbon,<sup>[74–76]</sup>  $\text{Na}_2\text{FeP}_2\text{O}_7$ ,<sup>[77,78]</sup>  $\text{Na}_{1.56}\text{Fe}_{1.22}\text{P}_2\text{O}_7$ ,<sup>[79]</sup>  $\text{Na}_2\text{MnSiO}_4$ ,<sup>[80]</sup>  $\text{TiO}_2$ ,<sup>[81]</sup>  $\text{NaFeO}_4$ ,<sup>[82]</sup>  $\text{Na}_2\text{Ti}_3\text{O}_7$ ,<sup>[83]</sup>  $\text{Na}_{2/3}\text{Fe}_{1/3}\text{Mn}_{2/3}\text{O}_2$ ,<sup>[84]</sup> demonstrating the suitability of the electrolyte for SIBs applications, evidencing that the SIBs employing the IL electrolyte perform well in the mid-high temperature range ( $60\text{--}80 \text{ }^\circ\text{C}$ ). However, the performance at RT suffers because of the lower conductivity and higher viscosity of the IL-based electrolyte in comparison to the conventional carbonate-based systems. Extensive research on IL-based electrolytes for application in SIBs has been conducted by Forsyth's group. In 2013,<sup>[85]</sup> the group investigated the physicochemical and electrochemical properties of  $\text{Pyr}_{14}\text{TFSI}-\text{NaTFSI}$  mixtures indicating that the addition of sodium salt leads to an increase of the glass transition ( $T_g$ ) value, and the disappearance of the crystallization ( $T_{\text{cry}}$ ) and melting ( $T_m$ ) temperatures. The viscosities and conductivities were well described by the Vogel–Tammann–Fulcher (VTF) equation. The detailed study was later extended to  $\text{Pyr}_{13}\text{FSI}-\text{NaTFSI}$  mixtures,<sup>[86]</sup> revealing similar behavior in respect to the previously reported system, in addition to a good stability against sodium metal. Temperature-dependent PFG-NMR diffusion measurements showed that both FSI and TFSI have a comparable behavior although the smaller FSI anion is more diffusive. Lately, the group reported an unexpected elevated solubility of NaFSI salt in the  $\text{Pyr}_{13}\text{FSI}$  IL, up to  $3.2 \text{ mol kg}^{-1}$  (50 mol %) at RT.<sup>[87]</sup> Despite the decrease of the ion diffusivity and lower conductivity with increasing Na-salt concentration, the authors demonstrated that the high  $\text{Na}^+$  content electrolytes can support high current densities ( $1 \text{ mA cm}^{-2}$ ) and prolonged stability upon continued cycling. Impedance measurements indicated that the interfacial resistance decreases at high salt concentration, resulting in faster charge transfer at the interface. The same group further investigated the effect of EC addition to the  $\text{Pyr}_{14}\text{FSI}-\text{NaFSI}$  mixture,<sup>[88]</sup> reporting that a 30 wt% EC addition to the  $3.2 \text{ mol kg}^{-1}$  NaFSI  $\text{Pyr}_{14}\text{FSI}$  greatly increases the ionic conductivity value. The suitability of the prepared electrolyte for sodium battery applications was tested in half-cells at RT using  $\text{Na}_3\text{V}_2(\text{PO}_4)_3$  as cathode material. High concentration of Na salt in phosphonium-based ILs for SIBs have also been investigated.<sup>[89]</sup> Both Forsyth and Hagiwara groups suggest that the reason for the improved performance at higher concentration of ILs in SIBs, despite the lower conductivity, is the higher transference number for the alkali cation.<sup>[90–92]</sup> Recently, this was also demonstrated by an in depth theoretical study of ion dynamics of concentrated IL ( $\text{NaFSI}:\text{Pyr}_{13}\text{FSI}$ ) focusing on how the solvation structure of a Na ion changes with salt concentration and how this affects its dynamics. The reported results evidenced a

decoupled motion for  $\text{Na}^+$  ions facilitated by a structural rearrangement in the IL structure with increasing salt addition. For elevated concentrations large Na-anion aggregate domains are formed, which gradually become interconnected when the fraction of salt is more than that of the IL. This can create preferential conduction pathways improving the mobility of the  $\text{Na}^+$  ion. Triisobutylmethylphosphonium bis(fluorosulfonyl)amide ( $\text{P}_{1444}\text{FSI}$ ) in mixtures with NaFSI or NaTFSI or  $\text{NaPF}_6$  salts was investigated. The ionic conductivities of FSI and TFSI mixtures were very similar at RT, both higher in respect to  $\text{PF}_6$  mixture. The highest  $\text{Na}^+$  transference number was reported for NaFSI mixture, being slightly higher in respect to TFSI mixture and double that of the  $\text{NaPF}_6$  sample. This suggests that the mechanism of  $\text{Na}^+$  diffusion is different in  $\text{PF}_6$  mixtures compared to that of FSI and TFSI mixtures and could be attributed to the different strength of speciation and the complex phases formed in the  $\text{PF}_6$  case. The applicability of  $\text{P}_{1114}\text{FSI}:\text{NaFSI}$  (2.3 m) electrolyte solution was demonstrated employing  $\text{O}_3\text{-Na}_{2/3}[\text{Fe}_{2/3}\text{Mn}_{1/3}]\text{O}_2$  and  $\text{P}_2\text{-Na}_{2/3}[\text{Fe}_{2/3}\text{Mn}_{1/3}]\text{O}_2$  cathodes in sodium cells.<sup>[93]</sup> Intensive investigation on the use of ILs based electrolytes for SIBs application has also been conducted by Passerini's group. The electrochemical performance of  $\text{Na}_{0.45}\text{Ni}_{0.22}\text{Co}_{0.11}\text{Mn}_{0.66}\text{O}_2$  was evaluated in 10 mol% NaTFSI (or 0.45 m) in  $\text{Pyr}_{14}\text{FSI}$  electrolyte and compared with a 0.5 m  $\text{NaPF}_6$  in PC, showing an improved stability in the IL-based electrolyte due to a lower solubility of manganese into the ionic liquid-based electrolyte (Figure 8).<sup>[94]</sup> Recently,  $\text{Pyr}_{14}\text{TFSI}-\text{NaTFSI}$  was tested in Na full cell, employing a nanostructured Sb–C composite anode and  $\text{P}_2\text{-Na}_{0.6}\text{Ni}_{0.22}\text{Fe}_{0.11}\text{Mn}_{0.66}\text{O}_2$  cathode. A capacity ranging from 100 to  $120 \text{ mAh g}^{-1}$  and a working voltage of about 2.7 V was demonstrated, once again showing the suitability of the IL for the realization of advanced SIBs.<sup>[95]</sup> The improved electrochemical performance of IL-based electrolyte in comparison to conventional carbonate electrolytes was also reported for a  $\text{Na}_4\text{Ni}_3(\text{PO}_4)_2(\text{P}_2\text{O}_7)$  high voltage cathode, which further evidenced an improvement by more than 60% in delivered capacity with  $\text{Pyr}_{13}\text{FSI}:\text{NaTFSI}$  (9:1 mole ratio) compared to the 1 m  $\text{NaPF}_6/\text{EC}:\text{DEC}$  (1:1 w:w) electrolyte, thanks to the superior electrochemical stability of the IL electrolyte, allowing the use

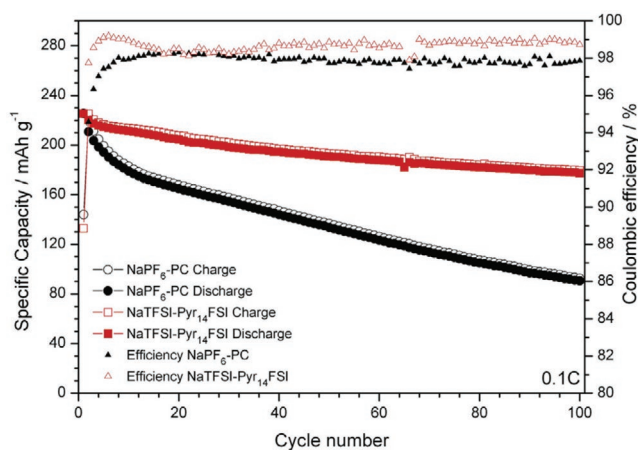


**Figure 8.** Cycling behavior of  $\text{Na}/\text{Na}_{0.45}\text{Ni}_{0.22}\text{Co}_{0.11}\text{Mn}_{0.66}\text{O}_2$  cells employing  $\text{NaPF}_6\text{-PC}$  electrolyte (circles) or  $\text{Pyr}_{14}\text{FSI}-\text{NaTFSI}$  electrolyte (squares). Current  $12 \text{ mA g}^{-1}$ , cutoff voltage limits: 4.6–1.5 V, and temperature at  $20 \text{ }^\circ\text{C}$ . Reproduced with permission.<sup>[94]</sup> Copyright 2013, Elsevier.

of a higher cutoff voltage.<sup>[96]</sup> The beneficial effect of IL-based electrolyte in SIBs has been also verified by Wang et al.<sup>[97]</sup> reporting improved electrochemical performances of quinone cathodes for organic SIBs employing IL-based electrolyte (0.3 M NaTFSI in Pyr<sub>13</sub>TFSI). The authors evidenced lower solubility of quinone cathodes in the IL based electrolyte, thus granting a superior cycle life of the organic cathode in Na-cells.

Chang's group investigated the electrochemical performance of NaFePO<sub>4</sub> in Pyr<sub>14</sub>TFSI–NaTFSI mixture ranging from 0.1 to 1 M, and reported that the best rate capability and capacity retention can be obtained at 0.5 and 1 M concentrations respectively.<sup>[98]</sup> The group explored the influence of sodium salt anion by testing NaBF<sub>4</sub>, NaClO<sub>4</sub>, NaPF<sub>6</sub>, and NaN(CN)<sub>2</sub> as conducting salts.<sup>[99]</sup> Pyr<sub>14</sub>TFSI–NaBF<sub>4</sub> showed the highest ionic conductivity and the best electrochemical behavior in Na/NaFePO<sub>4</sub> cell configuration at 50 °C, in terms of delivered capacity, rate capability and cycling stability. A similar investigation was performed using Na<sub>0.44</sub>MnO<sub>2</sub> as cathode material, but in this case, the best performances were achieved for NaClO<sub>4</sub> salt.<sup>[100]</sup> The electrochemical properties of Pyr<sub>13</sub>FSI–NaFSI electrolyte in a full cell configuration using hard carbon as anode and Na<sub>0.44</sub>MnO<sub>2</sub> as cathode materials was also reported.<sup>[101]</sup> The same electrolyte composition was employed in sodium cells in combination with a Sb<sub>2</sub>S<sub>3</sub>/graphene anode material, showing superior performance compared to conventional carbonate-based electrolyte.<sup>[102]</sup> Owing to its superior properties, Pyr<sub>13</sub>FSI–NaFSI has been applied for SIBs by several other research groups in different cell configurations,<sup>[103–107]</sup> nevertheless it is interesting to note the effects that the salt anion has on the performance and accordingly there is certainly much room to improve these IL-based electrolytes for future applications. Furthermore, while there has been significant investigation of the behavior of the electrode/electrolyte interphase in organic electrolytes, as discussed above, there is a lesser understanding of the interphase in the IL-based systems.

**IL + Cosolvent Electrolyte:** One of the main drawbacks of IL-based electrolytes is their high viscosity and limited ionic conductivity at RT. A possible solution to overcome this issue, already widely explored in lithium based systems,<sup>[108–112]</sup> is to mix the IL electrolyte with a (co)solvent(s) to improve electrochemical performances while maintaining a sufficient safety level and a limited flammability of the electrolyte. Monti et al.<sup>[113]</sup> reported a systematic study of physico-chemical properties and electrochemical performance of hybrid electrolytes for SIBs using both IL and organic electrolytes as references. Similar approach has been employed by Manohar et al.<sup>[114]</sup> reporting good electrochemical performances of sodium cells using a Na<sub>3</sub>V<sub>2</sub>(PO<sub>4</sub>)<sub>3</sub>/carbon (NVP@C) cathode and an electrolyte comprising a 1 M NaFSI in the mixture of xEC:PC (1:1 vol) + (1 – x)Pyr<sub>13</sub>TFSI (with x volume fraction x = 0, 0.25, 0.5, 0.75, 1). The best electrochemical performances have been reported for x = 0.5. Stettner et al.<sup>[115]</sup> studied mixtures of IL and glyme solvents for Na-battery systems. Further investigation of such mixed electrolyte systems is believed to play a key role in improving the performance of future SIBs.

#### 2.1.4. Concentrated Electrolytes

Conventionally, the salt concentration in the electrolyte system ranges between 1 and 1.2 M (molar) solutions. Recently, Chen

**Table 6.** Comparison of dilute and concentrated electrolyte systems.

Physicochemical property	Na <sup>+</sup> -electrolyte system	
	Dilute	Concentrated
Representative bulk components	Solvent-separated ion pairs and free solvent molecules	Contact ion pairs and cation–anion aggregates
Representative SEI species	Organic (solvent reduction) and inorganic (anion reduction)	Dominated by salt anion decomposed products (inorganic rich)
Thermal stability	Poor	Good
Flammability	High	Low
Oxidative stability	Low	High
Reductive stability	Low	High
Viscosity	Low	High
Ionic conductivity	High	Slightly low
Wettability	Good	Relatively poor
Electrode reaction kinetics	Slow	Fast
Power density	High	High
Energy density	High	High
Cost	Low	High

and co-workers<sup>[116]</sup> introduced a new class of high concentration electrolyte, named as “Solvent-in-Salt” electrolyte system (Table 6). The investigated ultrahigh salt concentration revealed a high lithium-ion transference number (0.73), an effective suppression of lithium dendrite/mossy growth and morphology change on the metallic lithium anode. The formation mechanism and the nature of the SEI layers derived from concentrated electrolytes could be fundamentally distinct from those of the traditional SEI and thus enable unusual functions that cannot be realized using regular (i.e., diluted) electrolytes. The use of glyme for the realization of “solvate ILs,” proposed for lithium system<sup>[117,118]</sup> has been also investigated for SIBs. Terada et al.<sup>[119]</sup> investigated the physicochemical properties of tetraethylene glycol dimethyl ether (tetraglyme/TEGDME) and NaTFSI mixtures. The authors revealed the formation of a “solvate ILs” in which [Na(tetraglyme)]<sup>+</sup> cationic charge carriers are formed for equimolar ratio of NaTFSI:tetraglyme. The prepared electrolyte is characterized by an ionic conductivity of 0.61 mS cm<sup>–1</sup> (30 °C) and with an anodic electrochemical window stability of 4 V versus Na/Na<sup>+</sup>. The same group<sup>[120]</sup> further investigated the NaTFSI:tetraglyme (1:1, mol) complex comparing the electrochemical properties with the NaTFSI:pentaglyme, showing that the population of contact ion-pair and/or ion aggregates is smaller for the pentaglyme system than for the tetraglyme, and that the pentaglyme-based electrolyte has higher ionic conductivity. The electrochemical properties of the two electrolytes were investigated in sodium cells employing a Na<sub>0.44</sub>MnO<sub>2</sub> cathode, revealing superior performances for the pentaglyme-based electrolyte in terms of delivered capacity and rate capability. Guo et al.<sup>[121]</sup> examined the performance of sodium batteries assembled using 9,10-anthraquinone (AQ), Na metal and a high-concentration NaFSI/triglyme as cathode, anode and electrolyte respectively. The authors evidenced that use of 4 M NaFSI electrolyte solution resulted in superior performance

enlisting higher capacity retention, delivered capacity and coulombic efficiency. Cao et al.<sup>[122]</sup> employed the same electrolyte composition (i.e., 4 m NaFSI/ triglyme) obtaining a highly reversible Na plating/stripping at ambient temperature with an extremely high coulombic efficiency. The highly concentrated ether–NaFSI mixtures enable the formation of an exceptionally stable SEI and thereby minimizing side degradation reactions during cycling. Schafzahl et al.<sup>[123]</sup> reported the electrochemical properties of a highly concentrated NaFSI in diglyme electrolytes against Na metal, hard carbon anodes and intercalation cathodes. The study proved that DME:NaFSI at a mole ratio of 2:1 grants a stable passivation of anode materials thanks to the formation of a stable SEI. Furthermore, the investigated electrolyte revealed a nondendritic Na metal cycling with approximately 98% coulombic efficiency up to 300 cycles. Lee et al.<sup>[124]</sup> investigated a similar system, using diglyme as solvent and NaFSI as salt in a 5.5 m concentration. The investigated electrolyte showed a very high Na plating/stripping coulombic efficiency (99.3%) on a stainless steel (SS) working electrode. Furthermore, the electrolyte displayed extremely good electrochemical window stability up to 4.9 V versus Na/Na<sup>+</sup>. The ultraconcentrated electrolyte was employed for the realization of sodium cells using high-voltage Na<sub>4</sub>Fe<sub>3</sub>(PO<sub>4</sub>)<sub>2</sub>(P<sub>2</sub>O<sub>7</sub>) and Na<sub>0.7</sub>(Fe<sub>0.5</sub>Mn<sub>0.5</sub>)O<sub>2</sub> cathodes, resulting in a remarkable cycling stability (delivered capacity of 109 mAh g<sup>-1</sup> for over 300 cycles for the Na<sub>4</sub>Fe<sub>3</sub>(PO<sub>4</sub>)<sub>2</sub>(P<sub>2</sub>O<sub>7</sub>) half-cell), revealing improved performances in respect to the conventional 1 m NaPF<sub>6</sub>/EC:PC electrolyte. He et al.<sup>[125]</sup> reported the electrochemical characteristics of a highly concentrated NaTFSI in DMSO (>3 mol kg<sup>-1</sup>). Raman spectra of NaTFSI/DMSO electrolytes in combination with the ab initio molecular dynamics simulation showed the formation of Na(DMSO)<sub>3</sub>(TFSI)-like solvation structure. The authors demonstrated an improved reversibility for Na-O<sub>2</sub> battery using the above mentioned concentrated electrolyte. Takada and co-workers<sup>[126]</sup> investigated a 5.86 m NaFSI in succinonitrile (SN) electrolyte, reporting excellent performance of sodium cell using hard carbon as working electrode. The improvement is attributed to the formation of a very stable SEI, mainly originated from the decomposition of the anion. Wang et al.<sup>[127]</sup> examined the use of a highly concentrated electrolyte using trimethyl phosphate (TMP) as solvent and NaFSI salt in a 3.3 m concentration, in a sodium cell employing HC negative electrode. The system showed excellent stability up to 1200 cycles, much higher in comparison to the conventional 1 m NaPF<sub>6</sub>/EC:DMC (Figure 9a). The reason behind the improved electrochemical behavior was addressed to the formation of a thinner, more adhesive and stable SEI (rich in NaSON, Na<sub>2</sub>S<sub>2</sub>O<sub>5</sub>, Na<sub>2</sub>S<sub>2</sub>O<sub>3</sub>, Na<sub>2</sub>S...) in the presence of a highly concentrated electrolyte (Figure 9b,c).

## 2.2. Aqueous Electrolytes

The use of water (H<sub>2</sub>O) instead of organic solvents in the electrolyte formulation offers many advantages, such as lower cost, elevated inherent safety, and environmentally friendliness. This, in combination with the elevated abundance and low cost of sodium, make the aqueous sodium-ion batteries (ASIBs) extremely appealing and promising. However, due to the electrochemical decomposition of H<sub>2</sub>O, the proper selection of the

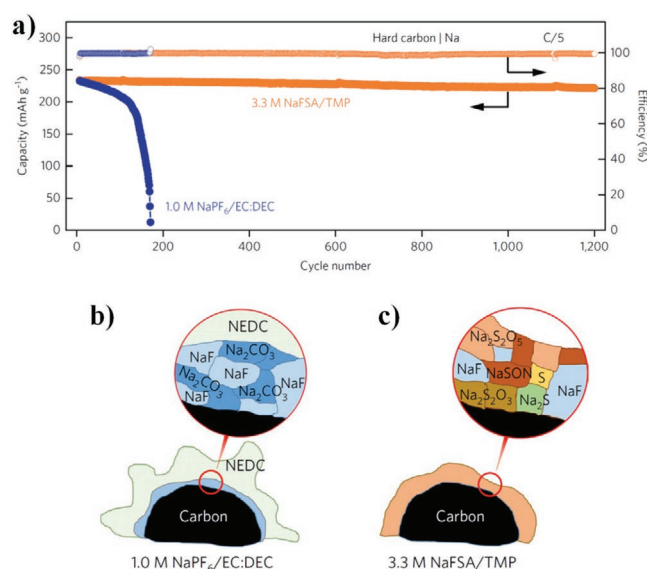


**Figure 9.** a) Cycling performance and Coulombic efficiency of the hard carbon half-cells using concentrated 3.3 m NaFSI/TMP electrolyte and conventional 1.0 m NaPF<sub>6</sub>/EC:DEC (1:1, vol) electrolyte. b,c) Schematic illustrations of passivation films derived from EC solvent in b) a conventional dilute electrolyte and c) from NaFSI salt in the concentrated electrolyte. The former has a typical organic–inorganic hybrid structure with the organic compounds (for example, sodium ethylene dicarbonate, NEDC) as the main component, while the latter shows a single inorganic structure. Reproduced with permission.<sup>[126]</sup> Copyright 2017, American Chemical Society.

electrode materials could be one of the most critical challenges in practical ASIBs. An aqueous electrolyte is further complicated because of: i) needs to eliminate residual O<sub>2</sub> in electrolyte, ii) protection of the electrode stability in aqueous electrolyte, iii) inhibition of H<sub>3</sub>O<sup>+</sup> cointercalation into the electrode, and iv) efficient internal consumption of O<sub>2</sub> and H<sub>2</sub> produced at cathode and anode sides after over (charge/discharge) (Figure 10).<sup>[128]</sup> These issues are of paramount importance for the realization of an aqueous battery system.

One of the first demonstration of ASIBs has been reported by Whitacre et al., assembling an 80 V, 2.4 kW h battery pack employing λ-MnO<sub>2</sub> as cathode and activated carbon as anode in 1 m Na<sub>2</sub>SO<sub>4</sub> aqueous electrolyte.<sup>[129]</sup> Employing the same electrolyte, Wu et al.<sup>[130]</sup> coupled NaTi<sub>2</sub>(PO<sub>4</sub>)<sub>3</sub> and Na<sub>2</sub>NiFe(CN)<sub>6</sub> as cathode and anode respectively, obtaining a battery system with an average output voltage of 1.27 V, an energy density of 42.5 Wh kg<sup>-1</sup> and a capacity retention of 88% after 250 cycles at 5 C rate. Park et al.<sup>[131]</sup> evidenced better performance of the 2 m Na<sub>2</sub>SO<sub>4</sub> in respect to 4 m NaOH in an ASIB employing NASICON-type NaTi<sub>2</sub>(PO<sub>4</sub>)<sub>3</sub> cathode material, obtaining a reversible capacity of 124 mAh g<sup>-1</sup> at 2.0 mA cm<sup>-2</sup> current, with a plateau voltage of 2.1 V versus Na/Na<sup>+</sup>. Surprisingly Minakshi and Meyrick reported good performances of maricite NaMn<sub>1/3</sub>Co<sub>1/3</sub>Ni<sub>1/3</sub>PO<sub>4</sub> in aqueous NaOH based electrolyte, as maricite is not favorable to ion diffusion.<sup>[132]</sup> Li et al. reported excellent performance of a NaTi<sub>2</sub>(PO<sub>4</sub>)<sub>3</sub>/Na<sub>0.44</sub>MnO<sub>2</sub> system employing 1 m Na<sub>2</sub>SO<sub>4</sub> electrolyte. The authors demonstrated an exceptionally high rate capability and excellent stability of more than 1000 cycles, evidencing extremely interesting values

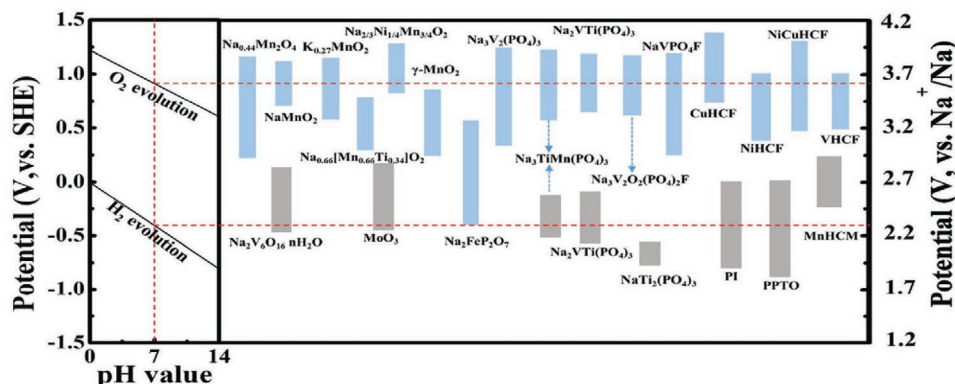


**Figure 10.** Electrochemical window of aqueous solution and the intercalation potential of some electrode materials that could be employed for aqueous Na-ion batteries. (AC: activated carbon; PVAQ: poly (2-vinylanthraquinone); PI: polyimides; PTVE: poly-2,2, 6,6-tetramethylpiperidine-oxy-4-vinyl ether. Reproduced with permission.<sup>[128]</sup> Copyright 2018, Wiley.

of energy and power densities.<sup>[133]</sup> Several other systems based on 1 M Na<sub>2</sub>SO<sub>4</sub> aqueous electrolyte has been developed such as NASICON-type Na<sub>3</sub>V<sub>2</sub>(PO<sub>4</sub>)<sub>3</sub>,<sup>[134]</sup> Na<sub>2</sub>FeP<sub>2</sub>O<sub>7</sub>,<sup>[135]</sup> NaFePO<sub>4</sub>,<sup>[136]</sup> Na<sub>2</sub>CuFe(CN)<sub>6</sub>,<sup>[137]</sup> NaFe<sub>2</sub>(CN)<sub>6</sub>,<sup>[138]</sup> Na<sub>3</sub>MnTi(PO<sub>4</sub>)<sub>3</sub>,<sup>[139]</sup> Na<sub>2</sub>VTi(PO<sub>4</sub>)<sub>3</sub>,<sup>[140]</sup> Whitacre and co-workers performed a detailed study on the effect of the electrolyte concentration on a NaTi<sub>2</sub>(PO<sub>4</sub>)<sub>3</sub>/Na<sub>0.44</sub>MnO<sub>2</sub> ASIB in NaClO<sub>4</sub> based electrolyte with molarities ranging from 1 to 5. The study showed an improved cell rate capability when employing high concentration electrolyte. Furthermore, the concentration of the electrolyte affects the self-discharge rate of the cell due to the lower oxygen solubility in the high concentration electrolytes.<sup>[141]</sup> Nakamoto et al.<sup>[142]</sup> studied the effect of various Na-salts (i.e., Na<sub>2</sub>SO<sub>4</sub>, NaNO<sub>3</sub>, and NaClO<sub>4</sub>) at different concentration on Na<sub>2</sub>FeP<sub>2</sub>O<sub>7</sub>/NaTi<sub>2</sub>(PO<sub>4</sub>)<sub>3</sub> rechargeable aqueous sodium-ion battery. NaNO<sub>3</sub>-based electrolyte exhibited a large irreversible capacity due to H<sub>2</sub> gas evolution and corrosive side reactions, while good performances have been reported for Na<sub>2</sub>SO<sub>4</sub>, and NaClO<sub>4</sub> based aqueous electrolytes, with slightly superior performance for 4 M NaClO<sub>4</sub>. However, due to the explosiveness and oxidizing abilities of NaClO<sub>4</sub>, the 2 M Na<sub>2</sub>SO<sub>4</sub> has been selected as the best electrolyte candidate for the investigated aqueous sodium-ion battery system.<sup>[142]</sup> Investigations on different electrolyte composition for ASIBs, and in particular on the so called “water in salt” electrolyte has been conducted by Xu and co-workers.<sup>[143]</sup> Similar investigation has been reported by the same authors previously on lithium system,<sup>[144]</sup> presenting an operating electrochemical stability window of 3 V obtained by increasing the salt concentration to form “water-in-salt” electrolytes.<sup>[144]</sup> For aqueous solution with concentration below 5 M, the number of water molecules is much higher with respect to the salt, and in this condition, it is generally accepted that the solvation shell consists at least of two layers: the more tightly associated primary and the relatively loose secondary solvation shell (Figure 11a), with the first Na<sup>+</sup> solvation shell typically containing 6 oxygens. However, when salt concentration is higher than 9.00 M, the number of available water molecules is not enough to form the second solvation shell, and this leads to the formation of a “water-in-salt” solution that can be visualized as a liquefied salt (Figure 11a). With this new concept (i.e., water-in-salt solution), a series of new transport and interfacial properties are

acquired. Employing a “water-in-salt” solution based on sodium trifluoromethane sulfonate (NaCF<sub>3</sub>SO<sub>3</sub>), Xu and co-workers<sup>[143]</sup> demonstrated a superior electrochemical window stability up to 2.5 V (Figure 11b). The improvement is associated with the formation of a Na<sup>+</sup> conducting SEI on the NaTi<sub>2</sub>(PO<sub>4</sub>)<sub>3</sub> anode surface that effectively suppress H<sub>2</sub> evolution and to the reduced electrochemical activity of water, leading to hindered oxygen evolution on the Na<sub>0.66</sub>[Mn<sub>0.66</sub>Ti<sub>0.34</sub>]O<sub>2</sub> cathode. The assembled cell showed an excellent reversibility, and extraordinarily high coulombic efficiency (>99.2%) even at a low rate of 0.2 C for >350 cycles. At a high rate of 1 C, superior stability of >1200 cycles were also achieved, with negligible capacity losses (0.006% per cycle). One of the main issues of this concentrated “water-in-salt” electrolyte (WiSE) is the elevated cost of Na salt employed; generally, NaTFSI or NaCF<sub>3</sub>SO<sub>3</sub> are employed. Passerini’s group<sup>[145]</sup> recently proposed the use of a much cheaper potassium acetate (KAc) to prepare a dual cation highly concentrated electrolyte including sodium acetate (NaAc) as a charge carrier. The WiSE with composition 32 m KAc and 8 m NaAc is characterized by an elevated electrochemical stability window and a good compatibility with low-cost aluminum current collector.

### 2.3. Solid-State or Quasi-Solid-State Electrolytes

Though liquid electrolyte-based batteries possess excellent electrochemical performances, they pose serious safety hazards, resulting from the use of highly flammable/volatile organic solvents. This includes electrolyte leakage, possibly fire or explosion, dendrite formation, and side reactions between electrolytes and electrodes. The safety issue of Na-based rechargeable batteries is even expected to be more severe than that of LIBs, due to the higher reactivity of sodium, if any formed, with moisture and oxygen. As a result, the use of solid electrolytes (SEs) for applications in SIBs has drawn increasing attention from the scientific community. SEs grants intrinsically elevated safety level, high thermal stability, wider electrochemical stability window, longer cycle life, excellent mechanical properties, flexibility, and simple assembly processes because SEs serve both as ion transport pathway and the separator with no liquid/fluid

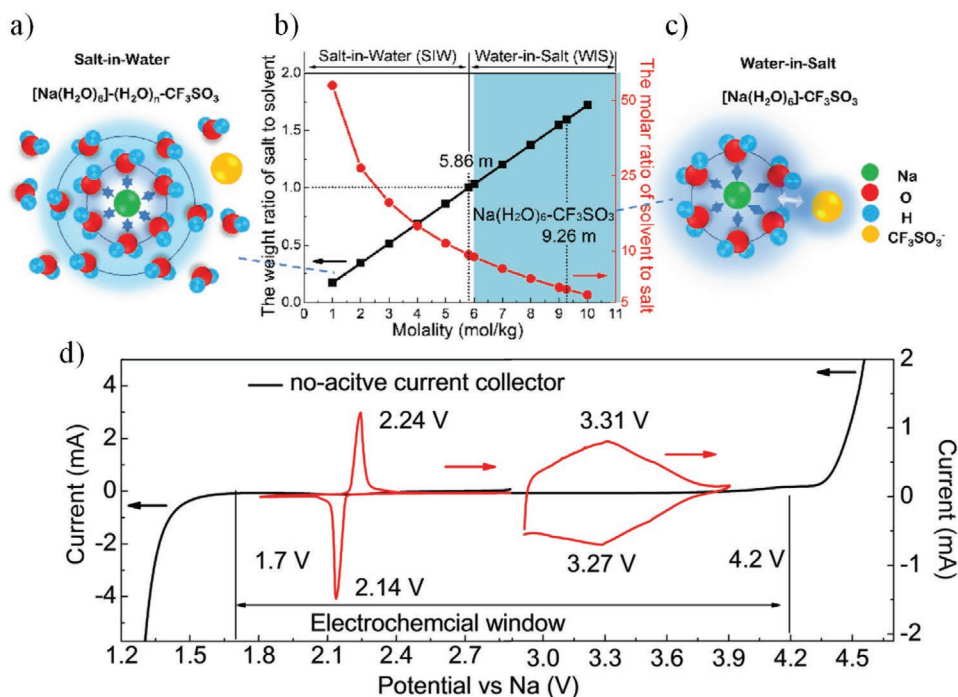


**Figure 11.** a) Scheme of the cation–anion and ion–solvent interactions in “salt in water” electrolyte. b) Trend of the weight ratio and of the molar ratio of solvent to salt as function of the molality. c) Scheme of the cation–anion and ion–solvent interactions in “water in salt” electrolyte. d) The CV curves measured on inert electrodes at the scanning rate of  $10 \text{ mV s}^{-1}$  (black line), which is overlaid with the first CV traces obtained on active anode ( $\text{NaTi}_2(\text{PO}_4)_3$ ) and cathode ( $\text{Na}_{0.66}\text{Mn}_{0.66}\text{Ti}_{0.34}\text{O}_2$ ) materials at the scanning rate of  $0.1 \text{ mV s}^{-1}$ . Reproduced with permission.<sup>[143]</sup> Copyright 2017, Wiley.

component. Hence, the development of solid-state batteries can lead to a breakthrough of the electrochemical storage systems for applications in mobility, stationary and utility/grid storage. However, the main drawbacks related to the use of SEs are their poor ionic conductivity compared to the liquid ones, harsh-to control interfaces between the electrodes/electrolytes (i.e., elevated interface resistance), and engineering process-related issues. In SEs, electrode wetting and the electrode/electrolyte interphase formation take place between two solids, which result in an extremely elevated interfacial resistance, being the main obstacle hindering their practical applications.<sup>[146,147]</sup> The field of solid electrolytes for Na-based rechargeable battery application mainly includes (solid) polymer electrolytes (SPEs), conductive inorganic solid electrolytes (ISEs) and their composite/hybrid versions.

### 2.3.1. Polymer Electrolytes

**Dry Polymer Electrolytes:** The discovery of ionically conducting polymers dates back four decades when the conductivity in complexes formed by alkali metal salts (i.e., Li, Na, K, Rb, and Cs) with poly (ethylene) oxide (PEO) was reported by Wright<sup>[148]</sup> and Armand<sup>[149]</sup> thus proposed for use in electrochemical devices. Polymer electrolytes (PEs) combine the ionic conductivity in the solid state with mechanical flexibility, making them ideal replacements for liquid electrolytes in electrochemical cells, thanks to their ability to form good interphases with solid electrodes. In addition, SPEs offer cost-effectiveness, light-weight (i.e., high energy density), improved safety, good processability

(shaping, patterning, and integration), highly flexible battery design, easier manipulation (including fabrication of ultrathin films) and strengthened resistance to volume change of the electrodes during the charge/discharge process. However, they are generally characterized by a limited conductivity at RT ( $10^{-5}$ – $10^{-7} \text{ S cm}^{-1}$ ) and for this reason, batteries employing SPEs generally operate at moderate temperatures ( $60$ – $90 \text{ }^\circ\text{C}$ ).<sup>[150,151]</sup> This temperature could be extremely critical for Na metal batteries as the melting point of Na metal (i.e.,  $98 \text{ }^\circ\text{C}$ ) is very close to the operating temperature of SPEs. PEO, with  $-\text{CH}_2\text{CH}_2\text{O}-$ , EO repeating units, is the most extensively studied polymer for SPEs preparation, due to its elevated solvation power ( $\text{DN} = 22$ ), and ion dissociating capacity. Besides PEO-based electrolytes, several other polymers have been investigated for SIB electrolyte application, such as the poly(vinyl pyrrolidone) (PVP),<sup>[152–154]</sup> poly(vinyl chloride) (PVC),<sup>[155]</sup> poly(vinyl alcohol) (PVA),<sup>[156,157]</sup> polyacrylonitrile (PAN),<sup>[158]</sup> and polycarbonates<sup>[159]</sup> (Table 7). The properties of PEO mixed with  $\text{NaClO}_4$  salt was reported by West et al.<sup>[160]</sup> in 1987, showing an ionic conductivity for the PEO/ $\text{NaClO}_4$  with  $\text{EO}/\text{Na} = 12$  of  $0.65 \text{ mS cm}^{-1}$  at  $80 \text{ }^\circ\text{C}$ . Hashmi and Chandra<sup>[161]</sup> investigated PEO/ $\text{NaPF}_6$  mixture reporting a conductivity of  $5 \times 10^{-6} \text{ S cm}^{-1}$  at RT and  $10^{-3} \text{ S cm}^{-1}$  at  $70 \text{ }^\circ\text{C}$  for  $\text{EO}/\text{Na} = 15$ . Following the initial studies, several other groups reported the properties of PEO with different Na salts such as  $\text{NaClO}_3$ ,<sup>[162]</sup>  $\text{NaLaF}_4$ ,<sup>[163]</sup>  $\text{NaClO}_4$ ,<sup>[162]</sup>  $\text{NaFSI}$ ,<sup>[164,165]</sup>  $\text{NaFNFSI}$ ,<sup>[166]</sup> and  $\text{NaTFSI}$ .<sup>[165,167]</sup> In particular, the latter fluorinated anions, proposed by Armand and co-workers,<sup>[168]</sup> act as a plasticizer for PEO based electrolytes, decreasing the crystallinity of the polymer and thereby enhancing its ionic conductivity at RT. The effect is mainly related to the possibility of rotations around

**Table 7.** Commonly used polymer solid electrolytes and their physicochemical properties.

Polymer matrix	Polymeric unit	$T_g$ [°C]	$T_m$ [°C]	Remark
PEO	$-(CH_2CH_2O)_n-$	-64	65	$-(CH_2CH_2O)_n-$ participates in the solvation of $Na^+$ cations
PPO	$-(CH(CH_3)CH_2O)_n-$	-60		$-(CH(CH_3)CH_2O)_n-$ participates in the solvation of $Na^+$ cations
PAN	$-(CH_2CH(CN))_n-$	125	217	$C\equiv N$ participates in the solvation of $Na^+$ cations through dipole interactions, elevated chemical stability
PMMA	$-(CH_2C(CH_3)(CO_2CH_3))_n-$	120		$C=O$ participates in the solvation of $Na^+$ cations through dipole interactions, widely used for cross-linked GPE
PVDF	$-(CF_2CH_2)_n-$	-30	171	$C-F$ bond contributes to the anodic stability, but does not solvate $Na^+$ cations, used preferentially for the preparation of GPE
PvDF-HFP	$-(CF_2CH_2)_n-(CF_2CF(CF_3))_m-$	-90	135	$C-F$ bond contributes to the anodic stability, but does not solvate $Na^+$ cations, used preferentially for the preparation of GPE
PVC	$-(CH_2CHCl)_n-$	80	220	

the two central S–N bonds providing mechanical flexibility, resulting in a plasticizing effect in the polymer electrolyte. Furthermore, the negative charge is delocalized over several atoms resulting in a weak coordinating power. This is of vital importance in applications where the formation of ion pairs would reduce the number of charge carriers and hence the ionic conductivity.

**Inclusion of Ceramic Additive to Polymer Electrolyte:** Besides the selection of Na salt, other methods can be used to improve the polymer electrolyte performances, such as the inclusion of nanometric ceramic powders (called fillers) that act as solid plasticizers, kinetically inhibiting crystallization and greatly improving the ionic conductivity at RT. The approach is well known since the first report by Scrosati and co-workers<sup>[169]</sup> in 1998, lately intensively studied for application in polymeric lithium batteries.<sup>[170–174]</sup> The same group<sup>[167]</sup> investigated the effect of nanometric  $SiO_2$  to a PEO/NaTFSI mixture. They demonstrated best performances with an EO/Na ratio of 20, and using the 5% wt  $SiO_2$ , giving an ionic conductivity of  $10^{-5}$  S  $cm^{-1}$  and a Na transference number ( $t_{Na^+}$ ) of 0.51. Further improvement in the performances of PEs can be obtained by proper functionalization of the metal oxide additives, for example,  $SiO_2$  nanoparticles covalently bonded to a dense brush of oligo-PEG chains, which outperform that of bare  $SiO_2$  nanoparticles.<sup>[175,176]</sup> Xu et al.<sup>[177]</sup> investigated the use of  $Na_3PS_4$ -polyethylene oxide synthesized by a solution-phase reaction method, obtaining an improved ionic conductivity up to  $9.4 \times 10^{-5}$  S  $cm^{-1}$  at room temperature. The electrolyte has been used to realize  $SnS_2/Na$  solid-state batteries, delivering enhanced electrochemical performance with 230 mAh  $g^{-1}$  after 40 cycles. The good stability of the system was associated to the capacity of PEO to isolate the NPS solid electrolyte and Na metal, alleviating the side reaction between NPS and Na foil.

**Na Polymer Single Ion Conductors:** The use of single ion-conductive polymers (so-called “ionomers”), generally composed by (block co-)polymers with the anion covalently tethered to the essentially immobile polymer backbone, possesses unique features in which the only mobile species is the cation. In such ionomers, no concentration gradients occur allowing the use of high charge/discharge current rates. Additionally, dendrite growth is limited.<sup>[178–182]</sup> Furthermore, with a cation transference equal to 1, it is possible to have comparable performances to an ambipolar electrolyte even with a tenfold reduction

in conductivity. Bronstein et al.<sup>[183]</sup> developed a composite polymer electrolyte consisting of a dispersion of poly(ethylene glycol) (PEG) and  $SiO_2$  nanoparticles, characterized by a RT conductivity of  $10^{-4}$  S  $cm^{-1}$  and a cation transference number of 0.9. Similar approach has been followed by Armand and co-workers<sup>[184]</sup> reporting a solid polymer hybrid electrolyte based on PEO ( $M_w \approx 5 \times 10^6$ ) and PEGDME ( $M_w \approx 250$ ) (1:1, wt) mixture, including  $SiO_2$  functionalized nanoparticles. Two different functionalized systems were tested, the first one employing sodium 2-[(trifluoromethane-sulfonylimido)-N-4-sulfonylphenyl]-ethyl trimethoxysilane anion ( $SiO_2$ -anion) surface functional group and a second one using  $SiO_2$ -anion with a polyethyleneglycol chain ( $SiO_2$ -PEG-anion) (**Figure 12a**). Both systems reached a conductivity of  $2 \times 10^{-5}$  S  $cm^{-1}$  at RT with EO/Na = 40 for the  $SiO_2$ -anion and a ratio of 20:1 for the  $SiO_2$ -PEG-anion system.  $^{23}Na$  and  $^{19}F$  NMR were used to evaluate the mobility of the cation and the anion in the system. Unfortunately, the very short spin-lattice relaxation times (typically less than 1 ms) of the  $^{23}Na$  make the diffusion measurement problematic. However,  $^{19}F$  NMR measurements of anion evidenced that it is effectively not mobile, most likely indicating that the ionic conductivity of the polymer electrolyte can be associated solely with  $Na^+$  cation diffusion.

A similar approach has been proposed by Forsyth and co-workers,<sup>[185–187]</sup> by preparing a “polyelectrolyte” with a backbone functionalized by sulfonyl(tri-fluoromethanesulfonyl) imide anion groups, and quaternary ammonium counter-ions (**Figure 12c**), obtaining a conductivity of  $\approx 10^{-6}$  S  $cm^{-1}$  at 90 °C (**Figure 12d**). The immobilization of the anion on the polymer chain makes the cation the only ionic mobile species in this class of electrolytes, thus minimizing the concentration gradient effect since the ion transference number can approach unity. The utilization of quaternary ammonium cations in ionomers leads to reduced association of counter-ions with sulfonic groups. The bulky ammonium counter-ions have weak ion–ion interactions and additionally, thanks to the mobility of the alkyl chain, act as plasticizers. However, these systems generate an additional problem as a result of the anion tethering, the interactions between the cation and the immobilized anion reduces the cation mobility, typically leading to low conductivity values. Several potential approaches exist to reduce this ion association and promote the mobility of the cation. Zhang et al. recently published a detailed review dedicated to single lithium-ion

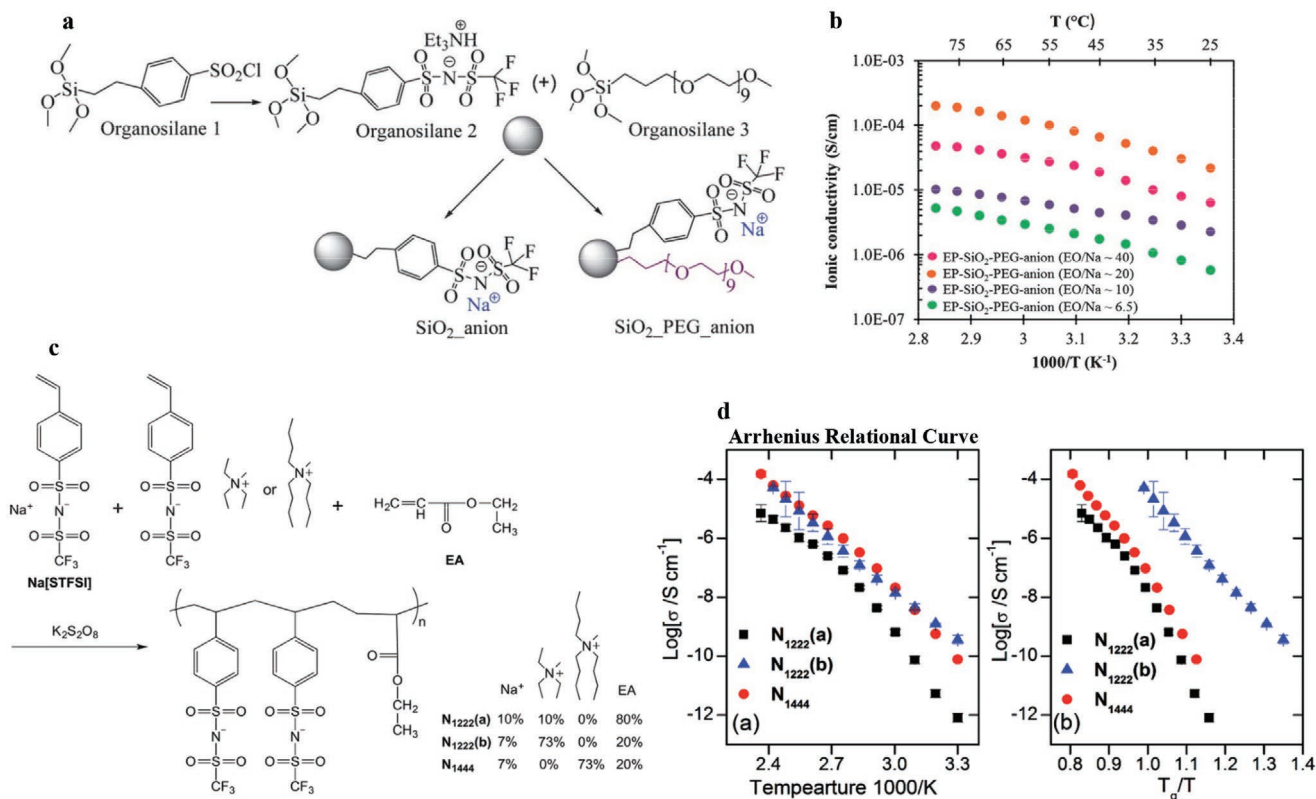


**Figure 12.** a) Schematic representation of the synthesis of inorganic–organic hybrid SiO<sub>2</sub> nanoparticles. b) Ionic conductivity of the polymer electrolytes prepared with SiO<sub>2</sub>-anion nanoparticles and SiO<sub>2</sub>-PEG-anion nanoparticles. Reproduced with permission.<sup>[184]</sup> Copyright 2013, Royal Society of Chemistry. c) Synthetic routes of the ionomers, the initial input molar percentage is listed. d) Ion conductivity of the ionomers  $\log(\sigma)$  versus  $T_g/T$ . Reproduced with permission.<sup>[187]</sup> Copyright 2015, Royal Society of Chemistry.

conducting solid polymer electrolytes whose approaches can also be considered for future Na electrolytes.<sup>[188]</sup>

**Gel-Polymer Electrolytes:** Gel polymer electrolytes (GPE) differentiate from “dry polymer electrolytes” because they incorporate a liquid component serving as plasticizer. Thus, the GPE has intermediate properties between liquid and dry-polymer electrolytes. They are generally characterized by higher conductivity with respect dry polymer electrolytes, being in the range of  $10^{-3}$  S cm<sup>-1</sup>, whereas dry polymer and liquid possess conductivities of  $\approx 10^{-4}$  S cm<sup>-1</sup> and  $\approx 10^{-2}$  S cm<sup>-1</sup> respectively. GPEs are characterized by a reduced flammability and limited electrolyte leakage issues, and in general by higher safety level compared to liquid-based but lower than that of dry polymer electrolytes.<sup>[189]</sup> These characteristics make them extremely appealing as next-generation electrolytes for practical battery applications. This topic has been extensively explored for lithium batteries.<sup>[189]</sup> In SIBs, several polymers have been investigated for the realization of GPEs, including polyethylene oxide (PEO),<sup>[190–193]</sup> perfluorinated sulfonic membranes (NAFION type),<sup>[194–196]</sup> polyacrylonitrile (PAN),<sup>[197,198]</sup> poly(methyl methacrylate) (PMMA),<sup>[199–201]</sup> and polyvinylidene fluoride (PVDF).<sup>[202–210]</sup> The mixture of PEO with short-chain length glyme leads to a homogeneous gel polymer electrolyte with highly isotropic properties. For sodium system, Bhide and Hariharan<sup>[190]</sup> reported the preparation of a PEO:NaPO<sub>3</sub> polymer electrolyte plasticized with PEG400, using an EO:Na ratio of 6:1, investigating the effect of the plasticizer in the range of 30 to 70 wt%,

obtaining conductivity values of  $8.9 \times 10^{-7}$  S cm<sup>-1</sup> at 40 °C. The developed GPE was tested in a sodium battery employing NaCoO<sub>2</sub> as cathode material.<sup>[192]</sup> Superior conductivity values of  $1.1 \times 10^{-4}$  S cm<sup>-1</sup> have been reported by Patel et al.<sup>[191]</sup> using PEO–NaCF<sub>3</sub>SO<sub>3</sub> mixture with succinonitrile (SN) as plasticizer. Kreuer et al.<sup>[211]</sup> proposed the use of perfluorinated sulfonic membranes (fully and half sulfonated poly phenylene-sulfone) for the realization of polyelectrolytes.<sup>[188]</sup> The GPE was prepared by an ion exchange of the membrane in aqueous NaOH or LiOH solution, obtaining exchange levels close to 100%. After water removal and drying, the polymer was swollen with dimethyl sulfoxide (DMSO). The same group has also investigated poly-vinyl phosphonic acid (PVPA2), sulfonated poly-ether ketone (SPEEK) and the n-ethyl- pyrrolidone (NEP) polymers, evidencing that the best conductivity of  $1.1 \times 10^{-3}$  S cm<sup>-1</sup> can be obtained using the full and half sulfonated poly phenylene-sulfone and pyrrolidone as swelling agents.<sup>[211]</sup> Lately, Li's group<sup>[194]</sup> employed a perfluorinated sulfonic membranes in Na-form (PSFA-Na) and a Nafion 115 swollen with EC-PC (1:1 v:v), solvent, obtaining transparent homogeneous membranes. The group showed that Nafion-based GPE is characterized by a conductivity of  $3 \times 10^{-4}$  S cm<sup>-1</sup> at RT, higher than that of PSFA-Na. The Nafion-based GPE was successfully tested in a sodium battery employing Na<sub>0.44</sub>MnO<sub>2</sub> cathode at 45 °C delivering superior capacity with better capacity retention in respect to the conventional liquid electrolyte. A perfluorinated sulfonic membrane, (PFSA-Na), swollen with EC-PC solvents has been

recently reported by Hou et al.<sup>[196]</sup> in a solid-state sodium battery employing a  $\text{Na}_{0.67}\text{Ni}_{0.23}\text{Mg}_{0.1}\text{Mn}_{0.67}\text{O}_2$  cathode displaying excellent cyclic performance up to 1000 cycles with a capacity retention of about 85% at a current density of  $48 \text{ mA g}^{-1}$ . PAN-based GPE have been extensively investigated for lithium battery applications, thanks to the possibility to make homogeneous, hybrid electrolyte films in which the salt and the plasticizer were molecularly dispersed.<sup>[189]</sup> In sodium systems, one of the first attempt of using PAN for GPE has been reported by Osman et al.,<sup>[158]</sup> comparing Li and Na PAN-based GPEs prepared with different salt concentrations. A RT conductivity of  $7.13 \times 10^{-4} \text{ S cm}^{-1}$  was reported for the GPE prepared from PAN + 24 wt%  $\text{NaCF}_3\text{SO}_3$ . PMMA is also one of the most widely investigated polymer host for lithium battery applications<sup>[212,213]</sup> because of its good affinity with organic electrolytes, its amorphous nature, and ability to exhibit a high RT ionic conductivity values. A PMMA-based GPE for sodium battery application with ionic conductivity of  $3.4 \times 10^{-3} \text{ S cm}^{-1}$  was reported by Kumar and Hashmi<sup>[199]</sup> using a 1 M  $\text{NaClO}_4/\text{EC:PC}$  (1:1 v:v) solution as swelling agent and 4 wt% of  $\text{SiO}_2$  nanoparticles. PVdF is one of the most widely investigated polymers for GPEs preparation because it is highly anodically stable due to the presence of a strong electron-withdrawing functional group ( $-\text{C}-\text{F}$ ) and possess an high dielectric constant ( $\epsilon = 8.4$ ), which helps the dissolution of lithium/sodium salts granting high concentration of charge carriers.<sup>[189]</sup> Park et al.<sup>[214]</sup> reported a PVDF-based GPE with a conductivity of  $5.1 \times 10^{-4} \text{ S cm}^{-1}$  at  $25^\circ\text{C}$  using tetraglyme and  $\text{NaCF}_3\text{SO}_3$  as plasticizer and salt respectively.

The GPE was successfully employed for the realization of a Na/GPE/S cell operating at RT. Lately, a similar system was reported by Kim et al.<sup>[202]</sup> showing a continuous increase of the Na/GPE/Na cell resistance with increasing storage time due to unstable passivation layer formation.

*Inclusion of Ceramics in GPE:* One of the main drawbacks of GPE is their poor mechanical properties. To overcome this issue, the inclusion of ceramic additive in the GPE is a widely explored approach to improve the GPE mechanical properties. Aravindan et al.<sup>[203]</sup> investigated the effect of nanosized  $\text{Sb}_2\text{O}_3$  as ceramic filler for GPE obtained by a blend of PVdF and PEMA, reporting a great improvement in the electrolyte conductivity and a decrease of the activation energy. This could be ascribed to the decrease of the crystallinity of the PVdF. The best performance was reported for the composition (in wt%) 23PVDF:10PEMA:27.5EC:27.5DMC:10 $\text{Sb}_2\text{O}_3$  which resulted in a conductivity of  $5.69 \times 10^{-4} \text{ S cm}^{-1}$  at ambient temperature. Goodenough's group<sup>[205]</sup> reported a PVDF-HFP blended with polyvinylpyrrolidone (PVP) in a 65:35 weight ratio and utilizing micrometric  $\text{Sb}_2\text{O}_3$  ceramic additive in 30 wt%. The use of micrometric powder instead to the nanometric ones greatly reduce the cost of the GPE. The obtained polymeric film was swollen with a 1 M  $\text{NaClO}_4/\text{EC:DEC}$  solution resulting in a conductivity of  $6 \times 10^{-3} \text{ S cm}^{-1}$ . Furthermore, the GPE was able to block Na metal dendrites from penetrating the membrane as evidenced by the symmetric Na/Na stripping deposition test (Figure 13a,b). The GPE was successfully employed for the realization of sodium cell using a Berlin-green  $\text{Fe}[\text{Fe}(\text{CN})_6]$  cathode

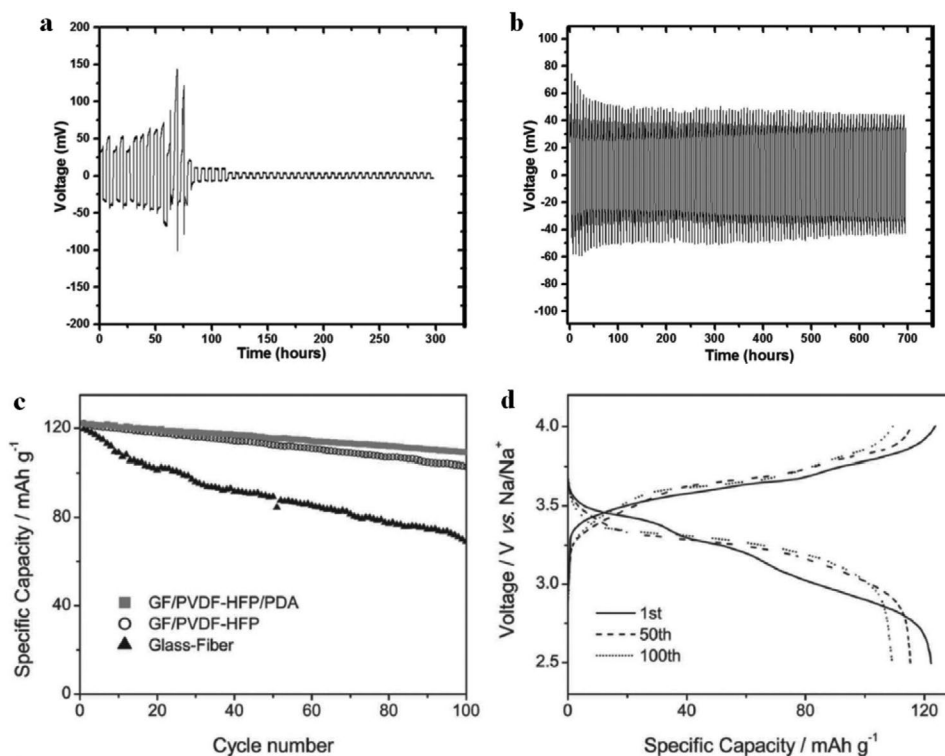


**Figure 13.** Voltage profiles for symmetric cells with sodium metal on both side with: a) pristine polymer electrolyte/separator (PVDF-HFP/PVP)/1 M  $\text{NaClO}_4/\text{EC:DEC}$ ; and b) polymer-composite electrolyte/separator (PVDF-HFP/PVP/ $\text{Sb}_2\text{O}_3$ )/1 M  $\text{NaClO}_4/\text{EC:DEC}$ , at constant current density of  $0.1 \text{ mA cm}^{-2}$ . Reproduced with permission.<sup>[205]</sup> Copyright 2014, Electrochemical Society. c,d) Electrochemical characterization of cells with  $\text{Na}_2\text{MnFe}(\text{CN})_6$  as cathode and glass-fiber paper, GF/PVDF-HFP and GF/PVDF-HFP/PDA as separators. Reproduced with permission.<sup>[206]</sup> Copyright 2015, Wiley.

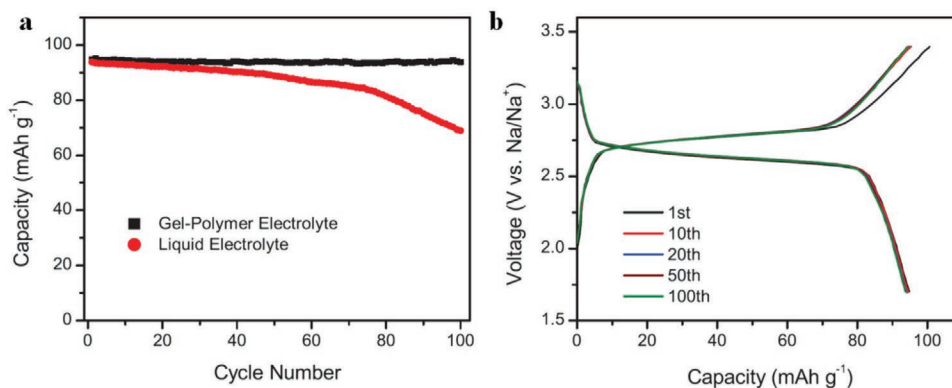


**Figure 14.** Electrochemical properties of the sodium-ion full-cell  $\text{Sb}/\text{Na}_3\text{V}_2(\text{PO}_4)_3$  with liquid electrolyte or gel-polymer electrolyte at 60 °C. a) Cycling performance of the sodium-ion full-cells at a constant current density of 1 C. b) Galvanostatic charge/discharge profiles of the sodium-ion full-cell with the gel-polymer electrolyte at a constant current density of 1 C. Reproduced with permission.<sup>[201]</sup> Copyright 2016, Wiley.

material. The developed cell delivered 115 and 65  $\text{mAh g}^{-1}$  at a current of 24 and 600  $\text{mA g}^{-1}$  respectively.

Lately, the same research group<sup>[206]</sup> reported the fabrication of a gel-polymer/glass-fiber electrolyte employing PVDF-HFP supported by a glass-fiber paper and modified by a polydopamine coating, soaked in a 1 M  $\text{NaClO}_4/\text{PC}$  electrolyte solution. The prepared membrane has a conductivity of  $5.9 \times 10^{-3} \text{ S cm}^{-1}$ , good mechanical strength, excellent thermal stability and a wide electrochemical window stability (stable up to 4.8 V vs  $\text{Na}/\text{Na}^+$ ). The GPE was tested in a sodium cell employing  $\text{Na}_2\text{MnFe}(\text{CN})_6$  as cathode material, and revealed superior electrochemical properties compared to the one employing the bare glass fiber separator [(Figure 13c,d)].

**Cross-Linked GPEs:** The poor mechanical stability is generally a problem for the GPE, and this can be alleviated by the inclusion of ceramic compound in the membrane as described previously. An alternative strategy is to cross-link the polymer used to prepare the GPE greatly improving the mechanical properties. This method is widely explored for lithium battery application.<sup>[189]</sup> Bella et al.<sup>[200]</sup> reported a photopolymerized electrolyte for a sodium-ion battery employing bisphenol A ethoxylate dimethacrylate (BEMA) and poly(ethylene glycol) methyl ether methacrylate (PEGMA) oligomers in a 35:65 weight ratio. The homogeneous transparent polymeric film obtained after UV curing was swollen in a 1 M  $\text{NaClO}_4/\text{PC}$  electrolyte solution, obtaining a GPE with a RT conductivity of  $5 \times 10^{-3} \text{ S cm}^{-1}$ . The GPE was finally successfully tested in sodium battery using  $\text{TiO}_2$  as working electrode. The cell presented relatively low coulombic efficiency in the initial cycles most likely due to residual of reaction products or of the Irgacure 1173 initiator used. A similar preparation process was described by Goodenough's group,<sup>[201]</sup> reporting the preparation of a GPE synthesized by a radical polymerization of methyl methacrylate (MMA) and tetraethylene glycol dimethacrylate (TEGDMA), with 2,2'-azobis(2-methylpropionitrile) (AIBN) initiator. After heating the precursor, the solution was drop-casted onto a porous cellulose membrane (0.1 mm thick) resulting in a transparent polymeric film. The obtained film was swollen in the 1 M  $\text{NaClO}_4/\text{PC:FEC}$  (9:1, vol) electrolyte, resulting in an ionic conductivity of  $6.2 \times 10^{-3} \text{ S cm}^{-1}$  at RT. The prepared GPE was tested in a sodium-ion battery utilizing a Sb-based

anode and a  $\text{Na}_3\text{V}_2(\text{PO}_4)_3$  cathode. The cell employing the GPE showed superior electrochemical performances in comparison to conventional liquid electrolyte (Figure 14a,b).

**IL-Based GPE Ionogels:** In general, GPEs are characterized by a higher conductivity in respect to “dry polymer electrolyte,” but the inclusion of organic solvent as plasticizer (EC, PC, DMC, DEC, etc.) lowers their safety level, compared with “dry polymer electrolytes.” The liquid organic electrolyte is confined by the polymer matrix; however, for volatile solvents, the problems of flammability and electrochemical instability (particularly, at elevated temperatures) exist, limiting the scope of applicability of the corresponding devices. The use of nonvolatile and non-flammable ionic liquids (ILs), instead of organic solvents, is a valuable alternative. Kumar and Hashmi<sup>[215]</sup> reported in 2010 a GPE with an ionic conductivity of  $5 \times 10^{-3} \text{ S cm}^{-1}$ , obtained by a mixture of PVdF-HFP, 1-ethyl 3-methyl imidazolium trifluoromethanesulfonate (EMIMTf) and sodium triflate (NaTf). Hashmi and co-workers<sup>[216]</sup> described a similar GPE composition (PVdF-HFP:EMIMTf:NaTf) while incorporating  $\text{Al}_2\text{O}_3$  and  $\text{NaAlO}_2$  particles as ceramic fillers reporting a conductivity of  $6.3\text{--}6.8 \times 10^{-3} \text{ S cm}^{-1}$  and  $5.5\text{--}6.5 \times 10^{-3} \text{ S cm}^{-1}$  for  $\text{Al}_2\text{O}_3$  and  $\text{NaAlO}_2$  dispersed GPEs respectively. The use of ceramic filler greatly improved the mechanical stability of the GPE. Kumar<sup>[217]</sup> studied the effect of ethylene carbonate and propylene carbonate addition to the PVdF-HFP:EMIMTf:NaTf GPE, and revealed a slightly higher conductivity of  $8.4 \times 10^{-3} \text{ S cm}^{-1}$  at RT. Singh et al.<sup>[218]</sup> investigated the PEO mixture with 1-butyl-3-methylimidazolium methylsulfate (BMIM-MS) and  $\text{NaCH}_3\text{OSO}_3$  salt (NaMS), exploring the compositions  $\text{PEO} + x \text{ wt}\% \text{ BMIM-MS}$  for  $x = 0$  and 20 and  $(\text{PEO} + 10 \text{ wt}\% \text{ NaMS}) + x \text{ wt}\% \text{ BMIM-MS}$  for  $x = 0, 20,$  and 60. The polymer electrolyte membrane containing 60 wt% BMIM-MS showed the higher ionic conductivity of  $1.05 \times 10^{-4} \text{ S cm}^{-1}$  at RT. The obtained GPE was characterized by limited electrochemical window stability, most likely due to the  $\text{CH}_3\text{OSO}_3^-$  decomposition, thus limiting its application in Na-ion batteries. Ionic liquids characterized by higher electrochemical stability, namely N-methyl-N-propylpyrrolidinium (Pyr<sub>13</sub>) with bis(trifluoromethanesulfonyl)imide (TFSI) and bis(fluorosulfonyl)imide (FSI) anion in combination with the PEO, and NaTFSI or NaFSI salts have been reported by Boschin

and Johansson.<sup>[219]</sup> Ternary electrolytes, NaTFSI(PEO)<sub>n</sub>-Pyr<sub>13</sub>TFSI and NaFSI(PEO)<sub>n</sub>-Pyr<sub>13</sub>FSI, with different ratio of EO:Na (*n*), i.e., 6, 9, and 20 containing different wt% of IL (5, 10, and 20) were tested. The study evidenced a general increase of the conductivity value with the increase of the IL content, attributed to the increased number of ionic species, to the role of the IL in enhancing the relative amount of conduction pathways and improving the polymer chain dynamics via a plasticizing effect. The conductivity at RT was lower than 10<sup>-5</sup> S cm<sup>-1</sup>, limiting the applicability of this system. A particular approach for obtaining a gel electrolyte for sodium batteries by simply mixing an IL with SiO<sub>2</sub> nanoparticles has been reported by Forsyth and co-workers;<sup>[220]</sup> the silica-gel type electrolyte (SiO<sub>2</sub>-GE) was compared with a PMMA-gel electrolyte. The latter one was prepared by polymerization of MMA-TEGDA mixture in Pyr<sub>14</sub>TFSI-NaTFSI ionic liquid electrolyte; while the SiO<sub>2</sub>-GE was obtained by mixing of SiO<sub>2</sub> nanoparticles (0.007 μm, 5 wt%) with Pyr<sub>14</sub>TFSI-NaTFSI (95 wt%), evaluating different salt concentration (from 0.1–0.5 M). Both GEs showed good ionic conductivity, i.e., 1.6 × 10<sup>-3</sup> S cm<sup>-1</sup> for the silica-gel electrolyte and 1.1 × 10<sup>-3</sup> S cm<sup>-1</sup> for the PMMA-based GPE but decreasing for increased Na salt concentrations. This behavior is common also in pure IL-based electrolytes.<sup>[221]</sup> It is associated with the higher charge density of the alkali metal cation, leading to the formation of ionic aggregates, thereby reducing the overall ion conductivity, although alkali metal ion transport numbers can actually increase.

### 2.3.2. Inorganic Solid Electrolytes

The research on inorganic compounds for solid-state electrolytes to be used in RT SIBs is mainly focused on glassy materials while NASICON and sodium β'-alumina are conventionally investigated for mid-high temperature application (Table 8).

**Na-β Alumina:** Na-β alumina can be obtained with two distinct crystal structures: β-Al<sub>2</sub>O<sub>3</sub> (hexagonal: P6<sub>3</sub>/mmc; a<sub>0</sub> = 0.559, c<sub>0</sub> = 2.261 mm) and β'-Al<sub>2</sub>O<sub>3</sub> (rhombohedral: R3m; a<sub>0</sub> = 0.560, c<sub>0</sub> = 3.395 mm). The β'-Al<sub>2</sub>O<sub>3</sub> phase was found to give better ionic conductivity than the β-Al<sub>2</sub>O<sub>3</sub> phase. In terms of conductivity, β'-Al<sub>2</sub>O<sub>3</sub> single crystals can reach 0.1 S cm<sup>-1</sup>

at RT, and 1 S cm<sup>-1</sup> at 300 °C. The conductivity decreases by almost five times for polycrystalline β'-Al<sub>2</sub>O<sub>3</sub> (0.2–0.4 S cm<sup>-1</sup>). Furthermore it is hard to get a uniform product because the synthesized β'-Al<sub>2</sub>O<sub>3</sub> is usually mixed with β-Al<sub>2</sub>O<sub>3</sub> which further decrease the conductivity values.<sup>[222]</sup> For these reasons, sodium β'-alumina is generally used in high-temperature batteries such as the high-T Na/S batteries.

**NASICON:** Sodium super ionic conductor (NASICON) is generally characterized by elevated ionic conductivity and can be used as solid-state electrolytes for SIBs. NASICON has a general formula Na<sub>1+2x+y+z</sub>M<sub>x</sub><sup>(II)</sup>M<sub>y</sub><sup>(III)</sup>M<sub>z-x-y</sub><sup>(IV)</sup>Si<sub>2</sub>R<sub>3-2z</sub>O<sub>12</sub> where M is replaced by divalent, trivalent, or tetravalent cations, and R can be Si or As. NASICON structure was firstly studied by Hagman et al.<sup>[223]</sup> in 1960, and afterward by Goodenough<sup>[224]</sup> and Hong.<sup>[225]</sup> This initial investigation evidenced that the NASICON ionic conductivity can be higher than 10<sup>-3</sup> S cm<sup>-1</sup>. Thanks to its good conduction properties NASICON was proposed as an alternative to the β'-alumina for high-temperature Na/S batteries, in fact the 3D conduction pathways of the NASICON is expected to guarantee superior performance in respect to the β'-alumina, which is characterized by 2D conduction pathways. The conductivity of NASICON is strongly related to the Na concentration and crystallographic structure, which is influenced by the size of the M cations. It has been concluded from literature survey<sup>[226]</sup> that the average ionic radius of M cations should be close to the ionic radius of Zr, i.e., Zr = 0.72 Å<sup>[227]</sup> to obtain highly conductive materials, comparable to β- and β'-alumina.<sup>[228,229]</sup> In addition, NASICON materials with the highest sodium ion conductivity contain 3–3.5 mol Na per formula unit showing a monoclinic distortion of the crystallographic lattice.<sup>[226]</sup> One of the first attempt of a RT sodium solid-state batteries employing NASICON electrolyte was reported by Noguchi et al.,<sup>[230]</sup> fabricating an all-solid-state sodium-ion symmetrical battery via combined screen printing and hot pressing using Na<sub>3</sub>Zr<sub>2</sub>Si<sub>2</sub>PO<sub>12</sub> (NASICON) as solid electrolyte and Na<sub>3</sub>V<sub>2</sub>(PO<sub>4</sub>)<sub>3</sub> (NVP) as active electrode materials. The NVP active material was characterized in solid-state sodium half-cells at 80 °C demonstrating its capability to reversibly intercalate sodium at potentials of 1.6 and 3.4 V versus Na/Na<sup>+</sup>. These insertion properties allow the use of NVP as active material for both positive and negative electrodes. The authors reported the electrochemical behavior of the sodium-ion cells cycled at RT within the voltage range of 0.01 and 1.9 V at a current density of 1.2 μA cm<sup>-2</sup>. They showed a first discharge capacity of 68 mAh g<sup>-1</sup>, validating the suitability of NASICON solid-state electrolyte for application in RT SIB. A similar approach has been followed by Lalère et al.<sup>[231]</sup> by developing a symmetrical Na<sub>3</sub>V<sub>2</sub>(PO<sub>4</sub>)<sub>3</sub>/Na<sub>3</sub>Zr<sub>2</sub>Si<sub>2</sub>PO<sub>12</sub>/Na<sub>3</sub>V<sub>2</sub>(PO<sub>4</sub>)<sub>3</sub> full battery characterized by an elevated electrode thickness (300 μm cathode and 130 μm anode thickness) which was assembled by spark plasma sintering at 900 °C. The solid-state cell was tested at 200 °C delivering the 85% of the theoretical capacity (Na<sub>3</sub>V<sub>2</sub>(PO<sub>4</sub>)<sub>3</sub> theoretical capacity 1176 mAh g<sup>-1</sup>) at C/10 with a working voltage of 1.8 V and good capacity retention, for an overall energy density of 1.87 × 10<sup>-3</sup> Wh cm<sup>-2</sup> and a capacity of 1.04 mAh cm<sup>-2</sup>. Based on these initial works, several studies focused on the development of NASICON-based electrolyte characterized by elevated conductivity values have been reported. Ma et al.<sup>[232]</sup> evidenced that the partial substitu-

**Table 8.** Composition, conductivity, and activation energy of selected Na solid electrolytes.

Na-solid-electrolyte	Conductivity	E <sub>a</sub>	Refs.
β-Al <sub>2</sub> O <sub>3</sub>	1.0 S cm <sup>-1</sup> (300 °C)		[222]
β'-Al <sub>2</sub> O <sub>3</sub>	0.2–0.4 S cm <sup>-1</sup> (300 °C)		[222]
Na <sub>3</sub> Zr <sub>2</sub> Si <sub>2</sub> PO <sub>12</sub> (NASICON)	9.4 × 10 <sup>-4</sup> S cm <sup>-1</sup> (25 °C)		[230]
Na <sub>3</sub> PS <sub>4</sub>	2.0 × 10 <sup>-4</sup> S cm <sup>-1</sup> (25 °C)	0.280 eV	[246]
Na <sub>2.375</sub> PS <sub>3.375</sub> Cl <sub>0.675</sub>	1.0 × 10 <sup>-3</sup> S cm <sup>-1</sup> (25 °C)	0.249 eV	[250]
Na <sub>3</sub> PSe <sub>4</sub>	1.16 × 10 <sup>-3</sup> S cm <sup>-1</sup> (25 °C)	0.210 eV	[252]
Na <sub>3</sub> SbS <sub>4</sub>	3.0 × 10 <sup>-3</sup> S cm <sup>-1</sup> (25 °C)	0.250 eV	[253]
Na <sub>2</sub> (Ga <sub>0.1</sub> Ge <sub>0.9</sub> ) <sub>2</sub> Se <sub>4.95</sub>	1.0 × 10 <sup>-5</sup> S cm <sup>-1</sup> (25 °C)	0.630 eV	[256]
Na <sub>3</sub> P <sub>0.62</sub> As <sub>0.38</sub> S <sub>4</sub>	1.46 × 10 <sup>-3</sup> S cm <sup>-1</sup> (25 °C)	0.256 eV	[258]

tion of zirconium with scandium can improve the ionic conductivity of the solid electrolyte, with an optimal composition of  $\text{Na}_3\text{Sc}_{0.4}\text{Zr}_{1.6}\text{Si}_2\text{PO}_{12}$ . Park et al.<sup>[233]</sup> evidenced improved ionic conductivity value for  $\text{Na}_3\text{Zr}_2\text{Si}_2\text{PO}_{12}$  with a 10% Na excess. Song et al.<sup>[234]</sup> reported a  $\text{Na}_{3.1}\text{Zr}_{1.95}\text{Mg}_{0.05}\text{Si}_2\text{PO}_{12}$  NASICON electrolyte exhibiting a RT conductivity of  $3.5 \times 10^{-3} \text{ S cm}^{-1}$ , that was successfully employed for the fabrication of a RT solid-state Na–S cell.

**NASICON Ceramic–Glass Composites:** Nevertheless, one of the main challenges for the application of NASICON in batteries is the elevated sintering temperature, usually as high as 1200 °C, which is needed to interconnect the particles and reduce the grain boundary resistance. This limits the possible scaling up of such system for cost issues; furthermore, the high temperature leads to problem-related to volatilization of light elements and undesirable side reactions with electrode materials. Honma et al.<sup>[235]</sup> proposed the use of glass–ceramic mixtures composed of  $\text{Na}_3\text{Zr}_2\text{Si}_2\text{PO}_{12}$  and 60 $\text{Li}_2\text{O}$ –10 $\text{Nb}_2\text{O}_5$ –30 $\text{P}_2\text{O}_5$  glass. It was found that the mixture of 90 wt.%  $\text{Na}_3\text{Zr}_2\text{Si}_2\text{PO}_{12}$ –10 wt.% 60 $\text{Li}_2\text{O}$ –10 $\text{Nb}_2\text{O}_5$ –30 $\text{P}_2\text{O}_5$  glass calcined at 900 °C for 10 min is characterized by a  $\sigma = 1.2 \times 10^{-4} \text{ S cm}^{-1}$  at RT. A similar approach has been proposed by Noi et al.<sup>[236]</sup> successfully reducing the sintering temperature at 900 °C using a 4.8%  $\text{Na}_3\text{BO}_3$  additive to  $\text{Na}_3\text{Zr}_2\text{Si}_2\text{PO}_{12}$  NASICON electrolyte, resulting in a conductivity of  $\approx 1.9 \times 10^{-3} \text{ S cm}^{-1}$  at RT. Suzuki et al.<sup>[237]</sup> lowered the sintering temperature of a  $\text{Na}_{1+x}\text{Zr}_2\text{Si}_x\text{P}_{3-x}\text{O}_{12}$  (NASICON)-based solid electrolytes with a  $\text{Na}_3\text{BO}_3$  additive at 700 °C.

**Glassy Materials:** Glassy materials are extremely interesting candidates for solid-state electrolytes, offering several advantages with respect to the crystalline ones such as wide range selection of compositions, isotropic properties, reduced grain boundaries issue, and easy film formation. They are generally characterized by a low melting temperature ( $T_m$ ) and/or glass transition temperature ( $T_g$ ), and for that reason can be molded to a desired shape providing a good contact to the entire surface area of small-particle cathodes.<sup>[238]</sup> Furthermore, they generally do not require high-temperature sintering process like  $\beta''$ -alumina or NASICON; instead isostatic pressure at RT is generally sufficient to ensure a good interphase interaction between electrode and electrolyte especially with sulfide-based materials. Because of the so-called open structure, the ionic

conductivity of amorphous materials is also generally higher. In addition, single-ion conduction can be realized because glassy materials belong to the so-called decoupled systems in which the mode of ion conduction relaxation is decoupled from the mode of structural relaxation. Amorphous or glassy materials are thus the most promising solid electrolytes candidates with single-ion conduction and high ionic conductivities.<sup>[239]</sup> Electrolytes of glassy systems denoted by the formula  $\text{Li}_2\text{O}$ – $\text{MO}_x$ <sup>[240–242]</sup> (M could be Si, P, B, etc.) have a high degree of disorder in the network structure. In 1966<sup>[242]</sup> an  $\text{Li}_2\text{O}$ – $\text{SiO}_2$ – $\text{B}_2\text{O}_3$  mixture was investigated showing an ionic conductivity of  $4 \times 10^{-4} \text{ S cm}^{-1}$  at 350 °C, revealing that the glassy structure could provide high ionic conductivity. However, to be practically applied at ambient temperature, extensive improvements are required. The sulfide glass-ceramic electrolytes were proposed to enhance the ionic conductivity at lower temperature. Sulfide glass-ceramic electrolytes for lithium batteries application have been studied comprehensively due to their outstanding ionic conductivity, wide electrochemical window and good mechanical characteristics.<sup>[243–245]</sup> In contrast, the research on Na analogues is in its infancy. In fact, only in 2012, Hayashi's group inspired by the research on  $\text{Li}_2\text{S}$ – $\text{P}_2\text{S}_5$  system, produced for the first time a sulfide glass-ceramic electrolyte for a sodium battery. The cubic  $\text{Na}_3\text{PS}_4$  phase was obtained from the glassy state by crystallization at high temperature (270 °C);<sup>[246]</sup> the glass component of the compound does not completely vanish by crystallization, and thus the remaining glass part have an important role in stabilizing a high-temperature phase, cubic  $\text{Na}_3\text{PS}_4$ , for that reason the material has been called glass ceramic. The study showed that the obtainment of a cubic phase upon thermal treatment (**Figure 15a**) is fundamental to obtain high conductivity values whereas the pure glassy state had a lower conductivity value. The glass ceramic containing the cubic  $\text{Na}_3\text{PS}_4$  phase has a conductivity of  $2 \times 10^{-4} \text{ S cm}^{-1}$  at RT and an activation energy of 27 kJ mol<sup>-1</sup>, whereas purely amorphous  $\text{Na}_3\text{PS}_4$  glass pellet has a conductivity of  $6 \times 10^{-6} \text{ S cm}^{-1}$  and an activation energy of 47 kJ mol<sup>-1</sup> under the same conditions. Furthermore, the electrolyte showed a good electrochemical stability against sodium metal and a wide electrochemical voltage window up to 5 V (**Figure 15b**). Hayashi's group also demonstrated the suitability of  $\text{Na}_3\text{PS}_4$  glass–ceramic electrolyte in an all-solid-state rechargeable sodium ion cell employing a sodiated tin anode

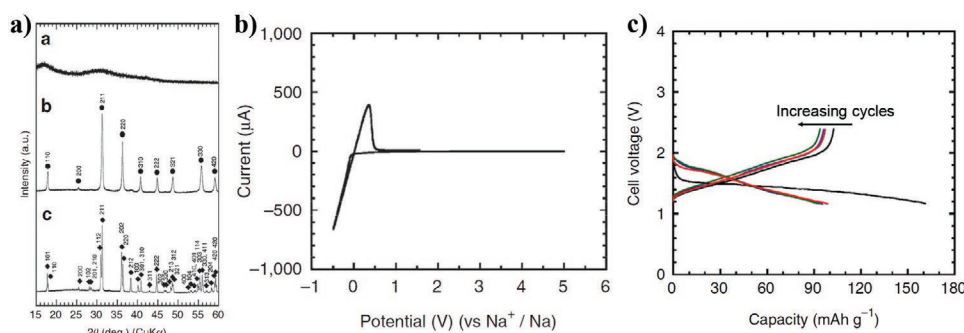


**Figure 15.** a) XRD patterns of the  $\text{Na}_3\text{PS}_4$  glass, b) glass-ceramic sample heated at 270 °C, c) and glass-ceramic sample heated at 420 °C. Closed circles and diamonds, respectively, denote the diffraction peaks attributable to the cubic  $\text{Na}_3\text{PS}_4$  phase and the tetragonal  $\text{Na}_3\text{PS}_4$  phase (JCPDS #081-1472). b) Cyclic voltammogram of the  $\text{Na}/\text{Na}_3\text{PS}_4/\text{SS}$  cell. Scan rate  $5 \text{ mV s}^{-1}$ , 25 °C. c) Charge–discharge curves of the all-solid-state rechargeable sodium cell  $\text{Na-Sn}/\text{Na}_3\text{PS}_4/\text{TiS}_2$ . 25 °C current density  $0.013 \text{ mA cm}^{-2}$ . Reproduced with permission.<sup>[246]</sup> Copyright 2012, Springer Nature.

(Na–Sn), Na<sub>3</sub>PS<sub>4</sub> glass–ceramic electrolyte and a TiS<sub>2</sub> cathode material. The Na–Sn/Na<sub>3</sub>PS<sub>4</sub>/TiS<sub>2</sub> cell was able to deliver a reversible capacity of about 90 mAh g<sup>-1</sup> with a cycling stability of 10 cycles (Figure 15c). Subsequently, the same research group verified a higher conductivity of the Na<sub>3</sub>PS<sub>4</sub> electrolyte<sup>[247]</sup> ( $4.6 \times 10^{-4}$  S cm<sup>-1</sup>, 56% improvement with respect to the previously reported result) can be obtained using high purity Na<sub>2</sub>S (99.1 wt% compared to 95.1 wt% used previously), optimizing the ball milling time (1.5 h) and thermal treatment time (1 h at 270 °C). More recently, Hayashi's group reported that, by using amorphous TiS<sub>3</sub><sup>[248]</sup> at the cathode, instead of the TiS<sub>2</sub> used in the previous study, higher capacity can be obtained (300 mAh g<sup>-1</sup> three times higher than the initial report) for the Na<sub>15</sub>Sn<sub>4</sub>/Na<sub>3</sub>PS<sub>4</sub>/a-TiS<sub>3</sub> cell configuration.

Yu et al.<sup>[249]</sup> performed a detailed DFT-based MD simulations indicating that an electrolyte characterized by elevated Na vacancies, possesses superior Na-ion mobility in both cubic and tetragonal phases; this was further confirmed by <sup>23</sup>Na solid-state NMR. The synthesis of Na<sub>3-x</sub>PS<sub>5</sub> materials with higher vacancy concentrations, for instance by halogen replacement of sulfur, may lead to even larger bulk Na-ion conductivities. The hypothesis was experimentally verified by Chu et al.<sup>[250]</sup> preparing a Cl-doped tetragonal Na<sub>3</sub>PS<sub>4</sub> (Na<sub>3-x</sub>PS<sub>4-x</sub>Cl<sub>x</sub>) solid electrolyte with a RT Na<sup>+</sup> conductivity exceeding 1 mS cm<sup>-1</sup>. The interface stability of the Na<sub>3</sub>PS<sub>4</sub> electrolyte against sodium metal was studied in detail by Janek's group<sup>[251]</sup> using time-resolved impedance and polarization resistance measurements together with in situ X-ray photoemission spectroscopy. The study evidenced that Na<sub>3</sub>PS<sub>4</sub> is unstable against Na metal, resulting in continuous growth of the solid electrolyte interphase layer with the formation of electronically insulating sodium sulfide and sodium phosphide, increasing the cell resistance and strongly deteriorating the cell performance. Besides the Na<sub>3</sub>PS<sub>4</sub>, several other sodium solid glassy-electrolytes have been proposed and investigated. Zhang et al.<sup>[252]</sup> investigated the Na<sub>3</sub>PSe<sub>4</sub> selenium chalcogenide (cubic phase, *I*-43 *m* space group) obtaining an ionic conductivity of 1.16 mS cm<sup>-1</sup> at RT and a low activation energy of 0.21 eV. The excellent properties of the compound were assigned to the large unit cell and the high polarizability of the Se ion providing fast Na<sup>+</sup> transport pathways in the 3D channels. The same group synthesized a new tetragonal Na<sub>3</sub>SbS<sub>4</sub> phase [(Figure 16a–c)], characterized by a high ionic conductivity of 3 mS cm<sup>-1</sup> at RT.<sup>[253]</sup> The same material was concurrently described by Liang and co-workers,<sup>[254]</sup> and Hong and co-workers<sup>[255]</sup> reporting a ionic conductivity of 1 mS cm<sup>-1</sup> and 1.1 mS cm<sup>-1</sup> respectively at RT. Hong and co-workers<sup>[255]</sup> reported scalable solution processes utilizing methanol or water to solubilize the Na<sub>3</sub>SbS<sub>4</sub> that, upon solvent elimination, still exhibits high conductivities of 0.1–0.3 mS cm<sup>-1</sup>. The proposed solution process was successfully employed to coat a NaCrO<sub>2</sub> cathode material, dramatically improving the electrochemical performance in all-solid-state batteries (Figure 16d).

Besides the studies on single pure phases, much effort has been dedicated to the investigation of binary or ternary systems. Kim et al.<sup>[256]</sup> proposed a ternary system of Na<sub>2</sub>Se–Ga<sub>2</sub>Se<sub>3</sub>–GeSe<sub>2</sub> providing a conductivity higher than 10<sup>-5</sup> S cm<sup>-1</sup> for the Na<sub>2</sub>(Ga<sub>0.1</sub>Ge<sub>0.9</sub>)<sub>2</sub>Se<sub>4.95</sub> composition. Tanibata et al.<sup>[257]</sup> investigated the mixture of (100-*x*) Na<sub>3</sub>PS<sub>4</sub>-*x*Na<sub>4</sub>Si<sub>4</sub> (mol%) glass-ceramics from the 0 to 8% of Na<sub>4</sub>Si<sub>4</sub>, showing that the 94Na<sub>3</sub>PS<sub>4</sub>·6Na<sub>4</sub>Si<sub>4</sub>

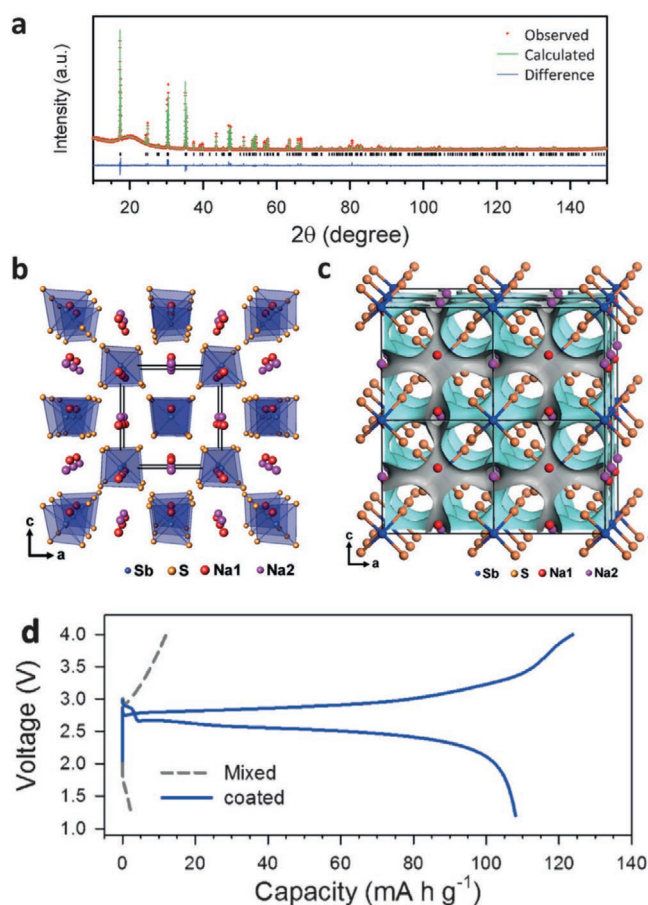


**Figure 16.** a) X-ray Rietveld refinement profile for the Na<sub>3</sub>SbS<sub>4</sub> powder. b) Crystal structure of Na<sub>3</sub>SbS<sub>4</sub> with the unit cell outlined. c) 3D bond valence map isosurfaces for Na<sub>3</sub>SbS<sub>4</sub> with an isovalue of  $\pm 0.3$  v.u. d) Comparison of the initial charge–discharge voltage profiles (50  $\mu$ A cm<sup>-2</sup>, 30 °C) of the Na–Sn/Na<sub>3</sub>SbS<sub>4</sub>/NaCrO<sub>2</sub> all-solid-state cells employing the mixed electrode (gray dash line) and the Na<sub>3</sub>SbS<sub>4</sub>-coated NaCrO<sub>2</sub> electrode (blue line). Reproduced with permission.<sup>[255]</sup> Copyright 2016, Wiley.

composition has an ionic conductivity value two times higher compared to the neat Na<sub>3</sub>PS<sub>4</sub>·electrolyte. The Rietveld analysis of the cubic Na<sub>3</sub>PS<sub>4</sub> in the 94Na<sub>3</sub>PS<sub>4</sub>·6Na<sub>4</sub>Si<sub>4</sub> evidenced a larger site-occupancy of Na<sub>2</sub> sites than that in the pure Na<sub>3</sub>PS<sub>4</sub> glass-ceramic, indicated as the parameter for the improved Na<sup>+</sup> conductivity. Yu et al.<sup>[258]</sup> studied the Na<sub>3</sub>P<sub>1-x</sub>As<sub>x</sub>S<sub>4</sub> (0  $\leq x \leq 1$ ) binary compounds obtaining a conductivity of 1.46 mS cm<sup>-1</sup> at RT for  $x = 0.38$  (i.e., Na<sub>3</sub>P<sub>0.62</sub>As<sub>0.38</sub>S<sub>4</sub>), which is higher than the pure Na<sub>3</sub>PS<sub>4</sub> and Na<sub>3</sub>SeS<sub>4</sub> compounds. The behavior of the conductivity with respect to Na<sub>3</sub>PS<sub>4</sub>:Na<sub>3</sub>SeS<sub>4</sub> ratio is influenced by variations in the Na–S bond length and the Na migration energy. In this regard, Na<sub>3</sub>PS<sub>4</sub> is characterized by a lower Na migration energy while Na<sub>3</sub>SeS<sub>4</sub> by a longer Na–S bond allowing an easier diffusion path for the Na<sup>+</sup> ion, and the ratio  $x = 0.38$  was found to be the best compromise between these two parameters. Moisture stability of Na<sub>3</sub>P<sub>1-x</sub>As<sub>x</sub>S<sub>4</sub> binary compounds was also investigated<sup>[259]</sup> demonstrating that the inclusion of arsenic greatly enhances the moisture stability of Na<sub>3</sub>P<sub>1-x</sub>As<sub>x</sub>S<sub>4</sub>, shifting the reaction products from the easy-forming oxy-sulfides (such as Na<sub>3</sub>POS<sub>3</sub> and Na<sub>3</sub>PO<sub>2</sub>S<sub>2</sub> with H<sub>2</sub>S release) to the difficult-forming

hydrates (such as  $\text{Na}_3\text{P}_{1-x}\text{As}_x\text{S}_4 \cdot n\text{H}_2\text{O}$  with  $n = 8$  and/or  $9$ ). This effect is attributed to the weaker As–O affinity compared to that of P–O. Adams and co-workers<sup>[260]</sup> systematically studied the doping of  $\text{Na}_3\text{PS}_4$  with  $\text{Ge}^{4+}$ ,  $\text{Ti}^{4+}$ ,  $\text{Sn}^{4+}$  and thereby optimizing the processing of these phases. The reported DFT calculation indicated that larger dopant ions increase the overcrowding of Na sites, rising the Na site energy, which has the beneficial effect of lowering the effective migration barrier for interstitialcy like motion, while it will also tend to slightly destabilize the doped phases. Hence, from the calculations, Sn-doping appeared to be particularly promising. In agreement with the calculation, the highest ionic conductivity value of  $2.5 \times 10^{-4} \text{ S cm}^{-1}$  was achieved for the  $\text{Na}_{3.1}\text{Sn}_{0.1}\text{P}_{0.9}\text{S}_4$  compound.

**Solid Electrolyte Interphase Optimization Approaches:** A different approach to optimize the interphase for solid-state sodium-ion batteries has been proposed by Liu et al.,<sup>[261]</sup> reporting the use of a “toothpaste-like electrode” composed by a layered oxide  $\text{Na}_{0.66}\text{Ni}_{0.33}\text{Mn}_{0.67}\text{O}_2$ , super P carbon additive and  $\text{Py}_{14}\text{FSI}$  ionic liquid. The prepared composite was directly cast on a  $\text{Na}\beta\text{-Al}_2\text{O}_3$  ceramic pellet without the need of sintering because the ionic conduction is granted by the presence of the ionic liquid in the “toothpaste-like electrode”. The assembled battery, tested at  $70^\circ\text{C}$  temperature, showed a superior stability and high reversibility, with a capacity retention of 90% after 10 000 cycles at  $6\text{C}$  ( $528 \text{ mA g}^{-1}$ ) rate. Furthermore, the cell configuration has been tested with high active material mass loading ( $6 \text{ mg cm}^{-2}$ ) and once again proved a capacity retention of 73.6% (initial delivered capacity of  $72 \text{ mAh g}^{-1}$ ) at a current rate of  $2\text{C}$  ( $176 \text{ mA g}^{-1}$ ) over 650 cycles. A similar approach has been used by Passerini and co-workers<sup>[262]</sup> combining a  $\text{Na}_3\text{Si}_2\text{Y}_{0.16}\text{Zr}_{1.84}\text{PO}_{12}$  NASICON solid electrolyte with a  $\text{NaTFSI-Py}_{14}\text{TFSI}$  ionic liquid electrolyte revealing that coating the ceramic conductor surface with an ionic liquid does not lead to any practical synergistic behavior between the solid and IL electrolyte. The authors suggested that a functionalization of the ceramic surface and/or ionic liquid, aiming to largely promote the  $\text{Na}^+$  cation transferring at the NASICON/ $\text{Py}_{14}\text{TFSI}$  interphase can lead to a beneficial effect. Another interesting approach has been suggested by Goodenough and co-workers,<sup>[263]</sup> proposing the inclusion of an interfacial polymeric interlayer between the metallic-sodium anode and the ceramic electrolyte, thus improving the wettability of the sodium on the interfacial interlayer. This in turn suppresses the Na dendrite formation and growth. The same polymer, a cross-linked poly(ethylene glycol) methyl ether acrylate (CPMEA)<sup>[264]</sup> was previously successfully used in lithium solid-state batteries.

### 3. Electrode/Electrolyte Interphases in Sodium Batteries

Interphases are extremely important in high-energy SIBs, as well as LIBs, which electrodes operates outside the stability window of the electrolytes. As a matter of fact, the success of LIBs is bound to the development of electrode/electrolyte interphases—the SEI on the negative electrode is the most famous—which prevent the reduction and/or oxidation of the electrolyte by avoiding electron transfer across them. The use of additives to the electrolyte solution is a well-established method to tune the inter-

phase properties and improve the battery performance.<sup>[265,266]</sup> In this section, the electrode/electrolyte interphases in SIBs and the effect of additives will be discussed. Because there is not a clear delineation between an additive and a cosolvent/salt in the literature, an arbitrary threshold of 10% (by wt% or vol%) is adopted.

#### 3.1. Negative Electrodes

The building blocks for the negative electrode/electrolyte interphase layer are usually obtained from reduction processes. Thus, the selection of the electrolyte composition, being the main source of the SEI building blocks, is of fundamental importance. The inclusion of additives is a widely used method to tune the SEI composition. Additives for negative electrodes usually feature higher reduction potential compared to the electrolyte components (solvents and salts). Accordingly, they preferentially get reduced into insoluble solids, covering the anode active materials and thereby deactivating further side reactions of the electrolyte constituents. As for Li-based additives, the LUMO energy, electron affinity (EA), ionization potential (IP) and chemical hardness ( $\eta$ ) could be considered as trustworthy descriptors to predict as well as screen these types of additives.<sup>[267]</sup> For instance, LUMO and EA describe the thermodynamic ability to accept a new electron and are utilized to evaluate the reduction potential, whereas  $\eta$  is a measure of reaction resistance and can serve as an indicator of the kinetics.<sup>[267]</sup> Dipole moment ( $\mu$ ), and the binding energy with a Li cation (BE) were also introduced, showing a higher  $\mu$  leads to a stronger nonbonding interaction with  $\text{Li}^+$ , whereas weak binding between the additive and the lithium cation ensures the rapid formation of the SEI.<sup>[268]</sup> In the following, the investigations on the SEI formation on  $\text{Na}^\circ$ , carbonaceous, and other negative electrodes for Na-batteries are reviewed, with particular regards to the electrolyte composition, including additives (Table 9).

##### 3.1.1. Sodium

The use of sodium metal as the negative electrode grants high theoretical specific capacity ( $1166 \text{ mAh g}^{-1}$ ) and low redox potential ( $-2.714 \text{ V vs SHE}$ ),<sup>[269–273]</sup> yielding to high energy batteries. In order to exploit these benefits in Na-metal batteries such as  $\text{Na-O}_2$ ,<sup>[274–276]</sup>  $\text{Na-S}$ ,<sup>[277,278]</sup> and  $\text{Na-CO}_2$ ,<sup>[279]</sup> the challenges related to dendritic metal growth and unwanted parasitic reactions at the electrode/electrolyte interphase need to be addressed. Similarly to Li metal batteries, the formation of a compact solid electrolyte interphase (SEI) layer, offering high mechanical stability, high ionic conductivity, and high impermeability to the electrolyte solvent, is a prerequisite for the long-term cycling of sodium metal batteries (SMBs).<sup>[280]</sup> In 1998, Peled proposed that for the spontaneously formed SEI on alkali metal electrodes to be protective, the molar volume of the SEI compounds must be larger than that of the metal.<sup>[281–283]</sup> In such a case, the corrosion products can, in fact, cover entirely the metal surface to form a continuous passivation layer disabling the further reaction. However, it must be considered that the electrolyte decomposition, and the associated SEI formation, may also occur upon battery operation.

**Table 9.** Summary of investigated electrolytes employing additives, and their effects on the electrochemical performance of SIBs (RT, room temperature; N-HCSs, nitrogen-doped hollow carbon nanospheres; AB, acetylene black; CB, carbon black; C, carbon; P, phosphorus; a-P, amorphous phosphorus; VGCF, vapor ground carbon fibers; CNF, carbon nanofiber).

Additive	Electrolyte formulation	Anode material	Voltage [V]	Capacity [mAh g <sup>-1</sup> ] (specific current or rate)	Cycle / # T [°C]	Capacity retention [%] <sup>a)</sup>	Refs.
FEC	1 M NaClO <sub>4</sub> /PC + 2 vol% FEC	HC	0–2	210 (25 mA g <sup>-1</sup> )	50 (RT)	+46	[372]
	1 M NaPF <sub>6</sub> /PC + 0.5% FEC			217 (25 mA g <sup>-1</sup> )	80 (RT)	+43	[303]
	1 M NaClO <sub>4</sub> /PC + 2 vol% FEC	N-HCSs	0.01–2	136 (200 mA g <sup>-1</sup> )	2600 (RT)	+60	[373]
	1 M NaPF <sub>6</sub> /PC + 5 wt% FEC	AlSb	0.005–1.3	300 (0.13 C)	20 (RT)	+67	[28]
	1 M NaPF <sub>6</sub> /EC:DEC (1:1, vol) + 5 vol% FEC	Sn <sub>3</sub> N <sub>4</sub> /AB	0.001–3	270 (50 mA g <sup>-1</sup> )	50 (RT)	+35	[374]
	1 M NaClO <sub>4</sub> /EC:PC (1:1, vol) + 5 vol% FEC	Mo <sub>3</sub> Sb <sub>7</sub> /AB	0–2	240 (100 mA g <sup>-1</sup> )	70 (RT)	+37	[375]
	1 M NaClO <sub>4</sub> /EC:DEC (1:1, vol) + 5 vol% FEC	Sn <sub>4+x</sub> P <sub>3</sub>	0–1.5	600 (100 mA g <sup>-1</sup> )	50 (RT)	+88	[376]
	1 M NaClO <sub>4</sub> /EC:DEC (1:1, vol) + 5 wt% FEC	Sn <sub>4</sub> P <sub>3</sub>	0–1.5	718 (0.15C)	50 (RT)	+97	[328]
	1 M NaPF <sub>6</sub> /EC:DMC (1:2, vol) + 5 vol% FEC	Sn–S–C	0.01–2	415 (100 mA g <sup>-1</sup> )	50 (RT)	+78	[377]
	1 M NaClO <sub>4</sub> /EC:DEC (1:1, vol) + 5 vol% FEC	SiC–Sb–C	0.01–2	492 (mA g <sup>-1</sup> )	70 (RT)	+50	[378]
	1 M NaPF <sub>6</sub> /EC:DEC (1:1, wt) + 5 wt% FEC	SnSb–CNF	0–2	345 (0.2C)	205 (RT)	+57	[379]
	1 M NaPF <sub>6</sub> /EC:DMC (1:1, vol) + 5 vol% FEC	SnCNF	0.01–0.8	189 (85 mA g <sup>-1</sup> )	45 (25)	+43	[380]
	1 M NaPF <sub>6</sub> /EC:DEC + 5% FEC	Sb/C	0–2	575 (100 mA g <sup>-1</sup> )	80 (RT)	+94	[27]
	1 M NaClO <sub>4</sub> /PC + 5 wt% FEC	Mo <sub>3</sub> Sb <sub>7</sub>	0–2	150 (3.5 C)	100 (RT)	+12	[381]
	1 M NaClO <sub>4</sub> /PC + 5 wt% FEC	Ge	0–1	280 (1 C)	50 (RT)	+94	[382]
	1 M NaClO <sub>4</sub> /PC + 5% FEC	Sb/CB/VGCF-S	0.02–1.5	576 (0.5 C)	150 (25)	+18	[26]
	1 M NaPF <sub>6</sub> /EC:DEC + 10% FEC	a-P/CB	0–2	1200 (250 mA g <sup>-1</sup> )	60 (RT)	+11	[383]
	1 M NaClO <sub>4</sub> /EC:PC (1:1, vol) + 2 wt% FEC	Sb/Cu <sub>2</sub> Sb–TiC–C	0–2	240 (100 mA g <sup>-1</sup> )	50 (RT)	+27	[374]
	1 M NaClO <sub>4</sub> /EC:PC (1:1, vol) + 2 vol% FEC	SnSb–TiC–AB	0–1.5	183 (100 mA g <sup>-1</sup> )	70 (RT)	+14	[384]
	1 M NaClO <sub>4</sub> /EC:PC (1:1, vol) + 2 vol% FEC	Cu <sub>6</sub> Sn <sub>5</sub> –TiC–C	0–2	150 (0.2 C)	100 (RT)	+60	[385]
1 M NaClO <sub>4</sub> /EC:PC (1:1, vol) + 2 vol% FEC	FeSb–TiC–AB	0–2	210 (100 mA g <sup>-1</sup> )	100 (RT)	+52	[386]	
FEC+CsPF <sub>6</sub>	0.8 M NaPF <sub>6</sub> + 0.05 M RbPF <sub>6</sub> /EC:PC (1:4, vol) + 2 wt% FEC	HC	0.01–2	293 (0.1 C)	100 (25)	+17	[387]
FEC+RbFP <sub>6</sub>	0.8 M NaPF <sub>6</sub> + 0.05 M RbPF <sub>6</sub> /EC:PC (1:4 vol) + 2 wt% FEC	HC	0.01–2	283 (0.1 C)		+15	
FEC+TMSP	1 M NaClO <sub>4</sub> /EC:PC (1:1, vol) + 5 wt% FEC + 0.5 wt% TMSP	Sn <sub>4</sub> P <sub>3</sub> /C	0–1.5	500 (0.1 C)	50 (RT)	+64	[388]
VC	1 M NaPF <sub>6</sub> /EC:DEC (1:1, vol) + 1 vol% VC	Black P/AB	0–2	1484 (125 mA g <sup>-1</sup> )	23 (RT)	+27	[389]

<sup>a)</sup>Capacity retention change after the addition of the additive.

Though the research account so far recorded is limited, several efforts have been made to understand the SEI layer in SMBs, including the formation and growth mechanisms, chemistry, characteristics, and functions. Palacin and co-workers<sup>[280]</sup> have compared the stripping/plating performance of Li/Li and Na/Na symmetric cells using 1 M LiPF<sub>6</sub> in EC<sub>0.5</sub>DMC<sub>0.5</sub> (LP30) and 1 M NaPF<sub>6</sub> in EC<sub>0.5</sub>DMC<sub>0.5</sub> and EC<sub>0.45</sub>PC<sub>0.45</sub>DMC<sub>0.1</sub>, respectively. While the Li/Li cells demonstrated low polarization and smooth charge/discharge profiles at current densities of 0.1 and 1 mA cm<sup>-2</sup>, large overpotential values were recorded for the Na/Na cells regardless of the nature of the electrolyte even at 0.1 mA cm<sup>-2</sup>. FTIR analysis confirmed the presence of a stable SEI on Li, while for the Na electrode a huge variation in the composition after polarization was evidenced. This finding was further corroborated by ex situ SEM images of the cycled electrode reported in the same work.<sup>[269]</sup> Due to the intrinsic high resistance towards reduction, ether-based solvents are among the most favored components of electrolytes for alkali-metal batteries.

Cui et al.<sup>[60]</sup> reported the use of 1 M NaPF<sub>6</sub> salt in various glymes (mono-, di-, and tetraglyme), EC:DEC and EC:DMC. Very high coulombic efficiencies for the Na stripping-deposition process, i.e., greater than 99.9%, were obtained with all glymes. In the same work, various salts (NaPF<sub>6</sub>, NaTFSI, NaFSI, NaOTf, NaClO<sub>4</sub>) dissolved in diglyme were evaluated, evidencing that NaPF<sub>6</sub> offers the best performance, i.e., the stable cycling of Na metal for over 300 cycles at 0.5 mA cm<sup>-2</sup>. The chemical composition of the SEIs on Na electrodes upon cycling in NaPF<sub>6</sub> in diglyme and EC:DEC was examined by XPS (Figure 17a,b). The detailed depth profile and elemental analysis evidenced that the SEI layer formed in diglyme is thinner (but enough accumulated volume to cover the Na surface) and uniform, composed mainly of inorganic Na<sub>2</sub>O and NaF species, while the one formed in EC:DEC is thicker and composed by mixed inorganic–organic compounds, making it more permeable towards the electrolyte, i.e., more prone to continuous breaking and formation. On the contrary the

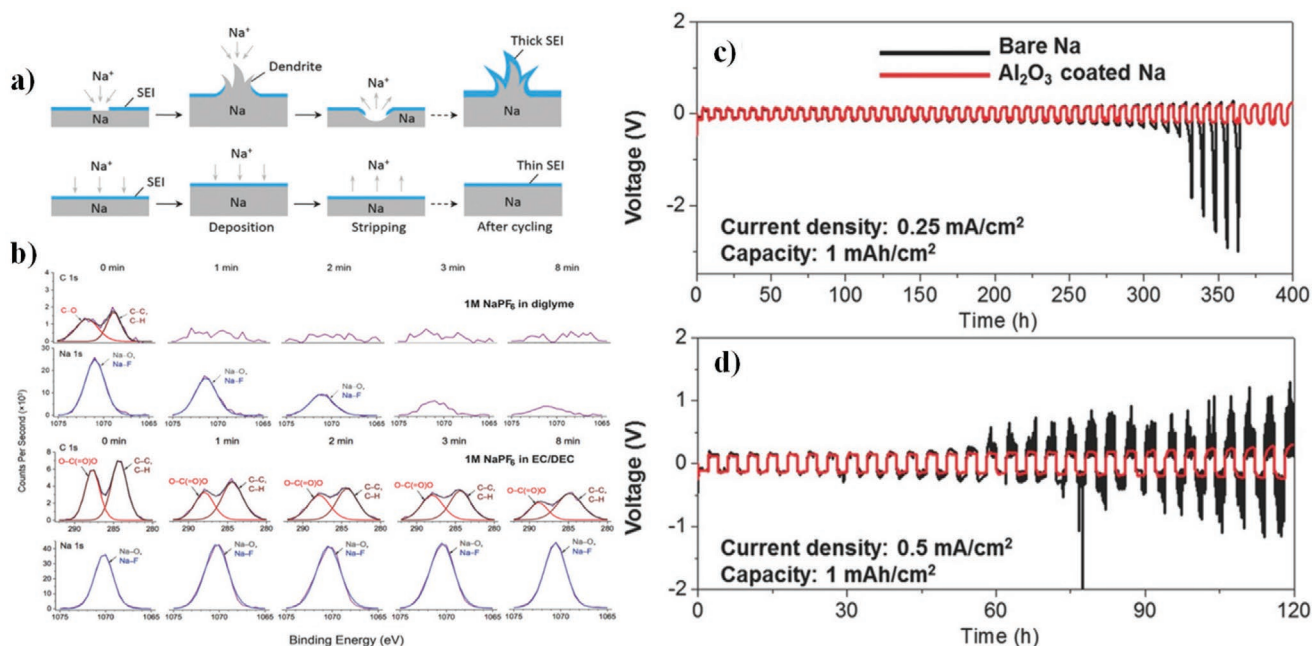


**Figure 17.** a) Schematic illustration of stripping/plating process of Na<sup>0</sup>-metal anode. b) XPS analysis of SEI layers on Na<sup>0</sup>-metal in diglyme and EC:DEC electrolytes. Reproduced with permission.<sup>[60]</sup> Copyright 2015, American Chemical Society. c,d) Cycling performance of symmetric cells using Al<sub>2</sub>O<sub>3</sub>-coated Na metal and bare Na metal at a current density of c) 0.25 mA cm<sup>-2</sup> and d) 0.5 mA cm<sup>-2</sup> with a total capacity of 1.0 mAh cm<sup>-2</sup>. The cycling stability of Na metal electrode is much improved by the Al<sub>2</sub>O<sub>3</sub> coating. Reproduced with permission.<sup>[285]</sup> Copyright 2017, Wiley.

thinner Na<sub>2</sub>O and NaF based SEI, granted a stable Na stripping deposition process.

As highlighted in Section 2.1.4, the use of concentrated electrolytes is a suitable strategy to modify the passivation layer on Na metal. In these electrolytes, the passivation layer is mostly formed by the decomposition products of the anion, frequently belonging to the bis-imide family.<sup>[126]</sup> This grants the formation of sulfidic compounds such as Na<sub>2</sub>S<sub>2</sub>O<sub>4</sub> and Na<sub>2</sub>S<sub>2</sub>O<sub>3</sub> expected to form SEI with superior properties.<sup>[283]</sup> Choi et al. reported 5 m NaFSI in DME to offer superior reversibility for Na stripping/plating in Na/SS as well as Na/Na cells.<sup>[284]</sup> Moreover, this formulation showed high oxidation stability (>4.9 V vs Na/Na<sup>+</sup>) without corrosion of the Al cathode current collector. Such an electrolyte was employed for the realization of sodium cells using high voltage cathodes materials, Na<sub>4</sub>Fe<sub>3</sub>(PO<sub>4</sub>)<sub>2</sub>(P<sub>2</sub>O<sub>7</sub>) and Na<sub>0.7</sub>(Fe<sub>0.5</sub>Mn<sub>0.5</sub>)O<sub>2</sub>, offering outstanding cycling stability. The reversible capacity of 109 mAh g<sup>-1</sup> for over 300 cycles was obtained with the Na/ Na<sub>4</sub>Fe<sub>3</sub>(PO<sub>4</sub>)<sub>2</sub>(P<sub>2</sub>O<sub>7</sub>) cell.

An approach to stabilize the Na metal electrode also relies in engineering its surface, i.e., build an artificial SEI layer, prior to exposing it to the electrolyte. Sun and co-workers<sup>[285]</sup> deposited an ultrathin layer of Al<sub>2</sub>O<sub>3</sub> on Na metal using atomic layer deposition (ALD), which resulted in the suppression of dendrite/mossy Na formation upon cycling. At high current density (5 mA cm<sup>-2</sup>) the Al<sub>2</sub>O<sub>3</sub>-coated Na metal electrode showed much lower overpotential (≈40 mV) than bare Na (≈300 mV) along with improved stability for 75 h cycling (Figure 17c,d). By further optimization of the Al<sub>2</sub>O<sub>3</sub> coating, Na/Na symmetric cells were realized delivering stable stripping/plating for 500 cycles without drastic increase of overpotential or short-circuiting.

The reversible plating of Na would allow the realization of metal-free “Na-batteries,” in which the Na metal is in situ deposited during the first battery charge.<sup>[286]</sup> An example of this approach has been reported by Mazzali et al.<sup>[286]</sup> employing 1 m NaPF<sub>6</sub> in diglyme as electrolyte and carbon-coated aluminum foil for the in situ plating of Na, showing very small voltage hysteresis up to an applied current of 2 mA cm<sup>-2</sup>. Zhao et al.<sup>[287]</sup> proposed an in situ solution-based methods to synthesize an artificial protective layer of Na<sub>3</sub>PS<sub>4</sub> (NaPS) on the surface of Na metal. Symmetric Na/Na cell, employed to verify the stripping deposition efficiency of the modified Na electrode, evidenced the superior cycling stability of the Na@NaPS with respect to the bare Na electrode.

The implementation of functional additives is also actively pursued since it is sought to be the simplest and most advantageous approach. As mentioned above, additives for SMBs must provide SEI-building materials offering high surface coverage (i.e., large molar volume) in addition to good ionic conductivity and elevated electrochemical and chemical stabilities.

Wang and co-workers introduced KTFSI as a bifunctional additive to 1 m NaOTf/TEGDME electrolyte for stabilizing Na metal electrodes.<sup>[288]</sup> The addition of KTFSI improves both the efficiency and cyclability of Na/Na symmetric cells, resulting in extended cycle life (more than 2700 h) with an average overpotential of only 14 mV. Moreover, this additive offered unprecedented cycling stability (>400 h) at high capacity (≈10 mAh cm<sup>-2</sup>). The enhanced performance is attributed to the TFSI decomposition which, by providing highly conductive and electrochemically stable Na<sub>3</sub>N and oxynitrides, builds up a robust SEI layer, and the preferential adsorption

of  $K^+$  on Na protrusions providing an electrostatic shielding effect to suppress dendrite growth. Howlett and co-workers recently investigated the effect of water as additive to an ionic liquid electrolyte on the stripping/plating performance of Na metal.<sup>[289]</sup> The addition of  $\approx 500$  ppm of water to N-methyl-N-propylpyrrolidinium bis(fluorosulfonyl)imide was found to promote the breakdown of the FSI<sup>-</sup> anion, thereby resulting in the formation of a smooth SEI layer on Na metal rich in inorganic compound.

Very recently, Li and co-workers evaluated sodium polysulfide ( $Na_2S_6$ ) as standalone and as coadditive with sodium nitrate ( $NaNO_3$ ) in ether-based electrolyte.  $Na_2S_6$  was found to boost the electrochemical performance of the Na electrode for over 100 cycles at high current density ( $10 \text{ mA cm}^{-2}$ ) and cycled capacity ( $5 \text{ mAh cm}^{-2}$ ).<sup>[290]</sup> However, while the combination of  $Li_2S_6$  and  $LiNO_3$  is reported to enhance the performance of Li-S battery via a synergistic effect, the use of only  $Na_2S_6$  is preferred with Na. In fact, XPS analysis revealed that the SEI layer contains  $Na_2O$ ,  $Na_2S_2$ , and  $Na_2O$ , which provide a mechanically stable SEI capable of suppressing (reducing) Na dendrite growth when only  $Na_2S_6$  is present (Figure 18a). In contrast, the SEI layer in the presence of both  $Na_2S_6$  and  $NaNO_3$  contains  $RCH_2ONa$  and  $Na_2S$ , resulting in Na dendrite/

mossy growth (Figure 18b–d). Zheng et al.<sup>[291]</sup> proposed the use of a small amount of  $SnCl_2$  additive ( $50 \times 10^{-3} \text{ M}$ ) to the 1.0 M  $NaClO_4$  EC:PC electrolyte. This leads to the formation, by the spontaneous reaction between  $SnCl_2$  and Na metal, of a Na–Sn alloy layer and a compact NaCl-rich SEI. Na/Na symmetric cells with stable cycling of over 500 h with low voltage hysteresis were obtained using the  $SnCl_2$  additive.

### 3.1.2. Carbon-Based Electrodes

Unlike to Li cells, graphite is inactive in Na cells, due to the inability of graphite to accommodate  $Na^+$  ions.<sup>[292,293]</sup> Only recently, the possibility to insert  $Na^+$  ions into graphite was demonstrated by using glyme-based electrolytes, thanks to the cointercalation of the solvent molecules together with the  $Na^+$  ion.<sup>[47]</sup> The SEI in SIBs employing graphite is subjected to huge stress.<sup>[294,295]</sup> In fact, a large volume expansion occurs upon the cointercalation of the  $Na^+$  solvated complex, as evidenced by Adelhelm and co-workers reporting a  $\approx 346\%$  increase of graphite interlayer distance upon intercalation.<sup>[47]</sup> Goktas et al.<sup>[294]</sup> proposed that no SEI is formed at the graphite surface, supporting this hypothesis with TEM images. In contrast, Maibach et al. conducted a detailed study of the SEI properties on graphite using Na-TEGDME. The authors found that NaFSI salt decomposes below 0.5 V versus Na/Na<sup>+</sup> playing a key role in the formation of a stable SEI.<sup>[54]</sup> The FSI leads to the formation of a SEI mainly composed of inorganic products and hydrocarbons, granting superior performances.<sup>[296]</sup> Hard carbon (HC) is the negative electrode material of choice for SIBs.<sup>[1,297–299]</sup> The properties of the SEI layer formed at the HC/electrolyte interphase have been at first studied by Komaba et al.<sup>[297]</sup> Combined XPS, and ToF-SIMS experiments with fully sodiated or lithiated HC in analogous electrolytes (i.e.,  $LiClO_4$  or  $NaClO_4$  in PC) revealed similar species for both cells (i.e.,  $M_2CO_3$ ,  $ROCO_2M$ ,  $-CH_2-$ ,  $-CO-O-$ , ester linkages, MF, MOH, MCl,  $M_2O$ , where  $M = Li$  or Na). However, the SEI formed in SIB is richer in inorganic species (i.e.,  $Na_2O$ , NaCl, and  $Na_2CO_3$ ), while the SEI in LIBs is dominated by organic compounds. SEM and TEM images further evidence that the SEI layer in SIBs is less homogeneous and thinner than the one in LIBs. Ponrouch et al. performed a comparative study on HC SEI layer composition employing 1 M  $NaPF_6$  or  $NaClO_4$  in  $EC_{(1-x/2)}:PC_{(1-x/2)}:DMC_x$  solvent mixtures with  $x$  varying from 0 to 0.5.<sup>[15]</sup> The authors evidenced, from the XPS C1s spectra, an increase in the amount of C–O groups when EC is present, thus associated to the EC ring-opening upon reduction, which leads to the formation of PEO oligomeric/polymeric species like for lithium. Passerini co-workers conducted FTIR analysis on the SEI layer formed on sodiated  $Na_x$ -HC in contact with 1 M  $NaPF_6$  in EC:DMC, EC:DEC, and EC:PC.<sup>[3]</sup> They evidenced the existence of sodium double alkyl carbonate (NEDC), a  $1e^-$  reduction product of EC, as the main component of the SEI layer and of  $Na_2CO_3$ , but in lower quantity. The same group investigated in detail the SEI composition at the HC surface employing different Na salts, i.e.,  $NaPF_6$ ,  $NaClO_4$ , NaTFSI, NaFSI, and NaFTFSI, all dissolved in EC:DEC (1:1, wt).<sup>[300]</sup> The authors evidenced the key role of the Na salt in determining the overall SEI layer composition, including its depth evolution and thickness. The SEI building species

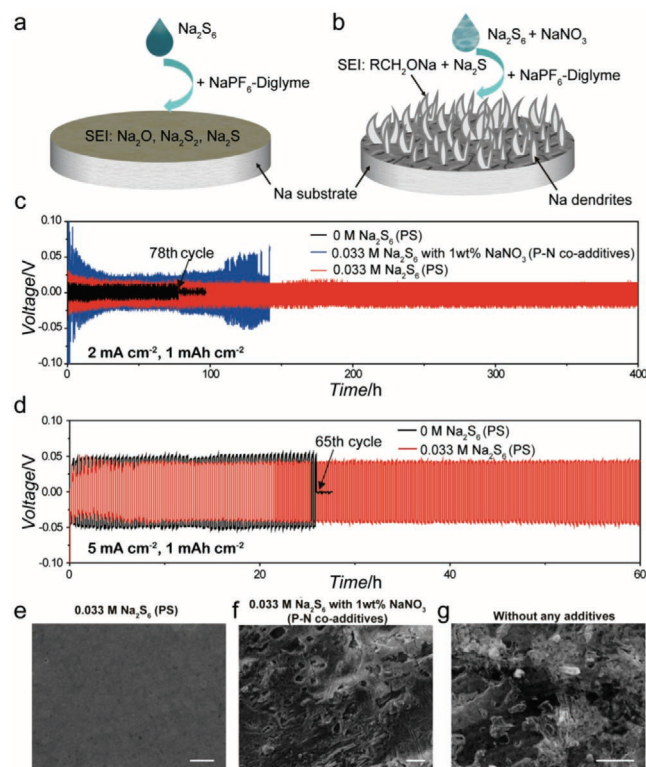


**Figure 18.** The role of  $Na_2S_6$  and  $Na_2S_6$ – $NaNO_3$  on the Na Plating/Stripping stability in 1 M  $NaPF_6$ /diglyme-based electrolyte. The Na surface morphology difference with a) PS alone and b) P-N co-additives. Galvanostatic cycling of symmetric cells at c)  $2 \text{ mA cm}^{-2}$  and  $1 \text{ mAh cm}^{-2}$  and d)  $5 \text{ mA cm}^{-2}$  and  $1 \text{ mAh cm}^{-2}$ . SEM images of the Na surface after 30 cycles at  $2 \text{ mA cm}^{-2}$  and  $1 \text{ mAh cm}^{-2}$  with e) 0.033 M PS alone, f) P-N co-additives, and g) 0 M PS (no additives). Scale bars in (e)–(g) are 10  $\mu\text{m}$ . Reproduced with permission.<sup>[290]</sup> Copyright 2018, Wiley.

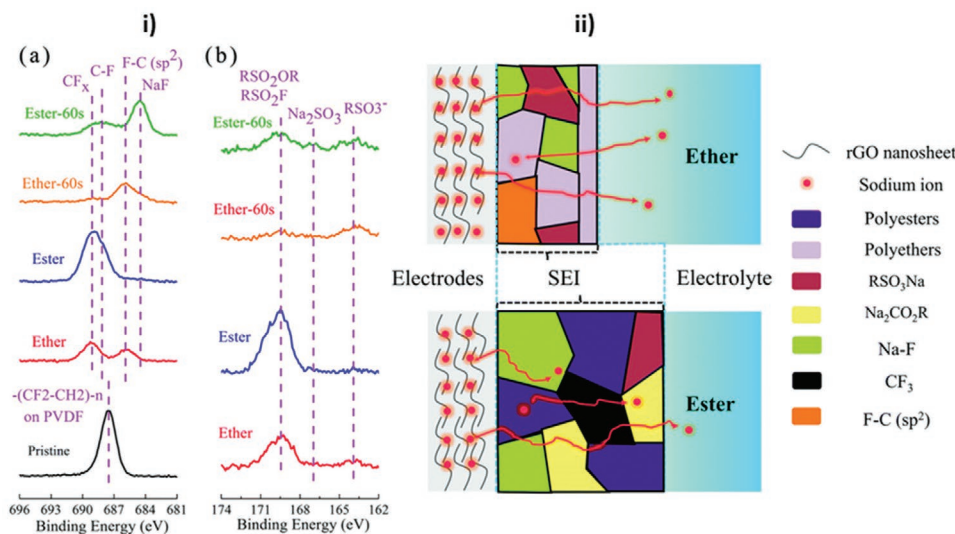


**Figure 19.** i) XPS spectra of SEI composition of pristine and cycled rGO electrodes in ether and carbonate ester-based electrolytes. ii) Schematic illustration of SEI components and configurations in carbonate and ether electrolytes. Reproduced with permission.<sup>[301]</sup> Copyright 2017, RSC Publishing group.

formed on HC by the solvent reduction were found to decrease with the various salts in the order: NaPF<sub>6</sub> > NaClO<sub>4</sub> ≈ NaTFSI > NaFTFSI > NaFSI. Yang and co-workers compared the passivation layers on reduced graphene oxide (rGO) anode cycled in 1 M NaOTf in carbonate ester (EC:DEC) and ether (diglyme)-based electrolytes.<sup>[301]</sup> The study shows a dramatic increase in the initial coulombic efficiency utilizing, as the solvent, diglyme instead of EC:DEC (i.e., 74.6% vs 39%). The improved performance is associated with the formation of a stable, thin and compact SEI in the ether-based electrolyte. On the contrary, in ester-based electrolytes, thicker SEI layer with poor protective properties are formed (Figure 19), in agreement with the results of glyme-based electrolyte and Na metal anode.<sup>[60]</sup>

Xu and co-workers conducted a detailed investigation on the SEI layer on HC, employing ester and ether-based electrolytes.<sup>[302]</sup> The study evidenced a larger gap between cathodic/anodic peaks for EC:DEC compared to DEGDME, indicating faster kinetics and more conductive/thinner SEI layer for the ether solvent. In fact, the SEM and XPS analyses showed that the ether-based electrolyte resulted in a compact, smooth and thinner SEI layer compared to the one in ester-based electrolyte. Also, the SEI formed in EC:DEC consists of more organic or polymeric species reduced from the ester solvents compared to the inorganic dominated DEGDME-derived SEI. Finally, the Young's modulus of the formed SEI, evaluated using AFM nanoindentation technique, is much higher in the presence of DEGDME (16280 MPa) than EC:DEC (1113 MPa). This implies that a stiffer SEI layer may be beneficial for the cycling of HC in SIBs.

Komaba et al. investigated and compared the electrochemical performance of Na cells in several well-known LIB additives, such as fluoroethylene carbonate (FEC), trans difluoroethylene carbonate (DFEC), ethylene sulfite (ES), and vinylene carbonate (VC), in 1 M NaClO<sub>4</sub>/PC, electrolyte solution.<sup>[25]</sup> All are known as anode film-forming additives for Li-ion batteries. Among the tested additives, FEC was found to be the most efficient in improving the reversibility Na half-cells employing HC and

NaNi<sub>0.5</sub>Mn<sub>0.5</sub>O<sub>2</sub> electrodes. On the contrary, the other tested additives revealed none or even negative effect on sodium cells. Later the same group extended their initial work, with a detailed study on the effect of FEC on HC when added to electrolytes solution of different compositions, i.e., 1 M NaClO<sub>4</sub> or NaPF<sub>6</sub> in PC or EC:PC electrolytes.<sup>[303]</sup> The study evidenced that NaPF<sub>6</sub>-based electrolytes provide superior reversibility and cyclability of sodium insertion into hard carbon compared with NaClO<sub>4</sub>-based ones. In agreement with the Komaba's group finding, Ponrouch and co-workers reported a negative effect of FEC both on the specific and coulombic efficiency of HC electrode, upon its addition into 1 M NaClO<sub>4</sub> in EC:PC.<sup>[304]</sup> Apart from FEC, Ma et al. recently proposed the use of rubidium (Rb<sup>+</sup>) and cesium (Cs<sup>+</sup>) ions as electrolyte additives for improving the performance of HC anode in SIBs.<sup>[305]</sup> The addition of 0.05 M MPF<sub>6</sub> (M = Rb or Cs) into EC:PC (4:1, vol%) + 2 wt% FEC reference electrolyte was reported to increase the cycling performance and capacity retention of the Na/HC cells up to 95.3% and 97.1% for Rb<sup>+</sup> and Cs<sup>+</sup> respectively, compared to the reference cell which showed ≈80.6% after 100 cycles. The improvement is attributed to the involvement of Rb<sup>+</sup>, and Cs<sup>+</sup> ions in the formation of a highly conductive and more stable SEI layer in respect to the one formed using the reference electrolyte.

### 3.1.3. Additional Negative Electrodes

**Ti-Based Materials:** Because of its low cost, environmental friendliness, intrinsic safety, and negligible volume expansion, nanoparticulated TiO<sub>2</sub> has been investigated as anode compound for rechargeable SIBs.<sup>[306–310]</sup> However, the high surface of such materials leads to excessive electrolyte's consumption for the SEI formation, negatively affecting the long-term performance of the battery. Lee et al. performed a detailed surface analysis using TEM and XPS on porous carbon/TiO<sub>2</sub> evidencing that the SEI layer formation increases on the anode having larger surface area, but the nature of the SEI appears to

depend on minor perturbations in the anode composition.<sup>[311]</sup> Xu et al. compared the SEI layers formed on anatase TiO<sub>2</sub> employing ether and carbonate-based electrolytes. Similarly to HC electrode,<sup>[302]</sup> the use of glyme-based electrolytes result in the formation of thinner and inorganic compounds-rich SEI layers, offering superior electrochemical performance in comparison to carbonate-based electrolytes.<sup>[308]</sup> This has been confirmed by Yang et al.<sup>[312]</sup> employing mesocrystal hollow TiO<sub>2</sub> spheres, demonstrating an improvement of 20% of the initial coulombic efficiency and of 30% on the delivered capacity using glyme-based electrolytes. Li et al.<sup>[313]</sup> performed a detailed investigation of the electrochemical interface of TiO<sub>2</sub> electrodes in diglyme-based electrolyte in comparison with ester electrolytes, showing that the charge transfer energy barrier (172 meV) is 1.4 times lower than that of EC:DEC-based electrolyte. This results in a much faster charge transfer across the electrolyte/TiO<sub>2</sub> electrode interphase.

Na<sub>2</sub>Ti<sub>3</sub>O<sub>7</sub> has also attracted large interest due to its elevated stability, low cost, and non-toxicity. With the capability to exchange up to 3.5 Na ions per formula unit, a capacity of 310 mAh g<sup>-1</sup> can be obtained at a rather low insertion potential (≈0.3 V versus Na/Na<sup>+</sup>), leading to promising energy densities for the corresponding batteries.<sup>[314]</sup> However, the instability of the SEI layer upon cycling is one of the main drawbacks of this material.<sup>[315,316]</sup> Munoz-Marquez co-workers conducted a detailed study on the interfacial chemistry of Na<sub>2</sub>Ti<sub>3</sub>O<sub>7</sub> electrode demonstrating the interface resistance's increase to be linked with the unstable SEI upon cycling.<sup>[316]</sup> Their XPS surface analysis evidenced that the SEI on the electrodes is composed of carbonates and semicarbonates (Na<sub>2</sub>CO<sub>3</sub>, NaCO<sub>3</sub>R), halides (NaF, NaCl), and poly(ethylene oxide) (PEO), but is unstable upon cycling, due to its partial dissolution upon each charge.

**Organic Materials:** The use of organic compounds as electrode material in SIB has the great advantages to avoid the use of transition metal elements, possibly resulting into lower costs and boosting environmental friendliness.<sup>[317–319]</sup> However, these compounds are prone to suffer from the dissolution of the active material in the electrolyte, which affects the cycling stability. A properly designed SEI can mitigate this drawback. Brandell and co-workers compared the SEI layers on benzene-diacrylate-based electrodes for LIB and SIBs in 1 M LiTFSI/EC:DMC (1:1) and 1 M NaFSI/EC:DEC (1:1.5) electrolytes, respectively.<sup>[320]</sup> The investigation by HAXPES analysis evidenced that salt-derived inorganic compounds dominate the SEI layer in SIBs, while organic species are the main SEI building materials in LIBs; however, the obtained results might be misleading as different salts, solvents mixtures, and their relative amounts were employed.

Zhao et al.<sup>[321]</sup> investigated the effect of an artificial layer of Al<sub>2</sub>O<sub>3</sub> deposited on the surface of Na<sub>2</sub>C<sub>8</sub>H<sub>4</sub>O<sub>4</sub> terephthalate electrodes by atomic layer deposition (ALD). Being Al<sub>2</sub>O<sub>3</sub> insulating, it reduces the SEI growth while limiting the active material solubility. In fact, the artificial layer significantly improved the initial coulombic efficiency (up to 91.1%), rate capability, and cycling performance.

**Alloying Materials:** Thanks to their elevated specific capacity, alloying-based compounds are considered extremely promising electrode materials for SIBs.<sup>[322,323]</sup> However, the mechanical stress caused by the volume variation upon charge/discharge

affects the stability of the SEI causing a further decomposition of the electrolyte constituents. This results in fast capacity fading and inferior coulombic and energy efficiency. Thus, a better understanding of the structure, composition, evolution, and function of the SEI layer is of utmost importance in alloying-type and their composite anode electrodes.

Baggetto et al. evidenced by XPS studies that the SEI layer on cycled Na–Sn electrodes is rich in carbonates (Na<sub>2</sub>CO<sub>3</sub> and NaCO<sub>3</sub>R) originating from the electrolyte (1 M NaClO<sub>4</sub> in PC) reduction.<sup>[324]</sup> However, the Sn<sup>4+</sup> formed upon de-sodiation (i.e., at 2 V) catalytically enhances the electrolyte's degradation. Komaba and co-workers systematically investigated the effect of cut-off voltage on the cyclability (and the SEI quality) of Sn–polyacrylate composite electrodes<sup>[325]</sup> showing that the electrolyte decomposition can be avoided limiting the desodiation potential to 0.65 V. Accordingly, the capacity retention and coulombic efficiency of the Sn-based composite electrode were enhanced. Tarascon et al. compared the performance of Sn electrodes in 1 M NaPF<sub>6</sub> in DEGDME and carbonate-based solvents.<sup>[326]</sup> The study evidenced that the glyme-based electrolyte enables high reversible capacity of the Sn electrodes via the formation of a stable SEI, in turns avoiding the isolation of active material's domains. The XPS investigation revealed that the SEI film contains both organic (RCH<sub>2</sub>ONa) and inorganic (NaF, NaPF<sub>6</sub>, Na<sub>2</sub>O, Na<sub>2</sub>CO<sub>3</sub>, and phosphates) components. In the PC-based electrolyte the SEI composition is similar, but different in relative proportions due to the high solubility of the sodium oxides and carbonates in PC.

Sn<sub>4</sub>P<sub>3</sub> is also an appealing alloying material for SIBs application thanks to elevated practical capacity (≈550–750 mAh g<sup>-1</sup>), and good volumetric capacity (700 vs 465 mAh cm<sup>-3</sup> of HC).<sup>[327,328]</sup> However, the volume expansion, reaching up to 100%, limits the stability of the electrode and its cycle life. Mogensen et al. conducted a detailed study on the quality of the SEI layer on Na/Sn<sub>4</sub>P<sub>3</sub> in contact with 1 M NaFSI in EC:DEC (1:1, wt) + 5% FEC (vol%).<sup>[329]</sup> The study indicated that the SEI formed at the Sn<sub>4</sub>P<sub>3</sub> electrode surface undergoes thickness and composition changes during the charge/discharge process, negatively affecting the cycling behavior of the electrode. Further electrolyte optimization is required to circumvent the stability issue of the Sn<sub>4</sub>P<sub>3</sub>.

Sb-based materials are also considered promising candidates for SIBs because of the high capacity (660 mAh g<sup>-1</sup>), good cycle stability and rate performance when incorporated in a carbon matrices, reducing the negative effects linked to the large volume expansion.<sup>[27,29,330]</sup> The investigation conducted on the effect of electrolyte salts and solvents on the SEI formed on Sb reveals a main contribution of carbonates and alkyl carbonates, identifying the role of the solvent in dictating the passivation in such types of anode systems.<sup>[34]</sup> XPS analysis on thin film of Cu<sub>2</sub>Sb confirmed that the SEI layer is mainly made of carbonates, with minor contribution from ethers and alkoxides.<sup>[331]</sup> However, similarly to Sn, the SEI layer is found to be dynamic, varying both electrochemically and mechanically during the cell expansion/contraction process.

**Conversion Materials:** Na-conversion electrodes also promise high specific capacity and, consequently, are considered a valid alternative to intercalation and alloying based systems. However, they are also affected by large volume variations during the electrochemical processes, hindering their efficient

Na-storage operation. Several strategies have been proposed to mitigate the negative effects of volume-changing such as the electrode optimization in term of composition, structure, and morphology, or the use of matrixes buffering the volume variation.<sup>[332]</sup>

Due to its abundance, low cost, and non-toxic nature, Fe<sub>2</sub>O<sub>3</sub> represents an appealing conversion-type anode material for SIBs. The conversion reaction



promises a capacity of 1007 mAh g<sup>-1</sup>, however, the poor initial reversibility, energy efficiency, and cycle life, limit the practical application of this conversion-type anode material. The limited performance is also caused by the poor stability of the electrode/electrolyte interphase. Studies on the SEI formed on Fe<sub>2</sub>O<sub>3</sub> in LIBs show that the passivation layer is stable in composition, however, it varies in thickness upon cycling, which means, it continuously consumes the electrolyte.<sup>[333]</sup> Edström et al. conducted a comparative study of the SEI layers formed on Fe<sub>2</sub>O<sub>3</sub> using Li and Na perchlorate in EC:DEC<sup>[334]</sup> showing that the nature of the SEI layers in the presence of Li or Na differs. In the Na system the SEI is thicker and richer in inorganic species. Furthermore, in Na cells, a layer composed of salt and solvent degradation byproducts forms by simple contact of the electrode with electrolyte.

Cupric oxide (CuO) has attracted attention as negative electrode for SIBs.<sup>[335,336]</sup> Adelmhelm et al.<sup>[337]</sup> investigated thin film electrodes (without carbon additive or polymer binder) to study the conversion reaction of CuO upon sodiation and lithiation. Beside the differences in the CuO conversion processes, the study evidenced as the SEI formed in the presence of Na is thicker and richer in inorganic components. In a following work, the same group investigated the interfacial chemistry of CuO composite electrodes employing 1 M LiPF<sub>6</sub> in EC:DMC (1:1, vol) and 0.5 M NaFSI in EC:DMC (3:7, vol),<sup>[338]</sup> showing clear differences in the SEI morphology and chemical composition. Once more, the SEI layer formed in the presence of Na is significantly thicker (6 μm vs 1 μm),

more homogeneous, and principally composed of inorganic species (Na<sub>2</sub>CO<sub>3</sub> and NaF). On the other hand, a heterogeneous, thinner, and richer in organic species SEI layer was obtained on CuO in the presence of Li. In spite of the apparently better morphology, in situ pressure monitoring cycling galvanostatic (PMCG) and differential electrochemical mass spectroscopy (DEMS) reveal the release of gaseous side products upon sodiation of CuO, indicating a continuous SEI formation and dissolution during cycling.

Overall, the formation of an SEI rich in inorganic species appears not to be appropriate for those electrode materials showing large volume changes, since the rigidity of the SEI cannot easily match with the volumetric expansion of the active materials' particles.

### 3.2. Positive Electrodes

Oxidative decomposition occurs at the positive electrode/electrolyte interphase when the cathode potential goes beyond the electrolyte's LUMO level. Unless a passivation layer, usually called cathode-electrolyte interphase or CEI, is formed, the electrolyte oxidation progresses continuously, negatively affecting the cell performance (Table 10).<sup>[146,339,340]</sup>

Hu et al. evaluated the effect of FEC on binder-free, Na<sub>2/3</sub>Fe<sub>1/2</sub>Mn<sub>1/2</sub>O<sub>2</sub>@graphene composite electrodes. The 1.0 M NaPF<sub>6</sub> PC + 2% FEC electrolyte enabled the charge cut-off voltage to be set at 4.3 V (vs 3.9 V without FEC), resulting in a rather high reversible capacity (156 mAh g<sup>-1</sup>).<sup>[341]</sup> Choi and co-workers evidenced by ex situ XPS analyses of cycled Na<sub>4</sub>Fe<sub>3</sub>(PO<sub>4</sub>)<sub>2</sub>(P<sub>2</sub>O<sub>7</sub>) cathodes that the FEC additive forms an NaF-rich resistive layer on the cathode surface leading to the excellent cycling performance of cathodes.<sup>[342]</sup> In agreement with the work of Hu and Choi, Passerini and co-workers showed the influence of FEC on Na half-cell employing a layered P2-Na<sub>0.7</sub>CoO<sub>2</sub> cathode, revealing enhanced cycle life, efficiency in the cell using the additive in carbonate based electrolyte.<sup>[57]</sup> Manohar et al.<sup>[343]</sup> investigated the use of Pyr<sub>13</sub>TFSI as additive to a 1 M NaClO<sub>4</sub> in PC electrolyte solution in sodium cells employing Na<sub>3</sub>V<sub>2</sub>(PO<sub>4</sub>)<sub>3</sub>/C (NVP/C) as

**Table 10.** Additives for improving the cathode/electrolyte interphase and their effect on the electrochemical performance of SIBs.

Additive	Electrolyte formulation	Cathode material	Charging voltage [V]	Capacity [mAh g <sup>-1</sup> ] (specific current or rate)	Cycle # T [°C]	Capacity retention <sup>a)</sup> [%]	Refs.
FEC	1 M NaClO <sub>4</sub> /PC + 2 vol% FEC	NaNi <sub>1/2</sub> Mn <sub>1/2</sub> O <sub>4</sub>	4.5	110 (0.1C)	20, (25)	+24	[390]
	1 M NaClO <sub>4</sub> /PC + 10 vol% FEC		3.8	80 (24 mA g <sup>-1</sup> )	50 (25)	+37	[372]
	1 M NaClO <sub>4</sub> /EC:PC (1:1, vol) + 5 vol% FEC	Na <sub>3.32</sub> F <sub>22.34</sub> (P <sub>2</sub> O <sub>7</sub> ) <sub>2</sub>	4.0	65 (5C)	1100 (25)	+7	[391]
	1 M NaPF <sub>6</sub> /EC:DEC (3:7, vol) + 2 wt% FEC	Na <sub>0.44</sub> MnO <sub>2</sub>	3.8	110 (0.2C)	40 (20)	+3	[35]
	1 M NaPF <sub>6</sub> /EC:PC (1:1, wt) + 2 wt% FEC			112 (0.2 C)		+8	
	1 M NaClO <sub>4</sub> /PC:FEC (8:2, wt)	Na <sub>0.6</sub> Ni <sub>0.22</sub> Fe <sub>0.11</sub> Mn <sub>0.66</sub> O <sub>2</sub>	4.6	157 (15 mA g <sup>-1</sup> )	10 (25)	+9	[33]
	1 M NaPF <sub>6</sub> /EC:DEC (1/1, vol) + 5 vol% FEC	Na <sub>1.95</sub> Fe <sub>2.08</sub> [Fe(CN <sub>6</sub> ) <sub>0.87</sub> Y <sub>0.07</sub> ] (Y' represents a [Fe(CN) <sub>6</sub> ] <sup>4-</sup> vacancy)	4.2	105 (100 mA g <sup>-1</sup> )	280 (25)	+4	[392]
	1 M NaPF <sub>6</sub> /EC:PC (1:1) + 2 vol% FEC	Na <sub>0.75</sub> Fe <sub>2.08</sub> (CN) <sub>6</sub> · 3.4H <sub>2</sub> O		115 (92 mA g <sup>-1</sup> )	40 (RT)	+3	[40]
	0.5 M NaClO <sub>4</sub> /EC:PC:DEC (5:3:2, vol) + 5 wt% FEC	Na <sub>4</sub> Fe <sub>3</sub> (PO <sub>4</sub> ) <sub>2</sub> (P <sub>2</sub> O <sub>7</sub> )	4.2	94 (50 mA g <sup>-1</sup> )	100 (NA)	+4	[342]
VC	10 M NaClO <sub>4</sub> /H <sub>2</sub> O + 2 vol% VC	Na <sub>3</sub> V <sub>2</sub> O <sub>2x</sub> (PO <sub>4</sub> ) <sub>2</sub> F <sub>3-2x</sub>	1.8	42 (1 C)	100 (NA)	+25	[393]
	1 M NaPF <sub>6</sub> /EC-PC (1/1, v/v) + 5 vol% FEC	Na <sub>2</sub> MnSiO <sub>4</sub>	4.3	210 (0.1 C)	10 (NA)	+61	[394]

<sup>a)</sup>Improvement with respect to the additive free electrolyte.

cathode. The results showed that the IL-containing electrolyte exhibited high discharge capacity of 107 mAh g<sup>-1</sup>, with capacity retention around 99.7%, and an average coulombic efficiency of 99.4% for the 50 cycles of the test, significantly improved in respect the performance of the IL-free electrolyte. The analysis of the composition of the CEI revealed the presence of sulfur in the surface film of the electrode cycled with IL-containing electrolyte. The presence of sulfur-based compound in the CEI composition was indicated as a responsible for the superior performances. Song et al.<sup>[344]</sup> reported the effect of adiponitrile (ADN) as additive to improve the performance of sodium ion battery using Na<sub>0.76</sub>Ni<sub>0.3</sub>Fe<sub>0.4</sub>Mn<sub>0.3</sub>O<sub>2</sub> as cathode and HC anode. The ADN can promote the formation of highly conductive and stable CEI film on the cathode material surface, as evidenced by TEM measurements, effectively improving the high/low temperature performance and cycling stability of the SIB.

Further investigations are required to understand the electrode/electrolyte interphase reactions. In particular, the investigation on gas evolution, being a significant hazard in high energy density systems, is not well explored in Na-systems as in conventional LIBs. The implementation of investigation methods such as DEMS is of fundamental importance to shed light on this topic.<sup>[338,345–350]</sup>

## 4. Safety of Na-Based Electrolytes

Safety is a stringent requirement for batteries characterized by high energy density. However, safety-related studies of Na-batteries and their components are still rather limited.

### 4.1. Thermal Reactivity of Na-Based Electrolytes

Okada and co-workers studied several electrolytes containing NaPF<sub>6</sub> or NaClO<sub>4</sub> dissolved in PC and EC:DMC, revealing that their thermal stability is dominated by the solvent.<sup>[351]</sup> The PC-based electrolytes are characterized by higher onset temperatures, but also higher heat generation compared to EC:DMC-based ones. Ponrouch et al.<sup>[14]</sup> studied the thermal stability of various pure solvents (DME, DMC, DEC, and PC), solvent blends (EC:DME, EC:DMC, EC:DEC, and EC:PC), Na-salts (NaPF<sub>6</sub>, NaTFSI, and NaClO<sub>4</sub>), and their corresponding electrolytes (NaPF<sub>6</sub>/EC:PC, NaClO<sub>4</sub>/EC:PC, NaClO<sub>4</sub>/PC, and NaClO<sub>4</sub>/EC:DEC). EC:PC showed the highest thermal stability among all tested solvent blends. The salts showed elevated thermal stabilities, following the order NaClO<sub>4</sub> (310 °C) > NaPF<sub>6</sub> (280 °C) > NaTFSI (250 °C). While outperforming all other salts, dry NaClO<sub>4</sub> cannot be employed in commercial applications because of explosion hazards. The trend for the first exothermic onset temperature of the four types of electrolytes is found to be as: NaClO<sub>4</sub>/EC:DEC < NaClO<sub>4</sub>/PC < NaClO<sub>4</sub>/EC:PC < NaPF<sub>6</sub>/EC:PC. Thus, considering the high first exothermic onset temperature and low total heat generated, the NaPF<sub>6</sub>/EC:PC is proposed as the optimal choice. Passerini and co-workers<sup>[3]</sup> evaluated additional Na-salts revealing their thermal stability to be in the order NaClO<sub>4</sub> > NaPF<sub>6</sub> > NaTFSI > NaFTFSI > NaFSI. The comparison with the same Li-salts revealed the higher stability of the Na-analogues (NaPF<sub>6</sub> have higher stability than

LiPF<sub>6</sub> by ≈200 °C), which is very promising for practical applications. The higher thermal stability of the Na salts can be associated to the higher Madelung energy of the Na salts, a parameter linked to the electrostatic energy in ionic crystals.

Wang et al.<sup>[352]</sup> reported for the first time a screening of a large family of flame retardants (FRs) for LIBs, including trimethyl phosphate. Following, several studies have focused on organohalogen, organophosphorus, and phosphazene compounds.

Feng et al. investigated the flame retardant characteristics of four well-known compounds, namely trimethyl phosphate (TMP), tri (2,2,2-trifluoroethyl) phosphite (TFEP), dimethyl methylphosphonate (DMMP), methyl nonafluorobutyl ether (MFE) in SIBs.<sup>[353]</sup> Among these, MFE is found to be stable against Na metal. The 0.3 M NaPF<sub>6</sub> in MFE:DEC:FEC (50:40:10 vol) electrolyte showed good electrochemical compatibility with both the Prussian blue (positive) and carbon nanotubes (negative) electrodes thus leading to good cell performance. However, the practical application of the tested FRs is limited by the relatively low ionic conductivity (5 × 10<sup>-4</sup> S cm<sup>-1</sup>) associated with the low dipole moment (2.37) and dielectric constant of MFE.

A more accurate approach to evaluate the thermal stability of an electrolyte consists of performing the measurements in the presence of the sodiated negative electrode or desodiated positive electrodes, including their interphase layers. In fact, the thermal stability of any electrolyte is influenced by the presence and the interaction with a polarized interface at the electrodes. In the following section, the thermal reactivity of electrolytes in contact with negative and positive electrodes is described in detail.

#### 4.1.1. Negative Electrode/Electrolyte Thermal Reactivity

A comparative study on the thermal reactivity of various electrolytes in the presence of lithiated (Li<sub>x</sub>-HC) or sodiated HC (Na<sub>x</sub>-HC) electrodes was conducted by Xia and Dahn using an accelerating rate calorimetry (ARC).<sup>[354]</sup> The results indicated higher reactivity of Na<sub>x</sub>-HC in NaPF<sub>6</sub>/EC:DEC and NaPF<sub>6</sub>/EC:DMC compared to EC:DEC and EC:DMC solvent mixture. Furthermore, the comparison shows that the electrolytes are more stable toward Li<sub>x</sub>-HC than Na<sub>x</sub>-HC. However, Zhao et al. compared the thermal stability of Na(Li)PF<sub>6</sub> or Na(Li)ClO<sub>4</sub> in EC:DMC or PC, in the presence of sodiated/lithiated HC C1600 (Sumitomo Chemical Co.).<sup>[351]</sup> The reported results showed that the Na-based electrolytes displayed similar or even better thermal stability than the Li-based one, in disagreement with the results reported by Xia and Dahn.<sup>[354]</sup> In particular, the DSC experiments demonstrated that NaPF<sub>6</sub>/EC:PC in contact with the fully sodiated Na<sub>x</sub>-HC electrode material exhibited the highest exothermic onset temperature and the lowest enthalpy of reaction amongst all tested electrolytes. This makes such an electrolyte very attractive for the development of SIBs.<sup>[14]</sup> Passerini et al. carried out a comprehensive study on the thermal stability of various electrolytes in contact with sodiated hard carbon (Na<sub>x</sub>-HC) electrodes. For a fixed solvent blend (e.g., EC:PC), the thermal reactivity was found to be in the order NaFSI > NaTFSI > NaPF<sub>6</sub> > NaFTFSI > NaClO<sub>4</sub> with respect to the onset temperature of the exothermal process, and NaFTFSI > NaPF<sub>6</sub> > NaClO<sub>4</sub> > NaTFSI > NaFSI in terms

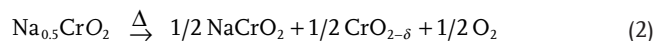
of the global heat generated. If the Na-salt is fixed, the thermal stability of the solvent mixtures follows the order EC:PC > EC:DEC > EC:DMC, implying that the salt and solvent mixture greatly influence the thermal behavior of the electrolyte in SIBs. To further understand the mechanism behind the thermal reactivity of electrolytes on Na<sub>x</sub>-HC anode electrodes, Passerini and co-workers investigated the thermal/chemical stability of the SEI layer decomposition (i.e., the onset reaction for all the cascading thermal phenomenon leading to run away in a given battery system) using the SEI layer's major/functional components, such as Na<sub>2</sub>CO<sub>3</sub>. Mixtures of Na<sub>2</sub>CO<sub>3</sub> and Na-salts or Na-based electrolytes were heated and analyzed using DSC. No noticeable heat release was observed below 90 °C for the mixtures of Na<sub>2</sub>CO<sub>3</sub> with dry NaPF<sub>6</sub> salt or the NaPF<sub>6</sub>/EC:DEC electrolyte (notice that similar experiments for LIBs showed that Li<sub>2</sub>CO<sub>3</sub> exothermically react with LiPF<sub>6</sub> and LiPF<sub>6</sub> in EC:DMC at temperature even below 90 °C). The presumably better thermal stability of Na-SEI layer is ascribed to the better stability of NaPF<sub>6</sub> salt compared to LiPF<sub>6</sub> and the weaker solvation of Na<sup>+</sup> than Li<sup>+</sup> with EC. In fact, NaPF<sub>6</sub> has good chemical and thermal stability, which is not the case of LiPF<sub>6</sub>. As a result, less of the acidic species, such as PF<sub>5</sub> and HF, are formed, mitigating the exothermic acid–base reaction with Na<sub>2</sub>CO<sub>3</sub>. Very recently, Mukai and Inoue<sup>[355]</sup> investigated the thermal stability of Na- and Li-HC electrodes, showing that they generate similar heat, ≈1200 J g<sup>-1</sup>. Although the onset temperature is nearly same, the maximum exothermic peak temperature differed between the two systems (i.e., 184 °C for C<sub>6</sub>Na<sub>0.65</sub> and 264 °C for C<sub>6</sub>Li<sub>0.65</sub>), indicating that Na-ion batteries are less thermally stable.<sup>[355]</sup> Additionally, similarly to Li,<sup>[356,357]</sup> Na metal plating might play an important role in the thermal runaway process during overcharge, causing a decrease of the onset temperature of the chemical reactions for the negative electrodes. Kondou et al. compared the thermal reactivity of plated Na on Ni substrates (using 1 M NaPF<sub>6</sub> in EC:DEC (1:1, wt)) with that of plated Li.<sup>[358]</sup> The heat flow measured in the presence of plated Na was found to be lower than with Li, which was ascribed to lower efficiency of the Na deposition in respect to Li. This is not an advantage for SMBs, but the low plating efficiency of Na can be considered a plus for SIBs.

#### 4.1.2. Positive Electrode/Electrolyte Thermal Reactivity

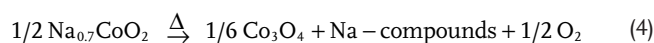
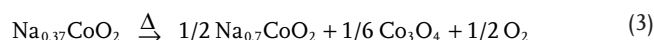
Only a limited number of studies addressing the thermal reactivity of electrolytes with charged positive electrode materials are available, made by accelerated rate calorimeter (ARC) and TGA-DSC.<sup>[359–366]</sup> Sodium-based positive materials share the same behavior of Li-based materials such as LiCoO<sub>2</sub>. Upon heating, the charged active material decomposes releasing oxygen, which can further react with the electrolyte and the carbonaceous anode.

However, the thermal behavior of Na-based cathodes is found to be comparable and/or even better to their analogous Li-based material. Xia and Dahn studied the thermal stability of desodiated Na<sub>0.5</sub>CrO<sub>2</sub> in the presence of 1 M NaClO<sub>4</sub>/PC reporting virtually no reactivity up to 350 °C,<sup>[360]</sup> which is even higher than that of delithiated LiFePO<sub>4</sub> in the corresponding electrolyte. Na<sub>0.5</sub>CrO<sub>2</sub> also demonstrated high

thermal stability in NaPF<sub>6</sub>-based electrolyte, which is better than that of Li<sub>0.5</sub>CoO<sub>2</sub> or Li<sub>x</sub>Ni<sub>1/3</sub>Mn<sub>1/3</sub>Co<sub>1/3</sub>O<sub>2</sub> under similar condition. From XRD study, the thermal decomposition of Na<sub>0.5</sub>CrO<sub>2</sub> was found to follow Reaction 2, evidencing that only small amount of oxygen (δ) will be released, explaining the low reactivity of the material towards the electrolyte solvents.



The same authors investigated the thermal stability of desodiated Na<sub>0.35</sub>CoO<sub>2</sub> in contact with the EC:DEC solvent mixture and the 1 M NaPF<sub>6</sub>/EC:DEC electrolyte using ARC under adiabatic condition.<sup>[362]</sup> The exothermic reactions were tracked when the sample self-heating-rate (SHR) exceeded 0.03 °C min<sup>-1</sup>. The Na<sub>0.35</sub>CoO<sub>2</sub> in contact with the electrolyte showed reactivity at a lower temperature than that of the solvent mixture alone (115 °C vs 140 °C). Based on XRD analysis, the authors attributed the exothermic phenomena observed in their ARC measurements to the following reactions



The total heat released by the first exothermic process (Reaction 3) was found to be roughly proportional to the molarity of the electrolyte. Lim et al. evaluated the thermal stability of 1 M NaClO<sub>4</sub> in PC electrolyte in contact with the Na<sub>3</sub>V<sub>2</sub>(PO<sub>4</sub>)<sub>3</sub> electrode material using TGA, DSC, and in situ XRD measurements.<sup>[363]</sup> The material maintained good thermal stability up to 450 °C, with no exothermic event, thanks to the intrinsic stability of the P–O bonding.<sup>[364]</sup> Zhao et al.<sup>[361]</sup> investigated the thermal stability of 1 M NaClO<sub>4</sub>/EC:DMC with charged NaFeO<sub>2</sub> electrodes. DSC thermograms showed that the charged material, Na<sub>0.58</sub>FeO<sub>2</sub>, powder in contact with the electrolyte displays exothermic heat at relatively high temperatures (220–300 °C).

## 4.2. Effect of Additives

### 4.2.1. Flame Retarding Additives

The increase of the SIBs energy density implies a rise of the risk associated with thermal runaway and consequent fire and explosion. The use of nonflammable electrolytes is the best solution to build safer devices. However, the design of such electrolytes has always been accompanied by detrimental compromises such as low ionic conductivities and/or failure to protect the electrodes resulting in continuous degradation. The incorporation of flame-retarding (FR) compounds in the electrolyte as additives or, even, co-solvents is among the most efficient strategies to mitigate fire-induced hazards with limited effect to the electrochemical battery performance.<sup>[265]</sup> The action of flame retardants is generally based on the catalytic removal of highly reactive radical species formed during the

thermal decomposition of organic solvents.<sup>[265]</sup> The radical species are responsible for initiating and maintaining the gas-phase combustion reactions via a cascading chain propagation reaction mechanism. Thus, FR additives must mitigate/stop the catalytic action of these reactive species by either chemically interacting and/or creating an insulator barrier via mechanical or physical means. It is known that FRs containing phosphorus, halogen and their combination, taking advantage of synergistic effects, are among the most effective. Feng et al.<sup>[367]</sup> studied ethoxy(pentafluoro)cyclotriphosphazene (EFPN) as potential FR utilizing self-extinguishing time (SET). By adding 5% EFPN to 1 M NaPF<sub>6</sub>/EC:DEC (1:1, vol%), the flammability of the carbonate-based electrolyte was significantly inhibited. Moreover, the EFPN-based electrolyte is stable toward Na metal and evidenced improved cyclability of acetylene black (negative) and Na<sub>0.44</sub>MnO<sub>2</sub> (positive) electrodes.

#### 4.2.2. Overcharge Protecting Additives

Overcharge is a major safety issue of batteries,<sup>[265,368]</sup> which can lead to the formation of flammable gases and eventually fire and/or explosion of the cell. To avoid this issue, considerable efforts have been dedicated towards designing overcharge inhibitors, such as redox shuttles and shutdown-type electrolyte additives, among others.<sup>[1]</sup> Shutdown-type additives polymerize at a characteristic potential to form insulating polymeric species on the electrode surface, avoiding any further degradation reaction. Their use is among the most promising, common and cost-efficient approaches proposed so far. Biphenyl (BP), the well-known overcharge protection additive for the 4 V-class positive electrode materials in commercial LIBs, has also been investigated for SIBs.<sup>[368]</sup> Electro-polymerizing at 4.3 V (vs Na/Na<sup>+</sup>), it has been shown capable of protecting the Na<sub>0.44</sub>MnO<sub>2</sub>/1 M NaPF<sub>6</sub> EC:DEC (1:1, vol) + 3% BP/Na battery cell from thermal runaway upon overcharge (Figure 20).

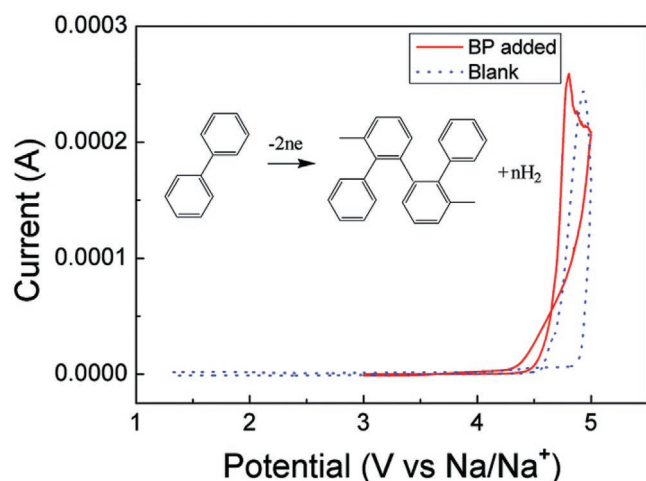


**Figure 20.** CV curves of 1 M NaPF<sub>6</sub>/ EC: DEC (1:1, v:v) with and without 3% BP and the overcharge protection mechanism of BP (inner graph). Reproduced with permission.<sup>[368]</sup> Copyright 2017, RSC Publishing group.

## 5. Conclusive Remarks and Outlook

The years between 2014 and 2019 beheld an exciting growth in the development of SIBs, where the number of publications has exponentially increased year by year. Based on our deep literature assessment, the research community seems to realize gradually that the key issue to the practical advancement of SIBs is the electrolyte along with the interfacial phenomena and safety-related issues. This is because the electrolyte and its electrodes interfaces affect the overall performance of the Na cells, enlisting the rate capability, energy density, power density, coulombic efficiency, long-term cycling life, self-discharge rate & fire-induced hazards. Herein, we surveyed the current status and future perspectives of the electrolytes for Na-based rechargeable batteries. The main summaries are presented as follows:

- i) *Electrolyte development:* The electrolyte formulation is the key enabling high-performance SIBs. An in-depth understanding of the electrolyte components influences on the electrochemical behavior of SIBs, will allow the design of electrolytes leading to superior electrochemical performance in SIBs. Of fundamental importance is the investigation of full cells configuration, since the electrolyte optimized for the negative electrode is usually incompatible with the positive one and vice versa. In terms of electrolyte composition, several studies suggested that linear carbonate should be avoided in the formulation due to their instability in SIBs. The use of high-throughput screening analysis methods of large numbers of electrolyte formulations via combined theoretical, electrochemical, and spectroscopic methods will speed up the search and optimization consistently. A systematic way of designing electrolytes is needed for future Na-based rechargeable batteries.
- ii) *Interphases in SIBs:* The detailed literature survey in this review clearly evidenced fundamental dissimilarities between the chemistries of the passivation layers formed on Li and Na. The larger size of Na metal, lower Lewis acidity, high solubility of Na-based SEI compounds, large equivalent volume of Na metal, higher reduction potential of Na, lower desolvation energy of Na etc. does undoubtedly affect the nature, composition and quality of the passivation layers and a detailed study considering all the underlying differences is urgently needed. Glyme-based electrolyte results are extremely promising, capable to originate SEI characterized by reduced thickness and higher mechanical and electrochemical stability. On the other hand, the limited stability upon oxidation of this class of electrolyte is a handicap. The achievement of deep understanding of the electrode/electrolyte interphase phenomena is extremely limited by the available experimental methods. The development of advanced characterization tools capable to shed light on this few nanometers region is the key for its comprehension.
- iii) *Safety:* Lastly, but not least, the large-scale deployment of large-format Na-based rechargeable batteries requires the systematic evaluation and detailed appraisal of the safety-related hazards. From the surveyed data, while the desodiated cathodes seem to be much safer than their Li counterparts, the anode proved to be less thermally stable. As most of the cascading thermal reactions start from the

anode side, the safety issue of Na-based batteries could be among the most detrimental factor for their future integration. Moreover, most of the safety tests are focused on thermal stability studies. However, fire-induced hazards such flammability and fire tests at cell level need to be systematically investigated.

## Acknowledgements

G.G.E. and G.A.E. contributed equally to this work. The financial support from the support Initiative and Networking Fund of the Helmholtz Association within the Network of Excellence on post-Lithium batteries (ExNet-0035) is kindly acknowledged.

## Conflict of Interest

The authors declare no conflict of interest.

## Keywords

additives, CEI, electrolytes, interphase, safety, SEI, sodium rechargeable batteries

Received: January 10, 2020  
Revised: February 25, 2020  
Published online: April 7, 2020

- [1] N. Yabuuchi, K. Kubota, M. Dahbi, S. Komaba, *Chem. Rev.* **2014**, *114*, 11636.
- [2] A. Ponrouch, D. Monti, A. Boschini, B. Steen, P. Johansson, M. R. Palacin, *J. Mater. Chem. A* **2015**, *3*, 22.
- [3] G. G. Eshetu, S. Grugeon, H. Kim, S. Jeong, L. Wu, G. Gachot, S. Laruelle, M. Armand, S. Passerini, *ChemSusChem* **2016**, *9*, 462.
- [4] H. Che, S. Chen, Y. Xie, H. Wang, K. Amine, X.-Z. Liao, Z.-F. Ma, *Energy Environ. Sci.* **2017**, *10*, 1075.
- [5] A. Mauger, C. M. Julien, A. Paoletta, M. Armand, K. Zaghib, *Mater. Sci. Eng., R* **2018**, *134*, 1.
- [6] C. Bommier, X. Ji, *Small* **2018**, *14*, 1703576.
- [7] E. Jónsson, P. Johansson, *Phys. Chem. Chem. Phys.* **2012**, *14*, 10774.
- [8] M. Okoshi, Y. Yamada, A. Yamada, H. Nakai, *J. Electrochem. Soc.* **2013**, *160*, A2160.
- [9] A. V. Cresce, S. M. Russell, O. Borodin, J. A. Allen, M. A. Schroeder, M. Dai, J. Peng, M. P. Gobet, S. G. Greenbaum, R. E. Rogers, K. Xu, *Phys. Chem. Chem. Phys.* **2017**, *19*, 574.
- [10] T. A. Pham, K. E. Kweon, A. Samanta, V. Lordi, J. E. Pask, *J. Phys. Chem. C* **2017**, *121*, 21913.
- [11] G. Kamath, R. W. Cutler, S. A. Deshmukh, M. Shakourian-fard, R. Parrish, J. Huether, D. P. Butt, C. Xiong, S. K. R. S. Sankaranarayanan, H. Xiong, S. K. R. S. Sankaranarayanan, *J. Phys. Chem. C* **2014**, *118*, 13406.
- [12] M. Shakourian-Fard, G. Kamath, K. Smith, H. Xiong, S. K. R. S. Sankaranarayanan, *J. Phys. Chem. C* **2015**, *119*, 22747.
- [13] H. Kumar, E. Detsi, D. P. Abraham, V. B. Shenoy, *Chem. Mater.* **2016**, *28*, 8930.
- [14] A. Ponrouch, E. Marchante, M. Courty, J.-M. Tarascon, M. R. Palacin, *Energy Environ. Sci.* **2012**, *5*, 8572.
- [15] A. Ponrouch, R. Dedryvère, D. Monti, A. E. Demet, J. M. Ateba Mba, L. Croguennec, C. Masquelier, P. Johansson, M. R. Palacin, *Energy Environ. Sci.* **2013**, *6*, 2361.
- [16] A. Ponrouch, M. R. Palacin, *Electrochem. Commun.* **2015**, *54*, 51.
- [17] J. Y. Jang, H. Kim, Y. Lee, K. T. Lee, K. Kang, N.-S. Choi, *Electrochem. Commun.* **2014**, *44*, 74.
- [18] H. Lee, Y.-I. Kim, J.-K. Park, J. W. Choi, *Chem. Commun.* **2012**, *48*, 8416.
- [19] A. Bhide, J. Hofmann, A. Katharina Dürr, J. J. Janek, P. Adelhelm, A. Katharina Durr, J. J. Janek, P. Adelhelm, *Phys. Chem. Chem. Phys.* **2014**, *16*, 1987.
- [20] A. Rudola, D. Aurbach, P. Balaya, *Electrochem. Commun.* **2014**, *46*, 56.
- [21] T. Hosaka, S. Muratsubaki, K. Kubota, H. Onuma, S. Komaba, *J. Phys. Chem. Lett.* **2019**, *10*, 3296.
- [22] T. D. Hatchard, M. N. Obrovac, *J. Electrochem. Soc.* **2014**, *161*, A1748.
- [23] J. Conder, C. Villevieille, *Chem. Commun.* **2019**, *55*, 1275.
- [24] G. Yan, D. Alves-Dalla-Corte, W. Yin, N. Madern, G. Gachot, J.-M. Tarascon, *J. Electrochem. Soc.* **2018**, *165*, A1222.
- [25] S. Komaba, T. Ishikawa, N. Yabuuchi, W. Murata, A. Ito, Y. Ohsawa, *ACS Appl. Mater. Interfaces* **2011**, *3*, 4165.
- [26] A. Darwiche, C. Marino, M. T. Sougrati, B. Fraise, L. Stievano, L. Monconduit, *J. Am. Chem. Soc.* **2012**, *134*, 20805.
- [27] J. Qian, Y. Chen, L. Wu, Y. Cao, X. Ai, H. Yang, *Chem. Commun.* **2012**, *48*, 7070.
- [28] L. Baggetto, M. Marszewski, J. Górka, M. Jaroniec, G. M. Veith, *J. Power Sources* **2013**, *243*, 699.
- [29] Y. Zhu, X. Han, Y. Xu, Y. Liu, S. Zheng, K. Xu, L. Hu, C. Wang, *ACS Nano* **2013**, *7*, 6378.
- [30] L. Ji, M. Gu, Y. Shao, X. Li, M. H. Engelhard, B. W. Arey, W. Wang, Z. Nie, J. Xiao, C. Wang, J. G. Zhang, J. Liu, *Adv. Mater.* **2014**, *26*, 2901.
- [31] V. Etacheri, O. Haik, Y. Go, G. A. Roberts, I. C. Stefan, R. Fasching, D. Aurbach, *Langmuir* **2012**, *28*, 965.
- [32] X. Chen, X. Li, D. Mei, J. Feng, M. Y. Hu, J. Hu, M. Engelhard, J. Zheng, W. Xu, J. Xiao, J. Liu, J.-G. Zhang, *ChemSusChem* **2014**, *7*, 549.
- [33] I. Hasa, S. Passerini, J. Hassoun, *RSC Adv.* **2015**, *5*, 48928.
- [34] A. Darwiche, L. Bodenes, L. Madec, L. Monconduit, H. Martinez, *Electrochim. Acta* **2016**, *207*, 284.
- [35] V. Dall'Asta, D. Buchholz, L. G. Chagas, X. Dou, C. Ferrara, E. Quartarone, C. Tealdi, S. Passerini, *ACS Appl. Mater. Interfaces* **2017**, *9*, 34891.
- [36] A. Ponrouch, A. R. Goñi, M. R. Palacin, *Electrochem. Commun.* **2013**, *27*, 85.
- [37] L. Wu, D. Buchholz, D. Bresser, L. Gomes Chagas, S. Passerini, *J. Power Sources* **2014**, *251*, 379.
- [38] M. Dahbi, T. Nakano, N. Yabuuchi, T. Ishikawa, K. Kubota, M. Fukunishi, S. Shibahara, J. Y. Son, Y. T. Cui, H. Oji, S. Komaba, *Electrochem. Commun.* **2014**, *44*, 66.
- [39] R. Dugas, A. Ponrouch, G. Gachot, R. David, M. R. Palacin, J. M. Tarascon, *J. Electrochem. Soc.* **2016**, *163*, A2333.
- [40] M. J. Piernas-Muñoz, E. Castillo-Martínez, J. L. Gómez-Cámer, T. Rojo, *Electrochim. Acta* **2016**, *200*, 123.
- [41] S.-M. Oh, S.-T. Myung, C. S. Yoon, J. Lu, J. Hassoun, B. Scrosati, K. Amine, Y.-K. Sun, *Nano Lett.* **2014**, *14*, 1620.
- [42] Z. Zeng, X. Jiang, R. Li, D. Yuan, X. Ai, H. Yang, Y. Cao, *Adv. Sci.* **2016**, *3*, 1600066.
- [43] Y. Yu, H. Che, X. Yang, Y. Deng, L. Li, Z. F. Ma, *Electrochem. Commun.* **2020**, *110*, 106635.
- [44] D. A. Stevens, J. R. Dahn, *J. Electrochem. Soc.* **2000**, *147*, 1271.
- [45] P. Thomas, D. Billaud, *Electrochim. Acta* **2002**, *47*, 3303.
- [46] K. Nobuhara, H. Nakayama, M. Nose, S. Nakanishi, H. Iba, *J. Power Sources* **2013**, *243*, 585.
- [47] B. Jache, P. Adelhelm, *Angew. Chem., Int. Ed.* **2014**, *53*, 10169.
- [48] H. Kim, J. Hong, Y.-U. Park, J. Kim, I. Hwang, K. Kang, *Adv. Funct. Mater.* **2015**, *25*, 534.

- [49] B. Jache, J. O. Binder, T. Abe, P. Adelhelm, M. Mizuno, W. Sirisaksoontorn, P. Adelhelm, *Phys. Chem. Chem. Phys.* **2016**, *18*, 14299.
- [50] H. Kim, J. Hong, G. Yoon, H. Kim, K.-Y. Park, M.-S. Park, W.-S. Yoon, K. Kang, *Energy Environ. Sci.* **2015**, *8*, 2963.
- [51] G. Yoon, H. Kim, I. Park, K. Kang, *Adv. Energy Mater.* **2017**, *7*, 1601519.
- [52] K. Gotoh, H. Maruyama, T. Miyatou, M. Mizuno, K. Urita, H. Ishida, *J. Phys. Chem. C* **2016**, *120*, 28152.
- [53] C. J. Yu, S. B. Ri, S. H. Choe, G. C. Ri, Y. H. Kye, S. C. Kim, *Electrochim. Acta* **2017**, *253*, 589.
- [54] J. Maibach, F. Jeschull, D. Brandell, K. Edström, M. Valvo, *ACS Appl. Mater. Interfaces* **2017**, *9*, 12373.
- [55] Z. Zhu, F. Cheng, Z. Hu, Z. Niu, J. Chen, *J. Power Sources* **2015**, *293*, 626.
- [56] M. Liu, L. Xing, K. Xu, H. Zhou, J. Lan, C. Wang, W. Li, *Energy Storage Mater.* **2020**, *26*, 32.
- [57] I. Hasa, X. Dou, D. Buchholz, Y. Shao-Horn, J. Hassoun, S. Passerini, B. Scrosati, *J. Power Sources* **2016**, *310*, 26.
- [58] G. A. Elia, N. A. Kyeremateng, K. Marquardt, R. Hahn, *Batteries Supercaps* **2019**, *2*, 83.
- [59] K. V. Kravchik, S. Wang, L. Piveteau, M. V. Kovalenko, *Chem. Mater.* **2017**, *29*, 4484.
- [60] Z. W. Seh, J. Sun, Y. Sun, Y. Cui, *ACS Cent. Sci.* **2015**, *1*, 449.
- [61] K. Westman, R. Dugas, P. Jankowski, W. Wiczczonek, G. Gachot, M. Morcrette, E. Irisarri, A. Ponrouch, M. R. Palacín, J.-M. Tarascon, P. Johansson, *ACS Appl. Energy Mater.* **2018**, *1*, 2671.
- [62] T. Nestler, E. Roedern, N. F. Uvarov, J. Hanzig, G. A. Elia, M. de Vivanco, *Phys. Sci. Rev.* **2018**, *4*, 2017.
- [63] M. Armand, F. Endres, D. R. MacFarlane, H. Ohno, B. Scrosati, *Nat. Mater.* **2009**, *8*, 621.
- [64] I. Osada, H. de Vries, B. Scrosati, S. Passerini, *Angew. Chem., Int. Ed.* **2015**, *55*, 500.
- [65] D. R. MacFarlane, M. Forsyth, P. C. Howlett, M. Kar, S. Passerini, J. M. Pringle, H. Ohno, M. Watanabe, F. Yan, W. Zheng, S. Zhang, J. Zhang, *Nat. Rev. Mater.* **2016**, *1*, 15005.
- [66] G. A. Elia, U. Ulissi, S. Jeong, S. Passerini, J. Hassoun, *Energy Environ. Sci.* **2016**, *9*, 3210.
- [67] G. G. Eshetu, S. Jeong, P. Pandard, A. Lecocq, G. Marlair, S. Passerini, *ChemSusChem* **2017**, *10*, 3146.
- [68] G. Gebresilassie Eshetu, M. Armand, B. Scrosati, S. Passerini, *Angew. Chem., Int. Ed.* **2014**, *53*, 13342.
- [69] L. S. Plashnitsa, E. Kobayashi, Y. Noguchi, S. Okada, J. Yamaki, *J. Electrochem. Soc.* **2010**, *157*, A536.
- [70] F. Wu, N. Zhu, Y. Bai, L. Liu, H. Zhou, C. Wu, *ACS Appl. Mater. Interfaces* **2016**, *8*, 21381.
- [71] D. Monti, E. Jónsson, M. R. Palacín, P. Johansson, *J. Power Sources* **2014**, *245*, 630.
- [72] T. Hosokawa, K. Matsumoto, T. Nohira, R. Hagiwara, A. Fukunaga, S. Sakai, K. Nitta, *J. Phys. Chem. C* **2016**, *120*, 9628.
- [73] C. Ding, T. Nohira, K. Kuroda, R. Hagiwara, A. Fukunaga, S. Sakai, K. Nitta, S. Inazawa, *J. Power Sources* **2013**, *238*, 296.
- [74] A. Fukunaga, T. Nohira, R. Hagiwara, K. Numata, E. Itani, S. Sakai, K. Nitta, S. Inazawa, *J. Power Sources* **2014**, *246*, 387.
- [75] C. Ding, T. Nohira, R. Hagiwara, A. Fukunaga, S. Sakai, K. Nitta, *Electrochim. Acta* **2015**, *176*, 344.
- [76] T. Yamamoto, T. Yamaguchi, T. Nohira, R. Hagiwara, A. Fukunaga, S. Sakai, K. Nitta, *Electrochemistry* **2017**, *85*, 391.
- [77] C.-Y. Chen, K. Matsumoto, T. Nohira, C. Ding, T. Yamamoto, R. Hagiwara, *Electrochim. Acta* **2014**, *133*, 583.
- [78] C.-Y. Chen, T. Kiko, T. Hosokawa, K. Matsumoto, T. Nohira, R. Hagiwara, *J. Power Sources* **2016**, *332*, 51.
- [79] C.-Y. Chen, K. Matsumoto, T. Nohira, R. Hagiwara, *J. Electrochem. Soc.* **2015**, *162*, A176.
- [80] C.-Y. Chen, K. Matsumoto, T. Nohira, R. Hagiwara, *Electrochem. Commun.* **2014**, *45*, 63.
- [81] C. Ding, T. Nohira, R. Hagiwara, *J. Mater. Chem. A* **2015**, *3*, 20767.
- [82] J. Hwang, K. Matsumoto, T. Nohira, R. Hagiwara, *Electrochemistry* **2017**, *85*, 675.
- [83] C. Ding, T. Nohira, R. Hagiwara, *J. Power Sources* **2017**, *354*, 10.
- [84] C. Ding, T. Nohira, R. Hagiwara, *Electrochim. Acta* **2017**, *231*, 412.
- [85] S. A. Mohd Noor, P. C. Howlett, D. R. MacFarlane, M. Forsyth, *Electrochim. Acta* **2013**, *114*, 766.
- [86] H. Yoon, H. Zhu, A. Hervault, M. Armand, D. R. MacFarlane, M. Forsyth, *Phys. Chem. Chem. Phys.* **2014**, *16*, 12350.
- [87] M. Forsyth, H. Yoon, F. Chen, H. Zhu, D. R. MacFarlane, M. Armand, P. C. Howlett, *J. Phys. Chem. C* **2016**, *120*, 4276.
- [88] S. A. M. Noor, N. C. Su, L. T. Khoon, N. S. Mohamed, A. Ahmad, M. Z. A. Yahya, H. Zhu, M. Forsyth, D. R. MacFarlane, *Electrochim. Acta* **2017**, *247*, 983.
- [89] F. Makhlooghiazad, R. Yunis, D. Mecerreyes, M. Armand, P. C. Howlett, M. Forsyth, *Solid State Ionics* **2017**, *312*, 44.
- [90] F. Chen, P. Howlett, M. Forsyth, *J. Phys. Chem. C* **2018**, *122*, 105.
- [91] F. Chen, M. Forsyth, S. Roy, K. Mazur, A. Nazet, R. Buchner, M. Bonn, J. Hunger, K. Hayamizu, S. Tsuzuki, M. Hattori, N. Terada, *Phys. Chem. Chem. Phys.* **2016**, *18*, 19336.
- [92] K. Matsumoto, Y. Okamoto, T. Nohira, R. Hagiwara, *J. Phys. Chem. C* **2015**, *119*, 7648.
- [93] M. Hilder, P. C. Howlett, D. Saurel, E. Gonzalo, M. Armand, T. Rojo, D. R. MacFarlane, M. Forsyth, *J. Power Sources* **2017**, *349*, 45.
- [94] L. G. Chagas, D. Buchholz, L. Wu, B. Vortmann, S. Passerini, *J. Power Sources* **2014**, *247*, 377.
- [95] I. Hasa, S. Passerini, J. Hassoun, *J. Power Sources* **2016**, *303*, 203.
- [96] H. Zhang, I. Hasa, D. Buchholz, B. Qin, D. Geiger, S. Jeong, U. Kaiser, S. Passerini, *NPG Asia Mater.* **2017**, *9*, e370.
- [97] X. Wang, Z. Shang, A. Yang, Q. Zhang, F. Cheng, D. Jia, J. Chen, *Chem* **2019**, *5*, 364.
- [98] N. Wongittharom, T.-C. Lee, C.-H. Wang, Y.-C. Wang, J.-K. Chang, *J. Mater. Chem. A* **2014**, *2*, 5655.
- [99] N. Wongittharom, C.-H. Wang, Y.-C. Wang, C.-H. Yang, J.-K. Chang, *ACS Appl. Mater. Interfaces* **2014**, *6*, 17564.
- [100] C.-H. Wang, Y.-W. Yeh, N. Wongittharom, Y.-C. Wang, C.-J. Tseng, S.-W. Lee, W.-S. Chang, J.-K. Chang, *J. Power Sources* **2015**, *274*, 1016.
- [101] C.-H. Wang, C.-H. Yang, J.-K. Chang, *Chem. Commun.* **2016**, *52*, 10890.
- [102] C. Y. Li, J. Patra, C. H. Yang, C. M. Tseng, S. B. Majumder, Q. F. Dong, J. K. Chang, *ACS Sustainable Chem. Eng.* **2017**, *5*, 8269.
- [103] L. Otaegui, E. Goikolea, F. Aguesse, M. Armand, T. Rojo, G. Singh, *J. Power Sources* **2015**, *297*, 168.
- [104] H. Usui, Y. Domi, M. Shimizu, A. Imoto, K. Yamaguchi, H. Sakaguchi, *J. Power Sources* **2016**, *329*, 428.
- [105] A. Fukunaga, T. Nohira, R. Hagiwara, K. Numata, E. Itani, S. Sakai, K. Nitta, *J. Appl. Electrochem.* **2016**, *46*, 487.
- [106] B. E. Gurkan, Z. Qiang, Y.-M. Chen, Y. Zhu, B. D. Vogt, *J. Electrochem. Soc.* **2017**, *164*, H5093.
- [107] M. Dahbi, M. Fukunishi, T. Horiba, N. Yabuuchi, S. Yasuno, S. Komaba, *J. Power Sources* **2017**, *363*, 404.
- [108] T. Vogl, S. Menne, A. Balducci, *Phys. Chem. Chem. Phys.* **2014**, *16*, 25014.
- [109] M. Montanino, M. Moreno, M. Carewska, G. Maresca, E. Simonetti, R. Lo Presti, F. Alessandrini, G. B. Appetecchi, *J. Power Sources* **2014**, *269*, 608.
- [110] S. Wilken, S. Xiong, J. Scheers, P. Jacobsson, P. Johansson, *J. Power Sources* **2015**, *275*, 935.
- [111] S. Menne, R.-S. Kühnel, A. Balducci, *Electrochim. Acta* **2013**, *90*, 641.
- [112] G. A. Elia, R. Bernhard, J. Hassoun, *RSC Adv.* **2015**, *5*, 21360.
- [113] D. Monti, A. Ponrouch, M. R. Palacín, P. Johansson, *J. Power Sources* **2016**, *324*, 712.
- [114] C. V. Manohar, A. Raj K, M. Kar, M. Forsyth, D. R. MacFarlane, S. Mitra, *Sustainable Energy Fuels* **2018**, *2*, 566.

- [115] T. Stettner, P. Huang, M. Goktas, P. Adelhelm, A. Balducci, *J. Chem. Phys.* **2018**, *148*, 193825.
- [116] L. Suo, Y. S. Hu, H. Li, M. Armand, L. Chen, *Nat. Commun.* **2013**, *4*, 1481.
- [117] T. M. Pappenfus, W. A. Henderson, B. B. Owens, K. R. Mann, W. H. Smyrl, *J. Electrochem. Soc.* **2004**, *151*, A209.
- [118] W. A. Henderson, F. McKenna, M. A. Khan, N. R. Brooks, V. G. Young, R. Frech, *Chem. Mater.* **2005**, *17*, 2284.
- [119] S. Terada, T. Mandai, R. Nozawa, K. Yoshida, K. Ueno, S. Tsuzuki, K. Dokko, M. Watanabe, *Phys. Chem. Chem. Phys.* **2014**, *16*, 11737.
- [120] S. Terada, H. Susa, S. Tsuzuki, T. Mandai, K. Ueno, Y. Urnebayashi, K. Dokko, M. Watanabe, *J. Phys. Chem. C* **2016**, *120*, 23339.
- [121] C. Guo, K. Zhang, Q. Zhao, L. Pei, J. Chen, J. Chen, C. Wang, H. X. Yang, D. Wang, X. Li, A. Maniyanan, D. Wang, *Chem. Commun.* **2015**, *51*, 10244.
- [122] R. Cao, K. Mishra, X. Li, J. Qian, M. H. Engelhard, M. E. Bowden, K. S. Han, K. T. Mueller, W. A. Henderson, J.-G. Zhang, *Nano Energy* **2016**, *30*, 825.
- [123] L. Schafzahl, I. Hanzu, M. Wilkening, S. A. Freunberger, *ChemSusChem* **2017**, *10*, 401.
- [124] J. J. Lee, Y. Lee, J. J. Lee, S.-M. Lee, J.-H. Choi, H. Kim, M.-S. Kwon, K. Kang, K. T. Lee, N.-S. Choi, *ACS Appl. Mater. Interfaces* **2017**, *9*, 3723.
- [125] M. He, K. C. Lau, X. Ren, N. Xiao, W. D. McCulloch, L. A. Curtiss, Y. Wu, *Angew. Chem., Int. Ed.* **2016**, *55*, 15310.
- [126] K. Takada, Y. Yamada, E. Watanabe, J. Wang, K. Sodeyama, Y. Tateyama, K. Hirata, T. Kawase, A. Yamada, *ACS Appl. Mater. Interfaces* **2017**, *9*, 33802.
- [127] J. Wang, Y. Yamada, K. Sodeyama, E. Watanabe, K. Takada, Y. Tateyama, A. Yamada, *Nat. Energy* **2018**, *3*, 22.
- [128] D. Bin, F. Wang, A. G. Tamirat, L. Suo, Y. Wang, C. Wang, Y. Xia, *Adv. Energy Mater.* **2018**, *8*, 1703008.
- [129] J. F. F. Whitacre, T. Wiley, S. Shanbhag, Y. Wenzhuo, A. Mohamed, S. E. E. Chun, E. Weber, D. Blackwood, E. Lynch-Bell, J. Gulakowski, C. Smith, D. Humphreys, *J. Power Sources* **2012**, *213*, 255.
- [130] X. Wu, Y. Cao, X. Ai, J. Qian, H. Yang, *Electrochem. Commun.* **2013**, *31*, 145.
- [131] S. Il Park, I. Gocheva, S. Okada, J. Yamaki, *J. Electrochem. Soc.* **2011**, *158*, A1067.
- [132] M. Minakshi, D. Meyrick, *J. Alloys Compd.* **2013**, *555*, 10.
- [133] Z. Li, D. Young, K. Xiang, W. C. Carter, Y.-M. Chiang, *Adv. Energy Mater.* **2013**, *3*, 290.
- [134] W. Song, X. Ji, Y. Zhu, H. Zhu, F. Li, J. Chen, F. Lu, Y. Yao, C. E. Banks, *ChemElectroChem* **2014**, *1*, 871.
- [135] Y. H. Jung, C. H. Lim, J.-H. Kim, D. K. Kim, *RSC Adv.* **2014**, *4*, 9799.
- [136] A. J. Fernández-Ropero, D. Saurel, B. Acebedo, T. Rojo, M. Casas-Cabanas, *J. Power Sources* **2015**, *291*, 40.
- [137] X. Y. Wu, M. Y. Sun, Y. F. Shen, J. F. Qian, Y. L. Cao, X. P. Ai, H. X. Yang, *ChemSusChem* **2014**, *7*, 407.
- [138] A. J. Fernández-Ropero, M. J. Piernas-Muñoz, E. Castillo-Martínez, T. Rojo, M. Casas-Cabanas, *Electrochim. Acta* **2016**, *210*, 352.
- [139] H. Gao, J. B. Goodenough, *Angew. Chem., Int. Ed.* **2016**, *55*, 12768.
- [140] J. Dong, G. Zhang, X. Wang, S. Zhang, C. Deng, *J. Mater. Chem. A* **2017**, *5*, 18725.
- [141] W. Wu, S. Shabag, J. Chang, A. Rutt, J. F. Whitacre, *J. Electrochem. Soc.* **2015**, *162*, A803.
- [142] K. Nakamoto, Y. Kano, A. Kitajou, S. Okada, *J. Power Sources* **2016**, *327*, 327.
- [143] L. Suo, O. Borodin, Y. Wang, X. Rong, W. Sun, X. Fan, S. Xu, M. A. Schroeder, A. V. Cresce, F. Wang, C. Yang, Y. S. Hu, K. Xu, C. Wang, *Adv. Energy Mater.* **2017**, *7*, 1701189.
- [144] L. Suo, O. Borodin, T. Gao, M. Olguin, J. Ho, X. Fan, C. Luo, C. Wang, K. Xu, *Science* **2015**, *350*, 938.
- [145] J. Han, H. Zhang, A. Varzi, S. Passerini, *ChemSusChem* **2018**, *11*, 3704.
- [146] K. Xu, *Chem. Rev.* **2014**, *114*, 11503.
- [147] K. Xu, *Chem. Rev.* **2004**, *104*, 4303.
- [148] D. E. Fenton, J. M. Parker, P. V. Wright, *Polymer* **1973**, *14*, 589.
- [149] C. Berthier, W. Gorecki, M. Minier, M. B. Armand, J. M. Chabagno, P. Rigaud, *Solid State Ionics* **1983**, *11*, 91.
- [150] G. B. Appetecchi, F. Alessandrini, M. Carewska, T. Caruso, P. P. Proisini, S. Scaccia, S. Passerini, *J. Power Sources* **2001**, *97–98*, 790.
- [151] W. H. Meyer, *Adv. Mater.* **1998**, *10*, 439.
- [152] K. Naresh Kumar, T. Sreekanth, M. Jaipal Reddy, U. V. Subba Rao, *J. Power Sources* **2001**, *101*, 130.
- [153] C. V. Subba Reddy, A.-P. Jin, Q.-Y. Zhu, L.-Q. Mai, W. Chen, *Eur. Phys. J. E* **2006**, *19*, 471.
- [154] K. Kiran Kumar, M. Ravi, Y. Pavani, S. Bhavani, A. K. Sharma, V. V. R. Narasimha Rao, *Phys. B* **2011**, *406*, 1706.
- [155] C. V. Subba Reddy, X. Han, Q.-Y. Zhu, L.-Q. Mai, W. Chen, *Eur. Polym. J.* **2006**, *42*, 3114.
- [156] P. Balaji Bhargav, V. M. Mohan, A. K. Sharma, V. V. R. N. Rao, *J. Appl. Polym. Sci.* **2008**, *108*, 510.
- [157] P. B. Bhargav, V. M. Mohan, A. K. Sharma, V. V. R. N. Rao, *Curr. Appl. Phys.* **2009**, *9*, 165.
- [158] Z. Osman, K. B. Md Isa, A. Ahmad, L. Othman, *Ionics* **2010**, *16*, 431.
- [159] J. Mindemark, R. Mogensen, M. J. Smith, M. M. Silva, D. Brandell, *Electrochem. Commun.* **2017**, *77*, 58.
- [160] K. West, B. Zachau-Christiansen, T. Jacobsen, E. Hiort-Lorenzen, S. Skaarup, *Br. Polym. J.* **1988**, *20*, 243.
- [161] S. A. Hashmi, S. Chandra, *Mater. Sci. Eng., B* **1995**, *34*, 18.
- [162] R. Chandrasekaran, S. Selladurai, *J. Solid State Electrochem.* **2001**, *5*, 355.
- [163] V. M. Mohan, V. Raja, P. Balaji Bhargav, A. K. Sharma, V. V. R. Narasimha Rao, *J. Polym. Res.* **2007**, *14*, 283.
- [164] X. Qi, Q. Ma, L. Liu, Y.-S. Hu, H. Li, Z. Zhou, X. Huang, L. Chen, *ChemElectroChem* **2016**, *3*, 1741.
- [165] A. Boschin, P. Johansson, *Electrochim. Acta* **2015**, *175*, 124.
- [166] Q. Ma, J. Liu, X. Qi, X. Rong, Y. Shao, W. Feng, J. Nie, Y.-S. Hu, H. Li, X. Huang, L. Chen, Z. Zhou, *J. Mater. Chem. A* **2017**, *5*, 7738.
- [167] J. Serra Moreno, M. Armand, M. B. Berman, S. G. Greenbaum, B. Scrosati, S. Panero, *J. Power Sources* **2014**, *248*, 695.
- [168] W. Gorecki, M. Jeannin, E. Belorizky, C. Roux, M. Armand, *J. Phys.: Condens. Matter* **1995**, *7*, 6823.
- [169] F. Croce, G. B. Appetecchi, L. Persi, B. Scrosati, *Nature* **1998**, *394*, 456.
- [170] B. Zewde, G. A. Elia, S. Admassie, J. Zimmermann, M. Hagemann, C. S. Isfort, B. Scrosati, J. Hassoun, *Solid State Ionics* **2014**, *268*, 174.
- [171] M. Forsyth, D. R. MacFarlane, A. Best, J. Adebahr, P. Jacobsson, A. J. Hill, *Solid State Ionics* **2002**, *147*, 203.
- [172] T. Itoh, *Solid State Ionics* **2003**, *156*, 393.
- [173] A. S. Best, A. Ferry, D. R. MacFarlane, M. Forsyth, *Solid State Ionics* **1999**, *126*, 269.
- [174] D. Golodnitsky, E. Livshits, R. Kovarsky, E. Peled, S. H. Chung, S. Suarez, S. G. Greenbaum, *Electrochem. Solid-State Lett.* **2004**, *7*, A412.
- [175] J. L. Nugent, S. S. Moganty, L. A. Archer, *Adv. Mater.* **2010**, *22*, 3677.
- [176] J. L. Schaefer, S. S. Moganty, D. A. Yanga, L. A. Archer, *J. Mater. Chem.* **2011**, *21*, 10094.
- [177] X. Xu, Y. Li, J. Cheng, G. Hou, X. Nie, Q. Ai, L. Dai, J. Feng, L. Ci, *J. Energy Chem.* **2020**, *41*, 73.
- [178] K. E. Thomas, S. E. Sloop, J. B. Kerr, J. Newman, *J. Power Sources* **2000**, *89*, 132.
- [179] M. Doyle, J. Newman, *Electrochim. Acta* **1995**, *40*, 2191.
- [180] M. Doyle, T. F. Fuller, J. Newman, *Electrochim. Acta* **1994**, *39*, 2073.
- [181] M. Rosso, C. Brissot, A. Teyssot, M. Dollé, L. Sannier, J.-M. Tarascon, R. Bouchet, S. Lascaud, *Electrochim. Acta* **2006**, *51*, 5334.

- [182] C. Brissot, M. Rosso, J.-N. Chazalviel, S. Lascaud, *J. Power Sources* **1999**, 81–82, 925.
- [183] L. M. Bronstein, R. L. Karlinsey, B. Stein, Z. Yi, J. Carini, J. W. Zwanziger, *Chem. Mater.* **2006**, 18, 708.
- [184] I. Villaluenga, X. Bogle, S. Greenbaum, I. Gil de Muro, T. Rojo, M. Armand, *J. Mater. Chem. A* **2013**, 1, 8348.
- [185] C. R. Pope, K. Romanenko, D. R. MacFarlane, M. Forsyth, L. A. O'Dell, *Electrochim. Acta* **2015**, 175, 62.
- [186] J. Li, H. Zhu, X. Wang, M. Armand, D. R. MacFarlane, M. Forsyth, *Electrochim. Acta* **2015**, 175, 232.
- [187] J. Li, H. Zhu, X. Wang, D. R. MacFarlane, M. Armand, M. Forsyth, *J. Mater. Chem. A* **2015**, 3, 19989.
- [188] H. Zhang, C. Li, M. Piszcz, E. Coya, T. Rojo, L. M. Rodriguez-Martinez, M. Armand, Z. Zhou, *Chem. Soc. Rev.* **2017**, 46, 797.
- [189] A. M. Stephan, *Eur. Polym. J.* **2006**, 42, 21.
- [190] A. Bhide, K. Hariharan, *Eur. Polym. J.* **2007**, 43, 4253.
- [191] M. Patel, K. G. Chandrappa, A. J. Bhattacharyya, *Solid State Ionics* **2010**, 181, 844.
- [192] A. Bhide, K. Hariharan, *Solid State Ionics* **2011**, 192, 360.
- [193] D. Praveen, S. V. Bhat, R. Damle, *Ionics* **2013**, 19, 1375.
- [194] C. Cao, W. Liu, L. Tan, X. Liao, L. Li, *Chem. Commun.* **2013**, 49, 11740.
- [195] C. Cao, H. Wang, W. Liu, X. Liao, L. Li, *Int. J. Hydrogen Energy* **2014**, 39, 16110.
- [196] H. Hou, Q. Xu, Y. Pang, L. Li, J. Wang, C. Zhang, C. Sun, *Adv. Sci.* **2017**, 4, 1700072.
- [197] N. K. Jyothi, K. V. Kumar, G. S. Sundari, P. N. Murthy, *Indian J. Phys.* **2016**, 90, 289.
- [198] K. Vignaroban, P. Badami, M. A. K. L. Dissanayake, P. Ravirajan, A. M. Kannan, *Ionics* **2017**, 23, 2817.
- [199] D. Kumar, S. A. Hashmi, *J. Power Sources* **2010**, 195, 5101.
- [200] F. Bella, F. Colò, J. R. Nair, C. Gerbaldi, *ChemSusChem* **2015**, 8, 3668.
- [201] H. Gao, W. Zhou, K. Park, J. B. Goodenough, *Adv. Energy Mater.* **2016**, 6, 1600467.
- [202] J.-S. S. Kim, H.-J. J. Ahn, I.-P. P. Kim, K.-W. W. Kim, J.-H. H. Ahn, C.-W. W. Park, H.-S. S. Ryu, *J. Solid State Electrochem.* **2008**, 12, 861.
- [203] V. Aravindan, C. Lakshmi, P. Vickraman, *Curr. Appl. Phys.* **2009**, 9, 1106.
- [204] D. Kumar, M. Suleman, S. A. Hashmi, *Solid State Ionics* **2011**, 202, 45.
- [205] Y. Ansari, B. Guo, J. H. Cho, K. Park, J. Song, C. J. Ellison, J. B. Goodenough, *J. Electrochem. Soc.* **2014**, 161, A1655.
- [206] H. Gao, B. Guo, J. Song, K. Park, J. B. Goodenough, *Adv. Energy Mater.* **2015**, 5, 1.
- [207] Y. Q. Yang, Z. Chang, M. X. Li, X. W. Wang, Y. P. Wu, *Solid State Ionics* **2015**, 269, 1.
- [208] S. Janakiraman, A. Surendran, S. Ghosh, S. Anandhan, A. Venimadhav, *Solid State Ionics* **2016**, 292, 130.
- [209] Y. Zhu, Y. Yang, L. Fu, Y. Wu, *Electrochim. Acta* **2017**, 224, 405.
- [210] J. Il Kim, Y. Choi, K. Y. Chung, J. H. Park, *Adv. Funct. Mater.* **2017**, 27, 1.
- [211] K. D. Kreuer, A. Wohlfarth, C. C. De Araujo, A. Fuchs, J. Maier, *ChemPhysChem* **2011**, 12, 2558.
- [212] J. Y. Song, Y. Y. Wang, C. C. Wan, *J. Power Sources* **1999**, 77, 183.
- [213] G. B. Appetecchi, F. Croce, B. Scrosati, *Electrochim. Acta* **1995**, 40, 991.
- [214] C.-W. Park, J.-H. Ahn, H.-S. Ryu, K.-W. Kim, H.-J. Ahn, *Electrochim. Solid-State Lett.* **2006**, 9, A123.
- [215] D. Kumar, S. A. Hashmi, *Solid State Ionics* **2010**, 181, 416.
- [216] S. A. Hashmi, M. Y. Bhat, M. K. Singh, N. T. K. Sundaram, B. P. C. Raghupathy, H. Tanaka, *J. Solid State Electrochem.* **2016**, 20, 2817.
- [217] D. Kumar, *Solid State Ionics* **2017**, 21, 1145.
- [218] V. K. Singh, S. Shalu, S. K. Chaurasia, R. K. Singh, *RSC Adv.* **2016**, 6, 40199.
- [219] A. Boschin, P. Johansson, *Electrochim. Acta* **2016**, 217, 1006.
- [220] S. A. Mohd Noor, H. Yoon, M. Forsyth, D. R. MacFarlane, *Electrochim. Acta* **2015**, 169, 376.
- [221] S. Seki, Y. Ohno, Y. Kobayashi, H. Miyashiro, A. Usami, Y. Mita, H. Tokuda, M. Watanabe, K. Hayamizu, S. Tsuzuki, M. Hattori, N. Terada, *J. Electrochem. Soc.* **2007**, 154, A173.
- [222] V. Palomares, P. Serras, I. Villaluenga, K. B. Hueso, J. Carretero-González, T. Rojo, *Energy Environ. Sci.* **2012**, 5, 5884.
- [223] L.-O. Hagman, P. Kierkegaard, P. Karvonen, A. I. Virtanen, J. Paasivirta, *Acta Chem. Scand.* **1968**, 22, 1822.
- [224] J. B. Goodenough, H.-P. Hong, J. A. Kafalas, *Mater. Res. Bull.* **1976**, 11, 203.
- [225] H.-P. Hong, *Mater. Res. Bull.* **1976**, 11, 173.
- [226] M. Guin, F. Tietz, *J. Power Sources* **2015**, 273, 1056.
- [227] R. D. Shannon, IUCr, *Acta Crystallogr. A* **1976**, 32, 751.
- [228] M. S. Whittingham, R. A. Huggins, *J. Chem. Phys.* **1971**, 54, 414.
- [229] J. L. Briant, G. C. Farrington, *J. Solid State Chem.* **1980**, 33, 385.
- [230] Y. Noguchi, E. Kobayashi, L. S. Plashnitsa, S. Okada, J. I. Yamaki, *Electrochim. Acta* **2013**, 101, 59.
- [231] F. Lalère, J. B. Leriche, M. Courty, S. Boulineau, V. Viallet, C. Masquelier, V. Seznec, *J. Power Sources* **2014**, 247, 975.
- [232] Q. Ma, M. Guin, S. Naqash, C.-L. Tsai, F. Tietz, O. Guillon, *Chem. Mater.* **2016**, 28, 4821.
- [233] H. Park, K. Jung, M. Nezafati, C.-S. Kim, B. Kang, *ACS Appl. Mater. Interfaces* **2016**, 8, 27814.
- [234] S. Song, H. M. Duong, A. M. Korsunsky, N. Hu, L. Lu, *Sci. Rep.* **2016**, 6, 1.
- [235] T. Honma, M. Okamoto, T. Togashi, N. Ito, K. Shinozaki, T. Komatsu, *Solid State Ionics* **2015**, 269, 19.
- [236] K. Noi, K. Suzuki, N. Tanibata, A. Hayashi, M. Tatsumisago, *J. Am. Ceram. Soc.* **2018**, 101, 1255.
- [237] K. Suzuki, K. Noi, A. Hayashi, M. Tatsumisago, *Scr. Mater.* **2018**, 145, 67.
- [238] J. B. Goodenough, P. Singh, *J. Electrochem. Soc.* **2015**, 162, A2387.
- [239] T. Minami, M. Tatsumisago, M. Wakihara, C. Iwakura, S. Kohjiya, I. Tanaka, *Solid State Ionics for Batteries*, Springer-Verlag, Tokyo **2005**.
- [240] R. J. Charles, *J. Am. Ceram. Soc.* **1963**, 46, 235.
- [241] S. W. Martin, *J. Am. Ceram. Soc.* **1991**, 74, 1767.
- [242] R. J. Charles, *J. Am. Ceram. Soc.* **1966**, 49, 55.
- [243] E. Quartarone, P. Mustarelli, *Chem. Soc. Rev.* **2011**, 40, 2525.
- [244] P. Knauth, *Solid State Ionics* **2009**, 180, 911.
- [245] J. C. Bachman, S. Mui, A. Grimaud, H.-H. Chang, N. Pour, S. F. Lux, O. Paschos, F. Maglia, S. Lupart, P. Lamp, L. Giordano, Y. Shao-Horn, *Chem. Rev.* **2016**, 116, 140.
- [246] A. Hayashi, K. Noi, A. Sakuda, M. Tatsumisago, *Nat. Commun.* **2012**, 3, 856.
- [247] A. Hayashi, K. Noi, N. Tanibata, M. Nagao, M. Tatsumisago, *J. Power Sources* **2014**, 258, 420.
- [248] N. Tanibata, T. Matsuyama, A. Hayashi, M. Tatsumisago, *J. Power Sources* **2015**, 275, 284.
- [249] C. Yu, S. Ganapathy, N. J. J. de Klerk, E. R. H. van Eck, M. Wagemaker, K. Takeda, A. Goto, K. Deguchi, S. Ohki, K. Hashi, T. Shimizu, H. Ishida, J. Janek, *J. Mater. Chem. A* **2016**, 4, 15095.
- [250] I.-H. Chu, C. S. Kompella, H. Nguyen, Z. Zhu, S. Hy, Z. Deng, Y. S. Meng, S. P. Ong, *Sci. Rep.* **2016**, 6, 33733.
- [251] S. Wenzel, T. Leichtweiss, D. A. Weber, J. Sann, W. G. Zeier, J. Janek, *ACS Appl. Mater. Interfaces* **2016**, 8, 28216.
- [252] L. Zhang, K. Yang, J. Mi, L. Lu, L. Zhao, L. Wang, Y. Li, H. Zeng, *Adv. Energy Mater.* **2015**, 5, 1501294.
- [253] L. Zhang, D. Zhang, K. Yang, X. Yan, L. Wang, J. Mi, B. Xu, Y. Li, *Adv. Sci.* **2016**, 3, 1600089.
- [254] H. Wang, Y. Chen, Z. D. Hood, G. Sahu, A. S. Pandian, J. K. Keum, K. An, C. Liang, *Angew. Chem., Int. Ed.* **2016**, 55, 8551.
- [255] A. Banerjee, K. H. Park, J. W. Heo, Y. J. Nam, C. K. Moon, S. M. Oh, S.-T. T. Hong, Y. S. Jung, *Angew. Chem., Int. Ed.* **2016**, 55, 9634.

- [256] S. K. S. Kim, A. Mao, S. Sen, S. K. S. Kim, *Chem. Mater.* **2014**, *26*, 5695.
- [257] N. Tanibata, K. Noi, A. Hayashi, N. Kitamura, Y. Idemoto, M. Tatsumisago, *ChemElectroChem* **2014**, *1*, 1130.
- [258] Z. Yu, S.-L. Shang, J.-H. Seo, D. Wang, X. Luo, Q. Huang, S. Chen, J. Lu, X. Li, Z.-K. Liu, D. Wang, *Adv. Mater.* **2017**, *29*, 1605561.
- [259] S. L. Shang, Z. Yu, Y. Wang, D. Wang, Z. K. Liu, *ACS Appl. Mater. Interfaces* **2017**, *9*, 16261.
- [260] R. P. Rao, H. Chen, L. L. Wong, S. Adams, *J. Mater. Chem. A* **2017**, *5*, 3377.
- [261] L. Liu, X. Qi, Q. Ma, X. Rong, Y.-S. Hu, Z. Zhou, H. Li, X. Huang, L. Chen, *ACS Appl. Mater. Interfaces* **2016**, *8*, 32631.
- [262] C. de la Torre-Gamarrá, G. B. Appetecchi, U. Ulissi, A. Varzi, A. Varez, S. Passerini, *J. Power Sources* **2018**, *383*, 157.
- [263] W. Zhou, Y. Li, S. Xin, J. B. Goodenough, *ACS Cent. Sci.* **2017**, *3*, 52.
- [264] W. Zhou, S. Wang, Y. Li, S. Xin, A. Manthiram, J. B. Goodenough, *J. Am. Chem. Soc.* **2016**, *138*, 9385.
- [265] J. Kalhoff, G. G. Eshetu, D. Bresser, S. Passerini, *ChemSusChem* **2015**, *8*, 2154.
- [266] M. Dahbi, S. Komaba, *Fluorine Chemistry for Negative Electrode in Sodium and Lithium Ion Batteries*, Elsevier, Amsterdam **2015**.
- [267] P. Jankowski, W. Wiczorek, P. Johansson, *J. Mol. Model.* **2017**, *23*, 6.
- [268] M. H. Park, Y. S. Lee, H. Lee, Y. K. Han, *J. Power Sources* **2011**, *196*, 5109.
- [269] J. Zheng, S. Chen, W. Zhao, J. Song, M. H. Engelhard, J. G. Zhang, *ACS Energy Lett.* **2018**, *3*, 315.
- [270] H. Ryu, T. Kim, K. Kim, J. H. Ahn, T. Nam, G. Wang, H. J. Ahn, *J. Power Sources* **2011**, *196*, 5186.
- [271] X. Zheng, C. Bommier, W. Luo, L. Jiang, Y. Hao, Y. Huang, *Energy Storage Mater.* **2019**, *16*, 6.
- [272] C. D. Fincher, Y. Zhang, G. M. Pharr, M. Pharr, *ACS Appl. Energy Mater.* **2020**, *3*, 1759.
- [273] X. Zheng, W. Yang, Z. Wang, L. Huang, S. Geng, J. Wen, W. Luo, Y. Huang, *Nano Energy* **2020**, *69*, 104387.
- [274] G. A. Elia, I. Hasa, J. Hassoun, *Electrochim. Acta* **2016**, *191*, 516.
- [275] B. D. McCloskey, J. M. Garcia, A. C. Luntz, *J. Phys. Chem. Lett.* **2014**, *5*, 1230.
- [276] P. Hartmann, C. L. Bender, M. Vračar, A. K. Dürr, A. Garsuch, J. Janek, P. Adelhelm, *Nat. Mater.* **2013**, *12*, 228.
- [277] X. Lu, B. W. Kirby, W. Xu, G. Li, J. Y. Kim, J. P. Lemmon, V. L. Sprenkle, Z. Yang, *Energy Environ. Sci.* **2013**, *6*, 299.
- [278] Z. Qiang, Y. M. Chen, Y. Xia, W. Liang, Y. Zhu, B. D. Vogt, *Nano Energy* **2017**, *32*, 59.
- [279] X. Hu, J. Sun, Z. Li, Q. Zhao, C. Chen, J. Chen, *Angew. Chem., Int. Ed.* **2016**, *55*, 6482.
- [280] D. I. Iermakova, R. Dugas, M. R. Palacín, A. Ponrouch, *J. Electrochem. Soc.* **2015**, *162*, A7060.
- [281] G. G. Eshetu, X. Judez, C. Li, O. Bondarchuk, L. M. Rodriguez-Martinez, H. Zhang, M. Armand, *Angew. Chem., Int. Ed.* **2017**, *56*, 15368.
- [282] E. Peled, S. Menkin, *J. Electrochem. Soc.* **2017**, *164*, A1703.
- [283] E. Peled, *J. Electrochem. Soc.* **1998**, *145*, 3482.
- [284] J. Lee, Y. Lee, J. Lee, S. Lee, J. Choi, H. Kim, M. Kwon, K. Kang, K. T. Lee, N. Choi, *ACS Appl. Mater. Interfaces* **2017**, *9*, 3723.
- [285] Y. Zhao, L. V. Goncharova, A. Lushington, Q. Sun, H. Yadegari, B. Wang, W. Xiao, R. Li, X. Sun, *Adv. Mater.* **2017**, *29*, 1606663.
- [286] F. Mazzali, M. W. Orzech, A. Adomkevicius, A. Pisanu, L. Malavasi, D. Deganello, S. Margadonna, *ACS Appl. Energy Mater.* **2019**, *2*, 344.
- [287] Y. Zhao, J. Liang, Q. Sun, L. V. Goncharova, J. Wang, C. Wang, K. R. Adair, X. Li, F. Zhao, Y. Sun, R. Li, X. Sun, *J. Mater. Chem. A* **2019**, *7*, 4119.
- [288] Q. Shi, Y. Zhong, M. Wu, H. Wang, H. Wang, *Angew. Chem., Int. Ed.* **2018**, *57*, 9069.
- [289] A. Basile, S. A. Ferdousi, F. Makhlooghiyazad, R. Yunis, M. Hilder, M. Forsyth, P. C. Howlett, *J. Power Sources* **2018**, *379*, 344.
- [290] H. Wang, C. Wang, E. Matios, W. Li, *Angew. Chem., Int. Ed.* **2018**, *57*, 7734.
- [291] X. Zheng, H. Fu, C. Hu, H. Xu, Y. Huang, J. Wen, H. Sun, W. Luo, Y. Huang, *J. Phys. Chem. Lett.* **2019**, *10*, 707.
- [292] K. Kubota, S. Komaba, *J. Electrochem. Soc.* **2015**, *162*, A2538.
- [293] M. M. Doeff, M. M. Doeff, Y. Ma, Y. Ma, S. J. Visco, S. J. Visco, L. C. De Jonghe, L. C. De Jonghe, *J. Electrochem. Soc.* **1993**, *140*, L169.
- [294] M. Goktas, C. Bolli, E. J. Berg, P. Novák, K. Pollok, F. Langenhorst, M. v. Roeder, O. Lenchuk, D. Mollenhauer, P. Adelhelm, *Adv. Energy Mater.* **2018**, *8*, 1702724.
- [295] N. Karimi, A. Varzi, S. Passerini, *Electrochim. Acta* **2019**, *304*, 474.
- [296] D. M. Piper, T. Evans, K. Leung, T. Watkins, J. Olson, S. C. Kim, S. S. Han, V. Bhat, K. H. Oh, D. A. Buttry, S.-H. Lee, *Nat. Commun.* **2015**, *6*, 6230.
- [297] S. Komaba, W. Murata, T. Ishikawa, N. Yabuuchi, T. Ozeki, T. Nakayama, A. Ogata, K. Gotoh, K. Fujiwara, *Adv. Funct. Mater.* **2011**, *21*, 3859.
- [298] M. Dahbi, N. Yabuuchi, K. Kubota, K. Tokiwa, S. Komaba, *Phys. Chem. Chem. Phys.* **2014**, *16*, 15007.
- [299] Z. E. Yu, Y. Lyu, Y. Wang, S. Xu, H. Cheng, X. Mu, J. Chu, R. Chen, Y. Liu, B. Guo, *Chem. Commun.* **2020**, *56*, 778.
- [300] G. G. Eshetu, T. Diemant, M. Hekmatfar, S. Grugeon, R. J. Behm, S. Laruelle, M. Armand, S. Passerini, *Nano Energy* **2019**, *55*, 327.
- [301] J. Zhang, D.-W. Wang, W. Lv, S. Zhang, Q. Liang, D. Zheng, F. Kang, Q.-H. Yang, *Energy Environ. Sci.* **2017**, *10*, 370.
- [302] P. Bai, Y. He, P. Xiong, X. Zhao, K. Xu, Y. Xu, *Energy Storage Mater.* **2018**, *13*, 274.
- [303] M. Dahbi, T. Nakano, N. Yabuuchi, S. Fujimura, K. Chihara, K. Kubota, J. Y. Son, Y. T. Cui, H. Oji, S. Komaba, *ChemElectroChem* **2016**, *3*, 1856.
- [304] E. Irisarri, A. Ponrouch, M. R. Palacin, *J. Electrochem. Soc.* **2015**, *162*, A2476.
- [305] H. Che, J. Liu, H. Wang, X. Wang, S. S. Zhang, X.-Z. Liao, Z.-F. Ma, *Electrochem. Commun.* **2017**, *83*, 20.
- [306] Y. Zhang, C. Wang, H. Hou, G. Zou, X. Ji, *Adv. Energy Mater.* **2017**, *7*, 1600173.
- [307] L. Wu, A. Moretti, D. Buchholz, S. Passerini, D. Bresser, *Electrochim. Acta* **2016**, *203*, 109.
- [308] Z.-L. Xu, K. Lim, K.-Y. Park, G. Yoon, W. M. Seong, K. Kang, *Adv. Funct. Mater.* **2018**, *28*, 1802099.
- [309] M. N. Tahir, B. Oschmann, D. Buchholz, X. Dou, I. Lieberwirth, M. Panthöfer, W. Tremel, R. Zentel, S. Passerini, *Adv. Energy Mater.* **2016**, *6*, 1501489.
- [310] L. Wu, D. Bresser, D. Buchholz, G. A. Giffin, C. R. Castro, A. Ochel, S. Passerini, *Adv. Energy Mater.* **2015**, *5*, 1401142.
- [311] J. Lee, Y.-M. Chen, Y. Zhu, B. D. Vogt, *RSC Adv.* **2015**, *5*, 99329.
- [312] R. Yang, L. Sun, W. Liu, Y. Zhang, Y. Cui, Y. Du, S. Liu, H. Wang, M. Huang, *J. Mater. Chem. A* **2019**, *7*, 3399.
- [313] K. Li, J. Zhang, D. Lin, D.-W. Wang, B. Li, W. Lv, S. Sun, Y.-B. He, F. Kang, Q.-H. Yang, L. Zhou, T.-Y. Zhang, *Nat. Commun.* **2019**, *10*, 725.
- [314] J. Ni, S. Fu, C. Wu, Y. Zhao, J. Maier, Y. Yu, L. Li, *Adv. Energy Mater.* **2016**, *6*, 1502568.
- [315] M. A. Muñoz-Márquez, M. Zarrabeitia, E. Castillo-Martínez, A. Eguía-Barrio, T. Rojo, M. Casas-Cabanas, *ACS Appl. Mater. Interfaces* **2015**, *7*, 7801.
- [316] M. Zarrabeitia, F. Nobili, M. A. Muñoz-Marquez, T. Rojo, M. Casas-Cabanas, *J. Power Sources* **2016**, *330*, 78.
- [317] Z. Song, H. Zhou, *Energy Environ. Sci.* **2013**, *6*, 2280.
- [318] A. Abouimrane, W. Weng, H. Eltayeb, Y. Cui, J. Niklas, O. Poluektov, K. Amine, *Energy Environ. Sci.* **2012**, *5*, 9632.
- [319] A. Mauer, C. Julien, A. Paolella, M. Armand, K. Zaghbi, *Materials* **2019**, *12*, 1.
- [320] V. A. Oltean, B. Philippe, S. Renault, R. Félix Duarte, H. Rensmo, D. Brandell, *Chem. Mater.* **2016**, *28*, 8742.

- [321] L. Zhao, J. Zhao, Y.-S. Hu, H. Li, Z. Zhou, M. Armand, L. Chen, *Adv. Energy Mater.* **2012**, 2, 962.
- [322] H. Zhang, I. Hasa, S. Passerini, *Adv. Energy Mater.* **2018**, 8, 1702582.
- [323] I. Hasa, J. Hassoun, S. Passerini, *Nano Res.* **2017**, 10, 3942.
- [324] L. Baggetto, P. Ganesh, R. P. Meisner, R. R. Unocic, J. C. Jumas, C. A. Bridges, G. M. Veith, *J. Power Sources* **2013**, 234, 48.
- [325] M. Fukunishi, N. Yabuuchi, M. Dahbi, J. Y. Son, Y. Cui, H. Oji, S. Komaba, *J. Phys. Chem. C* **2016**, 120, 15017.
- [326] B. Zhang, G. Rousse, D. Foix, R. Dugas, D. A. D. Corte, J.-M. Tarascon, *Adv. Mater.* **2016**, 28, 9824.
- [327] J. Qian, Y. Xiong, Y. Cao, X. Ai, H. Yang, *Nano Lett.* **2014**, 14, 1865.
- [328] Y. Kim, Y. Kim, A. Choi, S. Woo, D. Mok, N. S. Choi, Y. S. Jung, J. H. Ryu, S. M. Oh, K. T. Lee, *Adv. Mater.* **2014**, 26, 4139.
- [329] R. Mogensen, J. Maibach, W. R. Brant, D. Brandell, R. Younesi, *Electrochim. Acta* **2017**, 245, 696.
- [330] L. Wu, X. Hu, J. Qian, F. Pei, F. Wu, R. Mao, X. Ai, H. Yang, Y. Cao, *Energy Environ. Sci.* **2014**, 7, 323.
- [331] L. Baggetto, E. Allcorn, A. Manthiram, G. M. Veith, *Electrochem. Commun.* **2013**, 27, 168.
- [332] I. Hasa, R. Verrelli, J. Hassoun, *Electrochim. Acta* **2015**, 173, 613.
- [333] B. Tian, J. Światowska, V. Maurice, S. Zanna, A. Seyeux, L. H. Klein, P. Marcus, *J. Phys. Chem. C* **2013**, 117, 21651.
- [334] B. Philippe, M. Valvo, F. Lindgren, H. Rensmo, K. Edström, *Chem. Mater.* **2014**, 26, 5028.
- [335] Y. Lu, N. Zhang, Q. Zhao, J. Liang, J. Chen, *Nanoscale* **2015**, 7, 2770.
- [336] S. Yuan, X. Huang, D. Ma, H. Wang, F. Meng, X. Zhang, *Adv. Mater.* **2014**, 26, 2273.
- [337] F. Klein, R. Pinedo, P. Hering, A. Polity, J. Janek, P. Adelhelm, *J. Phys. Chem. C* **2016**, 120, 1400.
- [338] F. Klein, R. Pinedo, B. B. Berkes, J. Janek, P. Adelhelm, *J. Phys. Chem. C* **2017**, 121, 8679.
- [339] J.-H. Kim, N. P. W. Pieczonka, P. Lu, Z. Liu, R. Qiao, W. Yang, M. M. Tessema, Y.-K. Sun, B. R. Powell, *Adv. Mater. Interfaces* **2015**, 2, 1500109.
- [340] K. Edström, T. Gustafsson, J. O. Thomas, *Electrochim. Acta* **2004**, 50, 397.
- [341] H. Zhu, K. T. Lee, G. T. Hitz, X. Han, Y. Li, J. Wan, S. Lacey, A. von W. Cresce, K. Xu, E. Wachsman, L. Hu, *ACS Appl. Mater. Interfaces* **2014**, 6, 4242.
- [342] Y. Lee, J. Lee, H. Kim, K. Kang, N. S. Choi, *J. Power Sources* **2016**, 320, 49.
- [343] C. V. Manohar, M. Forsyth, D. R. MacFarlane, S. Mitra, *Energy Technol.* **2018**, 6, 2232.
- [344] X. Song, T. Meng, Y. Deng, A. Gao, J. Nan, D. Shu, F. Yi, *Electrochim. Acta* **2018**, 281, 370.
- [345] R. Imhof, *J. Electrochem. Soc.* **1999**, 146, 1702.
- [346] M. Winter, R. Imhof, F. Joho, P. Novák, *J. Power Sources* **1999**, 81–82, 818.
- [347] M. Lanz, P. Novák, *J. Power Sources* **2001**, 102, 277.
- [348] F. La Mantia, P. Novák, *Electrochem. Solid-State Lett.* **2008**, 11, A84.
- [349] G. Xu, X. Wang, J. Li, X. Shangguan, S. Huang, D. Lu, B. Chen, J. Ma, S. Dong, X. Zhou, Q. Kong, G. Cui, *Chem. Mater.* **2018**, 30, 8291.
- [350] D. Lu, G. Xu, Z. Hu, Z. Cui, X. Wang, J. Li, L. Huang, X. Du, Y. Wang, J. Ma, X. Lu, H. J. Lin, C. Te Chen, A. A. Nugroho, L. H. Tjeng, G. Cui, *Small Methods* **2019**, 3, 1.
- [351] J. Zhao, L. Zhao, K. Chihara, S. Okada, J. I. Yamaki, S. Matsumoto, S. Kuze, K. Nakane, *J. Power Sources* **2013**, 244, 752.
- [352] X. Wang, E. Yasukawa, S. Kasuya, *J. Electrochem. Soc.* **2001**, 148, A1066.
- [353] J. Feng, Z. Zhang, L. Li, J. Yang, S. Xiong, Y. Qian, *J. Power Sources* **2015**, 284, 222.
- [354] X. Xia, J. R. Dahn, *J. Electrochem. Soc.* **2012**, 159, A515.
- [355] K. Mukai, T. Inoue, *Electrochem. Commun.* **2018**, 88, 101.
- [356] Q. Liu, C. Du, B. Shen, P. Zuo, X. Cheng, Y. Ma, G. Yin, Y. Gao, *RSC Adv.* **2016**, 6, 88683.
- [357] T. Ohsaki, T. Kishi, T. Kuboki, N. Takami, N. Shimura, Y. Sato, M. Sekino, A. Satoh, *J. Power Sources* **2005**, 146, 97.
- [358] H. Kondou, J. Kim, H. Watanabe, *Electrochemistry* **2017**, 85, 647.
- [359] P. Barpanda, G. Liu, C. D. Ling, M. Tamaru, M. Avdeev, S.-C. Chung, Y. Yamada, A. Yamada, *Chem. Mater.* **2013**, 25, 3480.
- [360] X. Xia, J. R. Dahn, *Electrochem. Solid-State Lett.* **2012**, 15, A1.
- [361] J. Zhao, L. Zhao, N. Dimov, S. Okada, T. Nishida, *J. Electrochem. Soc.* **2013**, 160, A3077.
- [362] X. Xia, J. R. Dahn, *J. Electrochem. Soc.* **2012**, 159, A647.
- [363] S. Y. Lim, H. Kim, R. a. Shakoor, Y. Jung, J. W. Choi, *J. Electrochem. Soc.* **2012**, 159, A1393.
- [364] A. Yamada, Y. Kudo, K.-Y. Liu, *J. Electrochem. Soc.* **2001**, 148, A747.
- [365] J.-Y. Hwang, C. S. Yoon, I. Belharouak, Y.-K. Sun, *J. Mater. Chem. A* **2016**, 4, 17952.
- [366] J. Zhao, J. Xu, D. H. Lee, N. Dimov, Y. S. Meng, S. Okada, *J. Power Sources* **2014**, 264, 235.
- [367] J. Feng, Y. An, L. Ci, S. Xiong, *J. Mater. Chem. A* **2015**, 3, 14539.
- [368] J. Feng, L. Ci, S. Xiong, *RSC Adv.* **2015**, 5, 96649.
- [369] S. Aladinli, F. Bordet, K. Ahlbrecht, J. Tübke, M. Holzapfel, *Electrochim. Acta* **2017**, 231, 468.
- [370] C. Ge, L. Wang, L. Xue, Z.-S. Wu, H. Li, Z. Gong, X.-D. Zhang, *J. Power Sources* **2014**, 248, 77.
- [371] J. Chen, Z. Huang, C. Wang, S. Porter, B. Wang, W. Lie, H. K. Liu, P. Isken, C. Dippel, R. Müller, M. Kunze, A. Lex-Balducci, M. Winter, H. J. Gores, *Chem. Commun.* **2015**, 51, 9809.
- [372] S. Komaba, T. Ishikawa, N. Yabuuchi, W. Murata, A. Ito, Y. Ohsawa, *ACS Appl Mater Interfaces* **2011**, 3, 4165.
- [373] Y. Wen, B. Wang, B. Luo, L. Wang, *Eur. J. Inorg. Chem.* **2016**, 2016, 2051.
- [374] X. Li, A. L. Hector, J. R. Owen, S. I. U. Shah, *J. Mater. Chem. A* **2016**, 4, 5081.
- [375] J. Hur, I. T. Kim, *Bull. Korean Chem. Soc.* **2015**, 36, 1625.
- [376] W. Li, S. L. Chou, J. Z. Wang, J. H. Kim, H. K. Liu, S. X. Dou, *Adv. Mater.* **2014**, 26, 4037.
- [377] S. A. Pervez, D. Kim, S. M. Lee, C. H. Doh, S. Lee, U. Farooq, M. Saleem, *J. Power Sources* **2016**, 315, 218.
- [378] H. Lu, L. Wu, L. Xiao, X. Ai, H. Yang, Y. Cao, *Electrochim. Acta* **2016**, 190, 402.
- [379] L. Ji, M. Gu, Y. Shao, X. Li, M. H. Engelhard, B. W. Arey, W. Wang, Z. Nie, J. Xiao, C. Wang, J. Zhang, J. Liu, *Adv. Mater.* **2014**, 26, 2901.
- [380] M. K. Sadan, S.-H. Choi, H. H. Kim, C. Kim, G.-B. Cho, K.-W. Kim, N. S. Reddy, J.-H. Ahn, H.-J. Ahn, *Ionics* **2018**, 24, 753.
- [381] W. Wei, G. Oltean, C.-W. Tai, K. Edström, F. Björefors, L. Nyholm, *J. Mater. Chem. A* **2013**, 1, 8160.
- [382] L. Baggetto, J. K. Keum, J. F. Browning, G. M. Veith, *Electrochem. Commun.* **2013**, 34, 41.
- [383] J. Qian, X. Wu, Y. Cao, X. Ai, H. Yang, *Angew. Chem., Int. Ed.* **2013**, 52, 4633.
- [384] I. T. Kim, S. O. Kim, A. Manthiram, *J. Power Sources* **2014**, 269, 848.
- [385] I. T. Kim, E. Allcorn, A. Manthiram, *J. Power Sources* **2015**, 281, 11.
- [386] I. T. Kim, E. Allcorn, A. Manthiram, *Phys. Chem. Chem. Phys.* **2014**, 16, 12884.
- [387] H. Che, J. Liu, H. Wang, X. Wang, S. Sheng, *Electrochem. Commun.* **2017**, 83, 20.
- [388] J. Y. Jang, Y. Lee, Y. Kim, J. Lee, S.-M. Lee, K. T. Lee, N.-S. Choi, *J. Mater. Chem. A* **2015**, 3, 8332.
- [389] M. Dahbi, N. Yabuuchi, M. Fukunishi, K. Kubota, K. Chihara, K. Tokiwa, X. F. Yu, H. Ushiyama, K. Yamashita, J. Y. Son, Y. T. Cui, H. Oji, S. Komaba, *Chem. Mater.* **2016**, 28, 1625.

- [390] S. Komaba, N. Yabuuchi, T. Nakayama, A. Ogata, T. Ishikawa, I. Nakai, *Inorg. Chem.* **2012**, *51*, 6211.
- [391] M. Chen, L. Chen, Z. Hu, Q. Liu, B. Zhang, Y. Hu, Q. Gu, J.-L. Wang, L. Wang, X. Guo, S. Chou, S.-X. Dou, *Adv. Mater.* **2017**, *29*, 1605535.
- [392] Y. Huang, M. Xie, J. Zhang, Z. Wang, Y. Jiang, G. Xiao, S. Li, L. Li, F. Wu, R. Chen, *Nano Energy* **2017**, *39*, 273.
- [393] P. R. Kumar, Y. H. Jung, B. Moorthy, D. K. Kim, *J. Electrochem. Soc.* **2016**, *163*, A1484.
- [394] M. Law, V. Ramar, P. Balaya, *J. Power Sources* **2017**, *359*, 277.